ABSTRACT

LYNCH, IYAM IRIE. Friction and Sliding of Polystyrene Micro Particles in the Presence and Absence of Capillary Adhesion. (Under the direction of Dr. Jacqueline Krim.)

This thesis presents the results of a Quartz Crystal Microbalance (QCM) study of how sample environment (air, nitrogen, vacuum) impacts the form of the friction laws that govern the polystyrene microparticles deposited onto one of its surface electrodes. Understanding of friction at both the macro- and nano- scales are far better understood than at this intermediate (micro) length scale range. Load geometries particularly micro particles are a rapidly growing field of research. One goal of this thesis was to determine whether the friction associated with the micron scale particles was similar in nature to typical friction classifications associated with either scale (Coulomb, granular, viscous, etc.)

The topic has profound implications, given the varied applications in the wide reaching areas of textiles, biodiagnostics, and nanotransportation. In order to probe the form of the friction law, studies of the amplitude dependence of particle coupling were performed, (referred to herein as a "decoupling curve") monitored both in terms of the QCM response as well as optically. In order to control, as well as document, the impact of capillary adhesion on the measurements, an experimental apparatus was designed and constructed to allow transfer of micro spheres in vacuum from a QCM loaded with spheres to a nearby QCM that was initially sphere-free. Measurements were performed in air, vacuum, and dry nitrogen, and the nature of the friction laws was inferred from well- documented QCM frequency response models. Measurements performed on 5 micron spheres deposited on the surface in air medium revealed, after an initial drying and "run-in" depinning period, behavior close to that expected for a physisorbed system governed by a linear viscous friction law. Slip times

for these particles were close to those previously reported for physisorbed water layers. Measurements performed on dry spheres exhibited far more pronounced decoupling, as well as a crossover to a friction law closer to conventional Coulomb-type friction observed at macroscopic length scales. Optical observations showed that the particle motion was dependent on the oscillation direction and surface topology of the QCM. Particle motion and dynamics are observed using a microscope with a camera attached. This investigation documents that the friction and adhesive properties of microspheres are strongly influenced by the presence or absence of water.

Friction and Sliding of Polystyrene Micro Particles in the Presence and Absence of Capillary Adhesion

by
Iyam Irie Lynch

A dissertation submitted to the Graduate Faculty of
North Carolina State University
in partial fulfillment of the
requirements for the Degree of
Doctor of Philosophy

Physics

Raleigh, North Carolina

2011

APPROVED BY:

_____	_____
Jacqueline Krim Committee Chair	David Aspnes
_____	_____
Daniel Dougherty	Orlando Rojas

DEDICATION

This thesis is dedicated to my grandmother Loretta Campbell for instilling in me the will to never give up as well as my loving wife Olivia for her constant encouragement.

BIOGRAPHY

Iyam Lynch was born April 7, 1982 at Forsyth Hospital in Winston-Salem, NC. He and his younger brother Ishum were raised in Mocksville, NC by his grand parents James and Loretta Campbell. Growing up Iyam was a very curious child who bugged his grandparents by asking too many questions. He was always active in sports and physical activity however, he maintained his strong curiosity for understanding how the world worked. It was this curiosity which led him to pursue physics. In high school Iyam discovered he had a knack for understanding concepts and most of his courses did not provide too much of a challenge. This changed when Iyam took a physics course which proved to be both challenging and humbling. It was then he realized he wanted to take on the challenge of studying this difficult but wonderfully fundamental discipline. Iyam was not the greatest test taker and his grades were always above average but nothing outstanding. Despite this fact Iyam was fortunate enough to obtain acceptance into North Carolina State University under the transition program. This program was designed to give students of their choosing who were rejected in the college in which they applied but, their credentials for entering the university were sufficient. This program was good for Iyam because it required mandatory study hall and constantly monitored work and grades. After his first semester Iyam received a GPA of 3.8 and was later allowed to matriculate into the physics department. Upon graduating he decided to stay at NC State to pursue a Ph.D. in physics which had long been his dream. He was fortunate enough to find a good group that aligned with his interest and personality.

ACKNOWLEDGMENTS

I ultimately realize that with out the help of numerous people I would not even be in a position to type these sentences on this page. With that said I would first like to acknowledge my thesis advisor and mentor Dr. Jacqueline Krim whom I respect and admire for having the patience to deal with me for all these years. I would also like to show my great appreciation for all of my lab mates past and present who have been extremely helpful and fun to work with. I would also like to acknowledge Troy Bradshaw, Jessica McNutt, Andrew Brown, Edward Stevens, and Ben Keller for all of the help they provided me with collecting data. Lastly, I would like to acknowledge all those individuals who helped keep my sanity throughout this process my wife Olivia, my family, close friends, and the RDU Wing Chun School family.

TABLE OF CONTENTS

LIST OF TABLES

LIST OF FIGURES

CHAPTER 1: INTRODUCTION

1.1 THE IMPORTANCE OF MICRO-SCALE FRICTION.

The notion of transporting micro/nano objects has been of interest to the scientific community since the early days of nanotechnology. Progress in this area requires an understanding of the frictional behavior of these objects when they are in motion. Transport and manipulation of nano and micro devices is a necessary application of both nano/micro technology that is as intriguing as it is complex. Obtaining this control can lead to many exciting advancements that span from drug delivery in nanobiotechnology[8], micro particle sorting and grouping by mass[5], particle monitoring for toxicological studies as well and many more favorable applications that span multiple disciplines. However, before these applications can become a reality several questions must be addressed. What forces contribute to the friction between the device and surface? How strong are these forces? Can they be manipulated and if so how? At the micro/nano scale it has been observed in the literature [9] that particle dynamics are dramatically different than what is seen for the macro or meso length scales. This is due to the fact that intermolecular and capillary forces become increasingly important as one approaches these length scales. It was suggested in a previous study [8] that quartz crystal microbalances (QCMs) could have wide spread potential applications for separation, sorting, and sizing. In the prior experiments, polystyrene microspheres were attached to the oscillating surface of a QCM by multiple interactions and detachment of the spheres from the QCM was achieved by varying the driving voltage of the QCM. The QCM was oriented horizontally with the spheres deposited on the top side of the

electrode. The detachment was inferred by measuring the "sound" the spheres emit upon detaching with respect to the voltage at which the crystal was being driven. The experimenters also measured the change in the resonant frequency of the QCM as a function of the driving voltage. They attributed the changes in frequency of the QCM to be a result of the spheres detaching from the surface and eventually rolling off the edge of the QCM causing the mass to decrease which results in a frequency change in the QCM. This explanation is theoretically sound however, a similar shift in frequency can be observed when a portion of spheres no longer track the motion of the resonator as a result of surface decoupling from slipping, sliding, and/or rocking in place in a bound region. In our study we focus on polystyrene microspheres, which are of growing interest due to their medical and textile applications. In particular microencapsulation of phase change materials (PCMs) using polystyrene microspheres, has potential applications toward medical hot/cold therapy as well as manufacturing clothing to handle extreme weather conditions.[10] The topic has also grown increasingly important in recent years in the biosensing community.

1.2 BIOSENSING APPLICATIONS: THE IMPACT OF FRICTION, ADHESION AND DECOUPLING ON EMERGING MEDICAL DIAGNOSTIC TECHNIQUES.

Recent applications involving the use of the quartz crystal microbalance (QCM) are of growing interest in the biosensor community.[1] The QCM provides several advantages in terms of particle detection. The QCM is low cost and relatively low maintenance in terms of operation and most importantly is extremely sensitive (can easily detect mass changes on the

order of micrograms) to surface changes which makes it ideal for gaining information regarding contact mechanics[2] in a non destructive way. One key advantage the QCM brings to the biosensor community is its ability to easily distinguish between the weak "non-specific" surface interactions from the stronger "specific" bonds of study particularly in complex serums such as blood.[1a] The use of a QCM also potentially eliminates the need for tedious labeling procedures during bond rupture scans[1b]. It has been observed in the literature[3] that varying surface and environmental conditions in particular water layers from humid air can lead to drastic changes in the binding energy of the particles of study. It has also been suggested within the biosensing community that the presence of water can result in unwanted additional effects rising from changes in the acoustic coupling of the adsorbed liquid layer (interfacial slip) which would cause difficulties during interpretation of data.[4] Sensing is not the only issue that is affected by the presence of capillaries from water vapor, the prospect of micro-sorting via QCM experiments[5] would be a cumbersome task in the presence of water vapor for various reasons. At the microscale inertial loading has little to no influence on the particles attachment to the surface which means that the particles adherence to the surface arises primarily from other means such as the van der Waals interaction and capillary adhesion. It has been observed[6] that during QCM experiments surface particles distributed on the electrode experience non uniform binding energies even when all surface particles are of the same size and material and deposited under the same conditions. It is also known[7] that the oscillation amplitude of the QCM decreases radially from the center of the electrode which would have an effect on bond rupture. As a result of

these factors it is not guaranteed that adsorbed particles of varying size will sort according to size alone.

The biosensing community would be well served by a carefully controlled study of the friction and adhesion of microscale particles. In particular the form of the friction laws that govern behavior at the micron scale, and how various environmental conditions (air, vacuum, nitrogen) impact the results.

1.3 THE WORK OF THIS THESIS

As outlined above, this thesis is motivated by a desire to examine how sample environment, (air, nitrogen, vacuum) impacts the form of the friction laws that govern the polystyrene microparticles deposited onto the surface electrodes of a QCM. In particular, the work for this thesis explored whether the friction associated with the micron scale particles investigated was similar in nature to typical friction classifications associated with classical friction forms such as Coulomb, granular, viscous, etc. In order to probe the form of the friction law, studies of the amplitude dependence of particle coupling were performed (referred to herein as a "decoupling curve") and monitored both in terms of the QCM response as well as optically. In order to control, as well as document, the impact of capillary adhesion on the measurements, an experimental apparatus was designed and constructed to allow transfer of micro spheres in vacuum from a QCM loaded with spheres to a nearby QCM that was initially sphere-free. Measurements were performed in air, vacuum, and dry nitrogen, and the nature of the friction laws was inferred from well- documented QCM frequency response models. Measurements performed on 5 micron spheres deposited in air revealed, after an initial drying and "run-in" depinning period, behavior close to that

expected for a physisorbed system governed by a linear viscous friction law. Slip times for these particles were close to those previously reported for physisorbed water layers. Measurements performed on dry spheres exhibited far more pronounced decoupling, as well as a crossover to a friction law closer to conventional Coulomb-type friction observed at macroscopic length scales. Optical observations showed that the particle motion was dependent on the oscillation direction and surface topology of the QCM. Particle motion and dynamics were observed using a microscope with a camera attached. As anticipated, this investigation revealed that the friction and adhesive properties of microspheres were strongly influenced by the presence or absence of water.

The thesis is organized as follows: The following chapter provides a description of the experimental chamber and data acquisition procedure. Chapter 3 overviews the various theories for QCM data analysis based on the assumption of varying forms of the friction laws assumed to be governing the particle interactions. Chapter 4 overviews the contact mechanics approaches for asperity contact with an oscillating QCM surface.

Chapters 5 and 6 report respectively a study of the friction law governing 5 micron spheres in air, and the impact of a dry environment on this law. Chapter 7 describes a unique investigation of the sliding friction behavior and QCM response to a single 15 micron sphere located at the center of the QCM electrode. Chapter 8 includes summary comments and suggestions for future work.

1.4 REFERENCES

1. (a) Hirst, E. R.; Yuan, Y. J.; Xu, W. L.; Bronlund, J. E., Bond-rupture immunosensors--A review. *Biosensors and Bioelectronics* 2008, *23* (12), 1759-1768; (b) Rivet, C.; Lee, H.; Hirsch, A.; Hamilton, S.; Lu, H., Microfluidics for medical diagnostics and biosensors. *Chemical Engineering Science* 2011, *66* (7), 1490-1507.

2. (a) Dybwad, G. L., A sensitive new method for the determination of adhesive bonding between a particle and a substrate. *Journal of Applied Physics* 1985, *58* (7), 2789-2789; (b) Flanigan, C. M.; Desai, M.; Shull, K. R., Contact Mechanics Studies with the Quartz Crystal Microbalance. *Langmuir* 2000, *16* (25), 9825-9829.

3. D'Amour, J. N.; Stålgren, J. J. R.; Kanazawa, K. K.; Frank, C. W.; Rodahl, M.; Johannsmann, D., Capillary Aging of the Contacts between Glass Spheres and a Quartz Resonator Surface. *Physical Review Letters* 2006, *96* (5), 058301-058301.

4. Ellis, J. S.; Thompson, M., Acoustic physics of surface-attached biochemical species. *HFSP Journal* 2008, *2* (4), 171-177.

5. Dultsev, F. N.; Ostanin, V. P.; Klenerman, D., “Hearing” Bond Breakage. Measurement of Bond Rupture Forces Using a Quartz Crystal Microbalance. *Langmuir* 2000, *16* (11), 5036-5040.

6. Vittorias, E.; Kappl, M.; Butt, H.-J.; Johannsmann, D., Studying mechanical microcontacts of fine particles with the quartz crystal microbalance. *Powder Technology* 2010, *203* (3), 489-502.

7. Seah, P. J. C. a. M. P., The quartz crystal microbalance; radial/polar dependence of mass sensitivity both on and off the electrodes. *Measurement Science and Technology* 1990, *1* (7), 544-555.

8. Medvedeva, N. V. I., O.M.; Ivanov, Yu. D.; Drozhzhin, A.I.; Archakov, A.I., Nanobiotechnology and nanomedicine. *Biomeditsinskaya Khimiya* 2006, *52* (6), 529-546.

9. Peri, M. D. M.; Cetinkaya, C., Rotational motion of microsphere packs on acoustically excited surfaces. *Applied Physics Letters* 2005, *86* (19), 194103-194103.

10. Sánchez, L.; Sánchez, P.; Lucas, A.; Carmona, M.; Rodríguez, J. F., Microencapsulation of PCMs with a polystyrene shell. *Colloid and Polymer Science* 2007, *285* (12), 1377-1385.

CHAPTER 2: EXPERIMENTAL SETUP

2.1 INTRODUCTION

One of the main purposes of our experimental design is to drastically reduce and/or eliminate capillary forces on the micro particles. Elimination/reduction of these forces greatly simplifies the analysis and also allows controlled comparisons to be performed in the presence and absence of capillary effects. An additional benefit of this setup is the ability to compare results in two different particle environments, dry and humid. Our design also allows us to study particle motion in both vertical and horizontal orientations which permits examination of the impact of gravity on particle motion and friction.

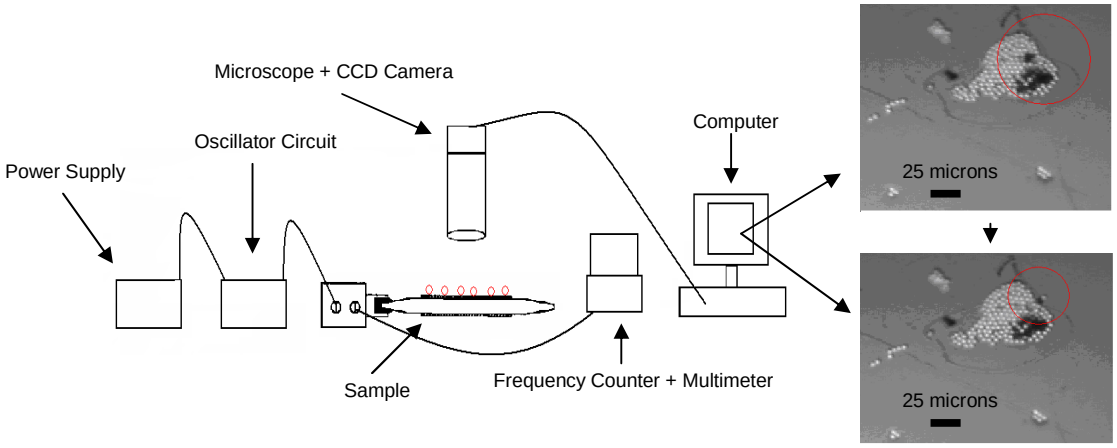

Figure 2.1 - Sketch of experimental apparatus

2.2 QUARTZ CRYSTAL MICROBALANCE (QCM)

QCM is the main experimental tool used in our experiments. In particular we employ two QCM's operating at very different frequencies (8 MHz and 5 MHz) to eliminate "cross talk" created by beat frequencies between the two QCM's. The following section provides an overview of the basic ideas underlying the design and operation of a QCM.

2.2.1 QCM DESIGN

Historically the QCM's were developed as timer components, and later adapted as "microbalances" to monitor film thickness and mass per unit area during gas uptake or thin film deposition.[1] They have since been adapted for a wide variety of more diverse applications[2,3,4,5,6,7]. A QCM is comprised of two main components, a precisely cut wafer of quartz and two conducting electrodes that are deposited on the top and bottom portions of the quartz wafer. The functional component of the QCM is the quartz wafer. Quartz is a crystalline form of SiO_2 and a piezoelectric material, which means that when a voltage is applied to the quartz it will respond mechanically. When the conducting electrodes are attached to the top and bottom of the quartz wafer, an alternating voltage can be applied to the plates to produce an oscillatory response in shear mode within it. The crystal will oscillate at its fundamental (or overtone) frequency, which is determined by the thickness of the wafer. A QCM has the favorable properties of high frequency stability as well as a high "quality factor" (Q) which is the ratio of energy stored to energy lost in the resonator per cycle. The manner in which a QCM is cut has a major impact on the fundamental properties of the oscillator, in particular the frequency, stress, and temperature dependence[8]. In our experiments we used AT cut crystals which are oriented 35 degrees 15 minutes with respect to the ZX crystal plane as shown in the figure below.

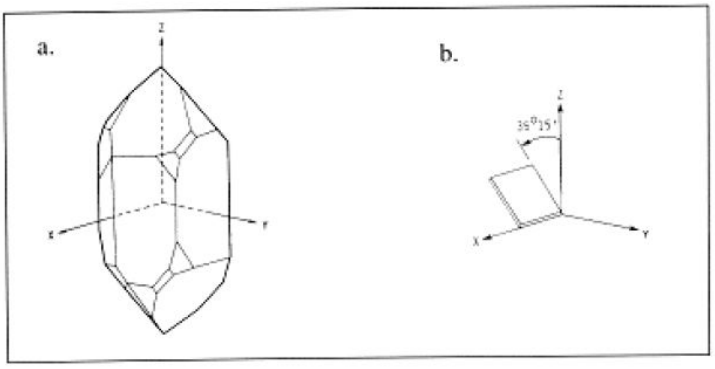

Figure 2.2 - The AT- Cut[9] as shown in 2.2b the cut is made along the zx axis.

The AT cut crystal that we employ operate with low temperature sensitivity (highest frequency stability and mass sensitivity) at room temperature. Our QCM(s) diameter was 0.375 and had a 0.01 inch flat on the –x axis was used to label the direction of oscillation. The crystals oscillated in the fundamental (8MHz and 5MHz) mode and had an optical (overtone) polished finish. The electrode was keyhole design with a diameter of 0.250 inches and it was made from gold deposited atop a thin chrome adhesion layer. Our QCM's where purchased from Laptech Precision Inc out of Ontario Canada[10].

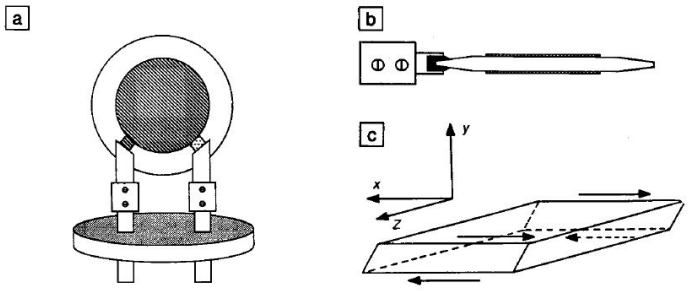

Figure 2.3 - QCM front view (a), side view (b), shear mechanical oscillatory response (c)[11]

2.2.2 BASIC QCM THEORY

In this section I review basic ideas discussed in the previous sections. I first discuss how the frequency of the QCM is determined by the thickness of the quartz disc and how that

thickness must be a multiple of the one half the wavelength of sound. When a QCM is in operation, acoustic (sound) waves propagate throughout the quartz. With this in mind the QCM (not dissimilar from a wind instrument) can be modeled as a wave cavity of length "T" (thickness) open at both ends such that the maximum amplitude of vibration occurs at the end points.

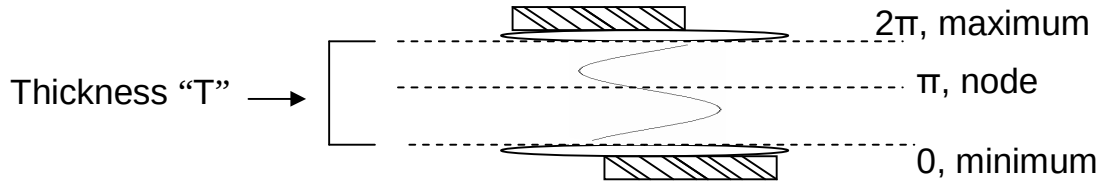

Figure 2.4 - The sound wave propagating through a QCM of thickness T.

The relationship between the frequency and thickness of the crystal is derived as follows:

Let

$$y(x,t) = A\cos(\omega t - kx) \qquad (2.1)$$

Cosine is used because the function is a maximum at the endpoints (the x coordinate is measured from the minimum up to the maximum in figure 2.4). Now applying the boundary conditions we have:

$$y'(0,t) = 0 \Rightarrow Ak\sin(\omega t) = 0 \qquad (2.2)$$

Using a familiar wave equation we can express ωt in terms of wavelength λ

$$v = \lambda f = \frac{\omega\lambda}{2\pi} \Rightarrow \qquad (2.3)$$

$$\omega = \frac{2\pi v}{\lambda} \Rightarrow \tag{2.4}$$

$$\omega t = \frac{2\pi v t}{\lambda} = \frac{2\pi x(t)}{\lambda} \tag{2.5}$$

Applying the boundary condition (2.2) we have

$$\sin(\omega t) = 0 \tag{2.6}$$

$$\Rightarrow \omega t = \frac{2\pi x}{\lambda} = n\pi, n = 0,1,2,... \tag{2.7}$$

$$\lambda = \frac{2\pi x}{n\pi} = \frac{2x}{m}, \tag{2.8}$$

$n \to m = 1,2,3,...$ n is replace with m to avoid divergence
Thus

$$x = \frac{m\lambda}{2} \tag{2.9}$$

Setting x equal to the "thickness" T we obtain the following relations

$$T = \frac{m\lambda_{\max}}{2} \tag{2.10}$$

$$f = \frac{v_s}{\lambda} = \frac{mv_s}{2T} \tag{2.11}$$

where v_s is the velocity of sound through quartz and $\lambda_{\max}$ is the maximum wavelength of a sound wave propagating through quartz. This derivation provides information on the relationship between QCM frequency (fundamental and higher modes "overtones") and thickness. It also shows the dependence a QCM's thickness has on the wavelength of sound.

The next section will elaborate on the QCM's sensitive dependence on changes in thickness, which is the heart of the approximation made when applying the QCM as a mass sensor.

2.2.3 THE SAUERBREY RELATION

The "microbalance" moniker for the QCM has its origins with the Sauerbrey[7] relation. The QCM has a narrow bandwidth and a high quality factor (Q) which makes its frequency of oscillation very sensitive to small changes in mass or more accurately thickness. The Sauerbrey[7] equation relates the change in QCM mass resulting from the deposition of a uniform thin film on the electrode surface to the change in the QCM's frequency from resonance. The derivation assumes that the mass is rigidly attached to the motion of the QCM and as a result can be considered as an effective increase in the thickness of the quartz itself. This assumption works quite well for sufficiently thin films.[12]

The following figure is a schematic demonstrating the problem that Sauerbrey wished to solve. In particular, Sauerbrey examined the shift in frequency of the resonator when a uniform thin layer of mass adsorbed to one side of the QCM surface.

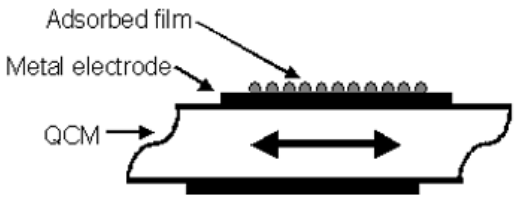

Figure 2.5 - Thin film adsorbed on the electrode surfaces of an oscillating QCM
Sauerbrey assumes equation (2.10), (2.11)

$$T = \frac{m\lambda_{\max}}{2}, \qquad (2.12)$$

$$f = \frac{v_s}{\lambda} = \frac{mv_s}{2T} \qquad (2.13)$$

Using the fundamental mode we set m=1

$$f = \frac{v_s}{2T} \qquad (2.14)$$

Since we are interested in how the frequency changes with thickness we will differentiate the above expression:

$$\frac{\delta f}{\delta T} = \frac{v_s}{2}\frac{\partial}{\partial T}\left(T^{-1}\right) + \frac{1}{T}\frac{\partial}{\partial T}\left(\frac{v_s}{2}\right) \qquad (2.15)$$

To a good approximation $\delta v_s/\delta T = 0$ since the mass film is thin and rigidly attached.

Applying this approximation yields the following result

$$\frac{\delta f}{\delta T} = \frac{-v_s}{2t^2} = \frac{-f_0}{T} \qquad (2.16)$$

Separating variables we have

$$\frac{\delta f}{f_0} = \frac{-\delta T}{T} \qquad (2.17)$$

We now need to relate the change in quartz thickness with the change in mass (to one side of the QCM) using the density of quartz (ρ_q).

$$m_q = \rho_q A T \Rightarrow \qquad (2.18)$$

$$T = \frac{m_q}{\rho_q A} \qquad (2.19)$$

$$\frac{\delta T}{\delta m} = \frac{1}{\rho_q A} \qquad (2.20)$$

Now applying the most important approximation that

$$m_f << m_q \qquad (2.21)$$

$$m_{total} = m_q + m_f \approx m_q \qquad (2.22)$$

$$\delta m \approx m_f \qquad (2.23)$$

Plugging this approximation into equation (2.20) yields an equation that relates the change in quartz thickness to the mass of the adsorbed film m_f

$$\delta T = \frac{\delta m}{\rho_q A} = \frac{m_f}{\rho_q A} \qquad (2.24)$$

We wish to express the frequency shift from resonance in terms of change in mass.

Combining the earlier equations (2.16) and (2.17) will accomplish this goal.

$$\frac{\delta f}{f_0} = \frac{-\delta T}{T} = \frac{-m_f}{m_q} \qquad (2.25)$$

$$\delta f = \frac{-m_f}{m_q} f_0 = \frac{-m_f}{\rho_q A T} f_0 \qquad (2.26)$$

Finally solving the earlier expression $f_0 = \frac{v_s}{2T}$ (2.14) for v_s and plugging the result in the previous equation we obtain the Sauerbrey equation for mass adsorbed to one side of the electrode.

$$\delta f = \frac{-2}{\rho_q v_s}\left(\frac{m_f}{A}\right) f_0^2 \qquad (2.27)$$

2.2.4 ELECTRONICS

The QCM was driven by a Pierce oscillator circuit whose output signal was mixed using a 0.5 to 500 MHz frequency mixer with a reference signal supplied by an 8 MHz can crystal oscillator driven by a different Pierce oscillator circuit. The mixed output ran through a low pass filter and was detected using a Hewlett Packard 5384A frequency counter. The crystal amplitude was measured using a Keithley 2000 multimeter. The reference "can" QCM was powered by an Elenco Precision model XP-15 regulated variable power supply and the experimental 8 MHz QCM was driven with a Keithley 2400 digital source meter. A second Keithley 2400 digital source meter was used to drive a 5 MHz QCM in experiments where both the 8 MHz and 5MHz crystal were oscillating simultaneously in close range. These source meters are extremely low noise instruments which allowed us to make accurate measurements while varying the drive voltage of one of the crystals. Below is a diagram of the Pierce oscillator circuit. The Pierce circuit was a convenient choice to power our crystals for several reasons. The Pierce oscillator operates well in the presence of high stray capacitances resulting from various mounting arrangements as well as maintaining high frequency stability even for low drive levels[13].

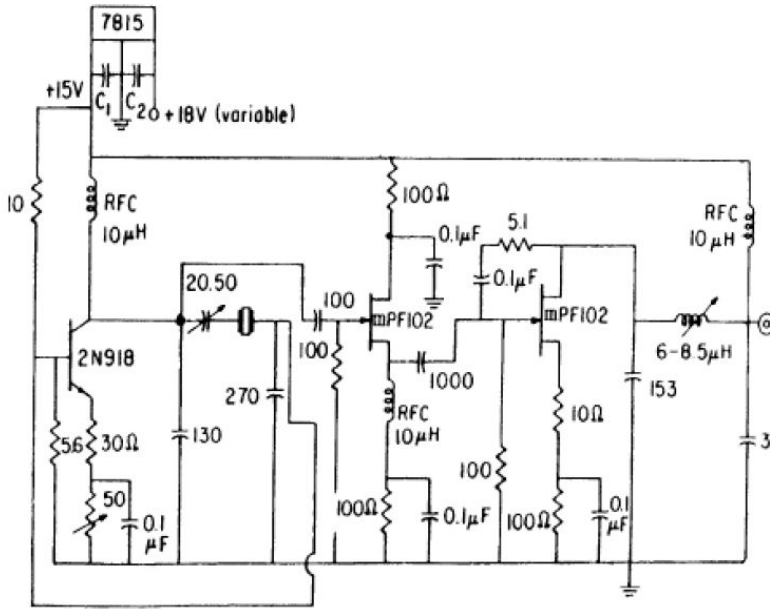

Figure 2.6 - Schematic of Pierce oscillator circuit[14]

When taking data we simultaneously read out the frequency and crystal amplitude of our experimental QCM. The Keithley 2000 multimeter was limited in its frequency range and could not handle frequencies in the MHz range. As a result of this we mixed the output from two Pierce boards one driving the experimental QCM and the other driving the reference "can" QCM. Both crystals were at similar fundamental frequencies only differing in the kHz range. The mixer circuit takes these frequencies and outputs both there sum and difference. Attaching a low pass filter to the mixer output gave us a frequency $f_{mixed} = \left| f_{\exp} - f_{ref} \right|$ (in the kHz range) that could be handled by our Keithley 2000 multimeter.

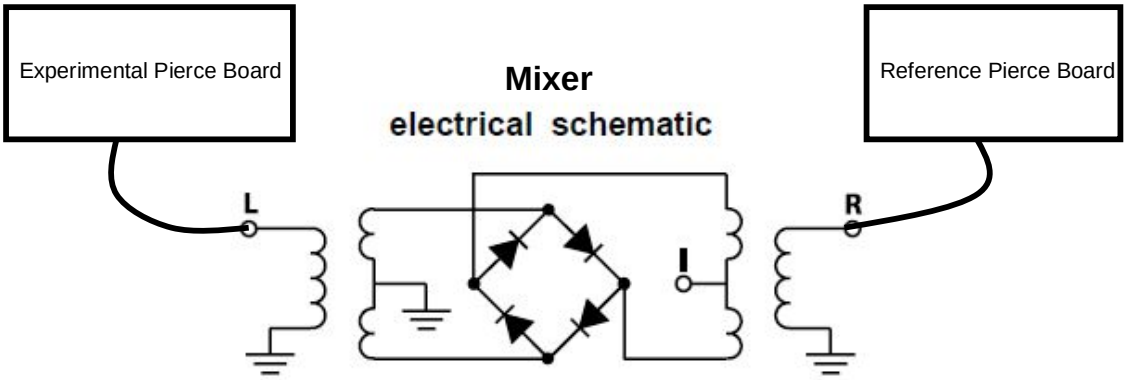

Figure 2.7 - Mixer circuit[15]

2.2.5 MICROSPHERES

In our experiment we deposited from aqueous solution a sub monolayer (1-10%) of polystyrene microspherical particles on the top electrode of a QCM. Our spheres were purchased from Bangs Laboratories, Inc. (Fishers, IN).

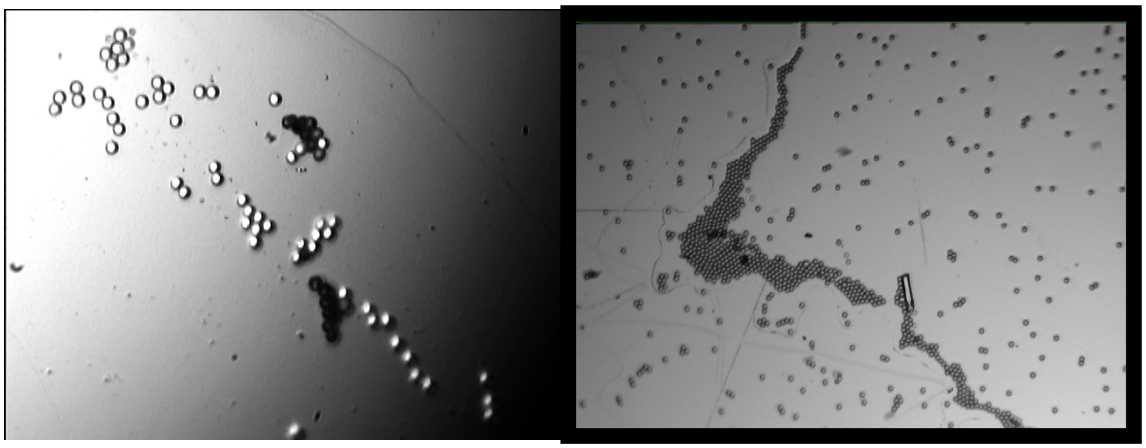

Figure 2.8 - Images from left to right 15 micron and 5 micron diameter polystyrene spheres.

2.2.6 CUSTOMIZED VACUUM CHAMBER

Experiments were performed in a vacuum chamber customized to rotate approximately 270 degrees in order to perform experiments in both vertical and horizontal orientations along with all angles in between. The horizontal and vertical experiments were both performed in the following environments: air, vacuum, and dry nitrogen. Inside of the chamber are two QCM holders one oriented in the horizontal plane while the other is oriented in the vertical plane with respect to the acceleration of gravity. These holders were placed in such a way to allow sphere transfer experiments to be performed in situ. Transfer experiments were performed by depositing microspheres on the 5 MHz QCM which were to be placed in the vertical holder. We then placed a blank 8 MHz QCM in the horizontal holder located directly below the vertical holder. Spheres were transferred by generating particle motion on the QCM in the vertical holder by strongly driving and rapidly varying the applied voltage. The projected particles landed on the oscillating 8 MHz QCM which was held at a fixed voltage. The choice of 5 and 8 MHz QCMs was chosen to eliminate "cross talk" from beat frequencies produced from the QCMs. Eliminating the cross talk allowed us to record QCM behavior during particle transfer. Particle motion was analyzed using an Edmund optics Proximity Series Infinitube microscope with a Mitutoyo 10X/0.28 lens illuminated by an Edmund Industrial Optics model 21AC illuminator. Attached to the microscope was a B/W CCD camera from *Industrial Vision Source* whose video output was sent to the computer program Flash Point 3D and a Toshiba DVD recorder to record movies of surface motion.

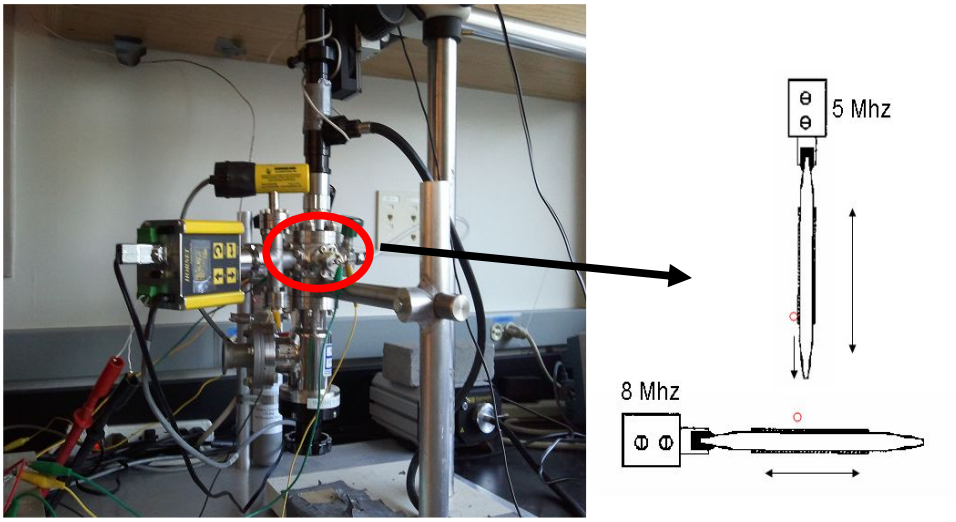

Figure 2.9 - Picture taken of the customized vacuum chamber.

The data recorded in this setup were analyzed in terms of both the frequency shift data and the optical information obtained with the camera. In the next chapter, I will describe the various theoretical approaches employed for analysis of frequency shift data, including analysis treatments of quality factor shifts when relevant.

2.3 REFERENCES

1. King, W. H., Piezoelectric Sorption Detector. Analytical Chemistry 1964, 36 (9), 1735-1739.

2. Dultsev, F. N.; Ostanin, V. P.; Klenerman, D., “Hearing” Bond Breakage. Measurement of Bond Rupture Forces Using a Quartz Crystal Microbalance. Langmuir 2000, 16 (11), 5036-5040.

3. Dybwad, G. L., A sensitive new method for the determination of adhesive bonding between a particle and a substrate. Journal of Applied Physics 1985, 58 (7), 2789-2789.

4. Flanigan, C. M.; Desai, M.; Shull, K. R., Contact Mechanics Studies with the Quartz Crystal Microbalance. Langmuir 2000, 16 (25), 9825-9829.

5. Krim, J.; Widom, A., Damping of a crystal oscillator by an adsorbed monolayer and its relation to interfacial viscosity. Physical Review B 1988, 38 (17), 12184-12184.

6. Laschitsch, A.; Johannsmann, D., High frequency tribological investigations on quartz resonator surfaces. Journal of Applied Physics 1999, 85 (7), 3759-3759.

7. Sauerbrey, G., Verwendung von Schwingquarzen zur Wägung dünner Schichten und zur Mikrowägung. Zeitschrift für Physik 1959, 155 (2), 206-222.

8. Varma, M. R. Vapor Phase Lubrication of Microelectro Mechanical Systems(MEMS): An Atomistic Approach to Solve Friction and Stiction in MEMS. North Carolina State University, Raleigh, 2003.

9. Crystallographic quartz axes figure reference.

10. Laptech Precision Inc, Part # XL1018, http://www.laptech.com.

11. Robbins, M. O., Energy Dissipation in Interfacial Friction. Krim, J., Ed. MRS Bulletin: MRS Bulletin, 1998; Vol. 23, pp 23-26.

12. Vogt, B. D.; Lin, E. K.; Wu, W.-l.; White, C. C., Effect of Film Thickness on the Validity of the Sauerbrey Equation for Hydrated Polyelectrolyte Films. The Journal of Physical Chemistry B 2004, 108 (34), 12685-12690.

13. Abdelmaksoud, M. Nanotribology of a Vapor Phase Lubricant: Quartz Crystal Microbalance Study of Tricresylphosphate (TCP) Uptake on Iron and Chrome North Carolina State University, Raleigh, 2001.

14. Winder, S. M. North Carolina State University, Raleigh, 2003.

15. Mini-Circuits, Mini-Circuits Frequency Mixer SRA-1 Data Sheet.

CHAPTER 3: THEORETICAL APPROACHES TO THE ANALYSIS OF QCM FREQUENCY SHIFT DATA.

3.1 INTRODUCTION

As previously discussed in chapter 2 the QCM traditionally is used to monitor mass uptake during thin film deposition. This is done by monitoring the change in frequency from resonance as mass adsorbs on the surface of one side of QCM layer by layer. The relationship between mass and frequency shift is given by the Sauerbrey relation and was described in detail in the previous chapter.

$$\delta f = \frac{-2}{\rho_q v_s}\left(\frac{m_f}{A}\right) f_0^2 \qquad (3.1)$$

We recall that the Sauerbrey relation related the change in QCM mass (adsorbed mass) to a change in the thickness of the quartz. This relation works well when dealing with thin monolayer depositions however, breaks down for significantly thick layers[1,2], submonolayer coverage, and other varying surface geometries. In the following sections specific examples of these varying geometries and how the QCM can be used to probe detailed information regarding the contact mechanics and friction of particles adsorbed on the surface. Knowledge of these varying geometries is extremely important for the analysis of the work presented in this thesis.

3.2 SLIDING FILMS

Equation (3.1) from the previous section assumes that the adsorbed mass is rigidly attached to the QCM electrode. As a result of the extreme shear vibrations the adsorbed particles experience on the electrode surface it is not hard to imagine the possibility of interfacial slip. When slip occurs on the surface, equation (3.1) is no longer a valid means of measuring mass due to the additional effects particles slipping on the surface have on the QCM. In 1986 researchers Krim and Widom[3] realized this possibility and developed methods to quantify the friction between the QCM electrode and the sliding "decoupled" particles. To address this behavior the researchers used a combination of fluid dynamics and driven oscillator mechanics to describe the experimental situation. To understand their methodology we examine the different ways a QCM can be modeled. The most common ways to model a QCM are as an equivalent circuit or a mass-spring system although other methods do exist (optical and purely mathematical) [4]. Krim and Widom modeled the QCM as a driven mass-spring system with damping. Writing out the sum of all the forces (considered) for this system gives:

$$F_0 \cos(\omega t) = m\ddot{x} + R_m\dot{x} + \frac{x}{C_m} \qquad (3.2)$$

Assuming solutions have the form

$$x(t) = Ae^{i(\omega t-\delta)} \qquad (3.3)$$

Then the velocity is written as

$$v = \frac{F}{R_m - i\left(\omega M_m - 1/\omega C_m\right)} \qquad (3.4)$$

Where R_m, M_m, C_m, and ω are the mechanical resistance, mass, compliance (1/(spring constant k), and frequency respectively and δ represents the phase angle. Equation (3.2) has obvious parallels with an RLC electrical circuit driven by and alternating emf V. For this system the mechanical impedance is

$$Z_m = \frac{F}{v} = R_m - iX_m = R_m - i(\omega M_m - 1/\omega C_m). \qquad (3.5)$$

The term X_m is the mechanical reactance of the system and is proportional to the inertial components of the system and R_m is proportional to the energy dissipation (loss) of the system. The authors realized that a QCM under a particular load would experience some increase in the impedance (3.5) of the system. If the components of the impedance R_m and X_m could be computed in terms of the properties of the loading material then detailed information regarding the behavior of the particles on the QCM surface could be extracted in particular whether the surface particles were rigidly attached or decoupled (sliding). In cases where the Sauerbrey equation (3.1) apply the resistive term of equation (3.5) would go to zero and the entire contribution of the impedance of the system would be inertial however, for systems where the films begin to decouple and slide the resistive term is greater than zero. In order to understand how a 2D film affects the impedance of a QCM it is beneficial to first examine the effect of a 3D fluid (or gas) interacting with the QCM. For a fluid interacting with an oscillating plane (QCM) the Navier-Stokes relation is sufficient to describe the behavior.

$$\rho_3 \frac{\partial v_x}{\partial t} = \eta_3 \frac{\partial^2 v_x}{\partial z^2} \ , \qquad (3.6)$$

where ρ_3 is the density of the 3D fluid, v_x is the velocity of the QCM in the x-direction such that $v_x = v_0 \cos(\omega t)$, and η_3 is the bulk viscosity of the 3D fluid. The 2D film adsorbed onto the surface of the QCM from the surrounding 3D fluid will have the following equation of motion,

$$\rho_2 (d\vec{v}_f / dt) = -\vec{\nabla}\phi - \eta_2 \vec{v}_f \qquad (3.7)$$

where η_2, ρ_2, ϕ, and v_f are the 2D film viscosity, density, spreading pressure, and velocity respectively. A 2D adsorbed monolayer film has a spreading pressure equal to zero thus it is implied from equation (3.7) that

$$\int dA \rho_2 (d\vec{v}_f / dt) = -\int dA \eta_2 \vec{v}_f \ . \qquad (3.8)$$

The classical shear impedance is found from the solution of equation (3.8)

$$Z_3 = R_3 - iX_3 = (1-i)\sqrt{\pi f \rho_3 \eta_3} \qquad (3.9)$$

where Z_3 is the acoustical shear impedance which is equivalent to the mechanical impedance (Z_m) per unit area. In order to compensate for excess momentum fluctuations resulting from gas particles with velocity components commensurate with the oscillation of the QCM the authors have replaced the viscosity term in equation (3.9) with the complex viscosity

$$\eta_3^* = \eta_3 \left[\frac{1}{1 - i\omega\tau_r} \right] \qquad (3.10)$$

where τ_r is the time it takes for the excess particle momentum to relax to 1/e of its initial equilibrium value. Taking into consideration equation (3.10) the components for equation (3.9) become,

$$R_3^* = \sqrt{\pi f \rho_3 \eta_3}\left\{\frac{\omega\tau_r}{1+(\omega\tau_r)^2}\left[\left(1+\frac{1}{\omega\tau_r}\right)+1\right]\right\}^{1/2} \qquad (3.11)$$

$$X_3^* = \sqrt{\pi f \rho_3 \eta_3}\left\{\frac{\omega\tau_r}{1+(\omega\tau_r)^2}\left[\left(1+\frac{1}{\omega\tau_r}\right)^{1/2}-1\right]\right\}^{1/2}. \qquad (3.12)$$

Equations (3.11) and (3.12) can be used to find the "excess dissipation per unit mass" from the momentum fluctuations of the 3D gas to the QCM surface. This is done by taking the ratio of (3.11) to (3.12) in the limit $\omega\tau_r << 1$ (short relaxation times) as shown in equation (13) below

$$\frac{R_3^*}{X_3^*} = 1+\omega\tau_r . \qquad (3.13)$$

For a 2D adsorbed film which is what we are mainly concerned with the authors found a similar expression for the ratio of the 2D counterparts of equation (3.13)

$$\frac{R_2^*}{X_2^*} = \omega\tau . \qquad (3.14)$$

where τ in (3.14) is the characteristic "slip time" or the time it takes for an adsorbed film to stop once slipping has begun. This term is analogous to the relaxation time introduced for the 3D fluid damping case. The authors discuss how the case of a film rigidly attached to the motion of the QCM (equation (3.1)) is an approximation of the actual situation of slip. When a film obeys equation (3.1) the slip time is much smaller than the period of oscillation of the

QCM thus slip is not observable. However, when the slip time is commensurate with the period of oscillation of the QCM the effects of slip can be probed via the added impedance to the QCM. The authors rigorously showed an agreement between the classical result of (3.14) and a result obtained from a quantum mechanical approach. They found the following results for the components of the added impedance a QCM experiences from a 2D adsorbed film on one side

$$R_2^* = \frac{\rho_2 \omega^2 \tau}{1+(\omega\tau)^2}, \qquad (3.15)$$

where ρ_2 is mass per unit area of the 2D adsorbed layer, in g/cm^2

$$X_2^* = \frac{\rho_2 \omega}{1+(\omega\tau)^2} \qquad (3.16)$$

where the ratio of (3.15) to (3.16) is in agreement with (3.14). As stated earlier the real and imaginary components of the impedance an adsorbed film adds to a QCM are related to the dissipative and inertial properties respectively. These expressions were derived by Stockbridge [5] and are

$$\delta\left[\frac{1}{Q}\right] = \frac{2R^*}{\omega\rho_q t_q}, \qquad (3.17)$$

$$\delta\omega = \frac{X^*}{\rho_q t_q}, \qquad (3.18)$$

where $\delta\left[\frac{1}{Q}\right]$ is the shift in inverse quality factor or "change in dissipation" of the system, $\delta\omega$ is the shift from resonance and t_q is the thickness of quartz. Plugging (3.15) and (3.16)

into (3.17) and (3.18) and taking the ratio of (3.17) to (3.18) the authors found the central result of their work which was an expression of slip time in terms of measurable changes in the QCM during deposition.

$$\delta\left[\frac{1}{Q}\right] = 2\tau\delta\omega \qquad (3.19)$$

Plugging (3.16) into (3.18) gives the frequency shift from resonance the QCM experiences from film slippage.

$$\delta f = \frac{\delta f_{film}}{1+(\omega\tau)^2} \qquad (3.20)$$

In equation (3.20) δf_{film} is the shift in frequency from mass loading (no slipping) and is therefore found by applying equation (3.1).

3.3 THE DYBWAD EXPERIMENT

In 1985 Dybwad performed an experiment where he placed a single gold microsphere on the center portion of an oscillating QCM [6]. He observed a positive shift in frequency which at first glance appears contradictory to the Sauerbrey equation. Similar to the authors from section 3.2, Dybwad modeled the QCM as a mechanical system. He explained his result by modeling the single sphere QCM geometry as a coupled mechanical oscillator. By doing so he justified the possibility of measuring a positive shift in frequency when a single particle is "lightly" coupled to the electrode of the QCM. This experiment was one of the first examples of how a QCM could be used to probe particle adhesion.

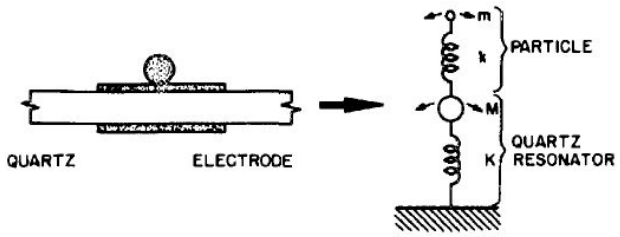

Figure 3.1 - Dybwad's coupled oscillator model [4]

Using figure 3.1 I will review Dybwad's published result for the system's frequency response as a function of the single sphere "attachment parameter" $\omega(k)$.

We begin by displacing each object in the coupled oscillator model by an arbitrary distance as shown in figure 3.2.

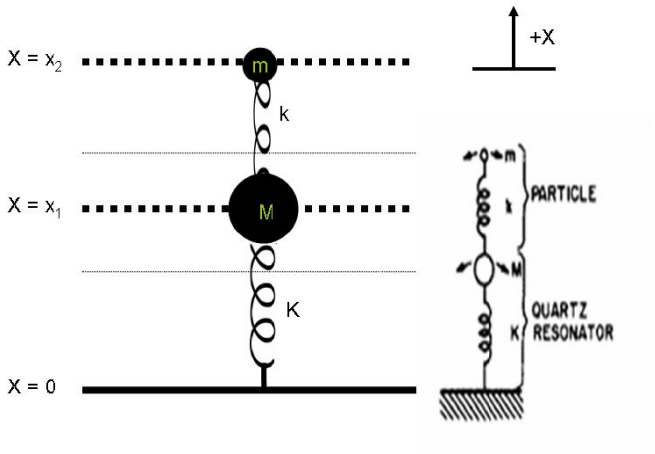

Figure 3.2 - Dybwad's coupled oscillator extended by arbitrary distances.

where M is the mass associated with the QCM, m is the mass of the sphere deposited to one side of the QCM, K is the spring constant associated with the QCM, and k is the spring constant of the sphere which is also referred to as the "attachment parameter" a value that describes the bond strength between the sphere and QCM surface. After applying this

displacement we write the equations of motion for objects M and m via Newton's 2nd law assuming x_2 larger than x_1.

$$M\ddot{x}_1 = -Kx_1 + k(x_2 - x_1) \quad (3.21)$$

$$m\ddot{x}_2 = -k(x_2 - x_1) \quad (3.22)$$

$$\ddot{x}_1 + \frac{K}{M}x_1 - \frac{k}{M}x_2 + \frac{k}{M}x_1 = 0 \quad (3.23)$$

$$\ddot{x}_2 + \frac{k}{m}x_2 - \frac{k}{m}x_1 = 0 \quad (3.24)$$

The differential equations (3.22) and (3.23) can be solved by assuming the following solutions for x_1 and x_2.

$$x_1 = C_1\cos(\omega t) \quad (3.25)$$

$$x_2 = C_2\cos(\omega t) \quad (3.26)$$

Since we are searching for the normal mode frequencies of this coupled oscillator system the frequency term ω must be the same for both equations (3.25) and (3.26). It is also necessary that there are exactly two normal mode solutions since there are two objects (QCM and single microsphere). Plugging (3.25) and (3.26) into (3.23) and 3. (24) we obtain:

$$-C_1(-\omega^2 + \frac{K}{M} + \frac{k}{M}) = C_2\frac{k}{M} \quad (3.27)$$

$$C_2(-\omega^2 + \frac{k}{m}) = C_1\frac{k}{m} \quad (3.28)$$

We now have 2 equations (3.27) and (3.28) with 3 unknown variables C_1, C_2, and ω. To solve this problem we must have 3 equations. The third equation comes from finding the ratio of the amplitudes C_1/C_2 . When solving this ratio for equations (3.27) and (3.28) then

equating the two expressions we effectively eliminate the ratio. The result is an expression for frequency as a function of "attachment parameter" ω(k).

$$\frac{C_1}{C_2} = \frac{\left(\frac{k}{M}\right)}{\left(-\omega^2 + \frac{K}{M} + \frac{k}{M}\right)} = \frac{\left(-\omega^2 + \frac{k}{m}\right)}{\left(\frac{k}{m}\right)} \qquad (3.29)$$

After some algebra, one arrives at the following expression from equation (3.29)

$$\omega^4 - \omega^2\left(\frac{K}{M} + \frac{k}{M} + \frac{k}{m}\right) + \frac{Kk}{Mm} = 0\,. \qquad (3.30)$$

Equation (3.30) is a quadratic equation that leads to two solutions (negative frequencies have no physical meaning) for the normal modes of the coupled oscillator system. Applying the quadratic equation to solve Equation (3.30), we obtain:

$$\frac{-b \pm \sqrt{b^2 - 4ac}}{2a} = \omega^2 \text{, where } \begin{array}{l} a = 1 \\ b = -\left(\frac{K}{M} + \frac{k}{M} + \frac{k}{m}\right) \\ c = \frac{Kk}{Mm} \end{array} \qquad (3.31)$$

After applying equation (3.31) we arrive at Dybwad's expression for $\omega(k)$, where m is the mass of a particle added on one side of the crystal.

$$2\omega^2 = \left(\frac{K}{M} + \frac{k}{M} + \frac{k}{m}\right) \pm \left[\left(\frac{K}{M} + \frac{k}{M} + \frac{k}{m}\right)^2 - 4\frac{K}{M}\frac{k}{m}\right]^{1/2}. \qquad (3.32)$$

Plotting the system frequency ω as a function of the attachment parameter k, Dybwad obtined the idealized behavior of the coupled system. This plot is shown in figure 3.3 where two coupling regimes, "strong" and "weak", are highlighted. In the strong region (large k values) the plot shows negative values for the frequency in accordance with equation (3.1).

Conversely in the weak region (small k values) the plot shows that when the sphere is "loosely" attached to the QCM, positive shifts in frequency are possible. This is a result of the additional "stiffness" the system experiences from the bond. In other words the bond is not strong enough for the sphere to track the motion of the QCM so the resonator does not detect its mass (inertial loading) however, it can sense the added stiffness from the sphere-electrode bond.

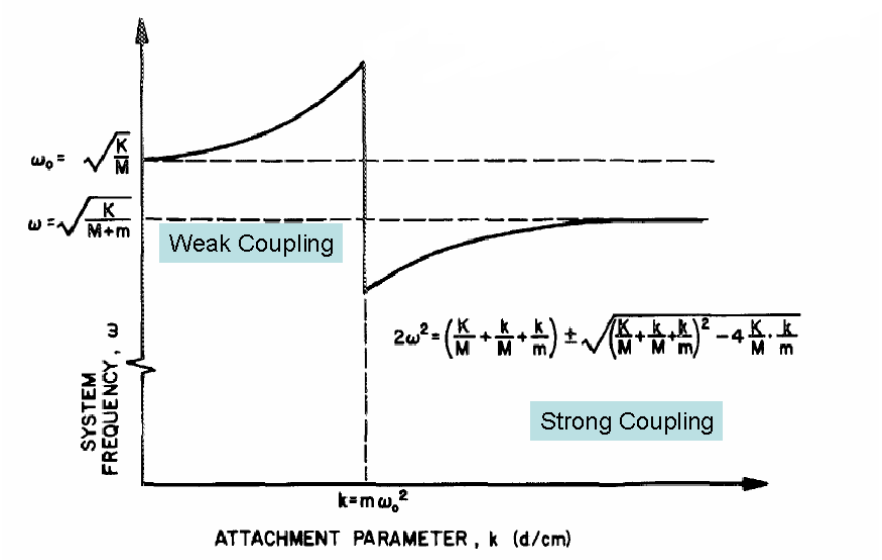

Figure 3.3 - System frequency ω as a function of attachment parameter k.[6]

3.4 QCM CIRCUIT MODEL

We next consider a theoretical treatment of the QCM that models it in terms of its equivalent electrical components, which can then be related back to the mechanical properties of the crystal. An unloaded QCM oscillating at or near resonance can be modeled as a Butterworth-Van Dyke equivalent circuit as shown in figure 3.4. The Butterworth-van Dyke (BVD) circuit is an approximation of the more rigorous Mason equivalent circuit [7].

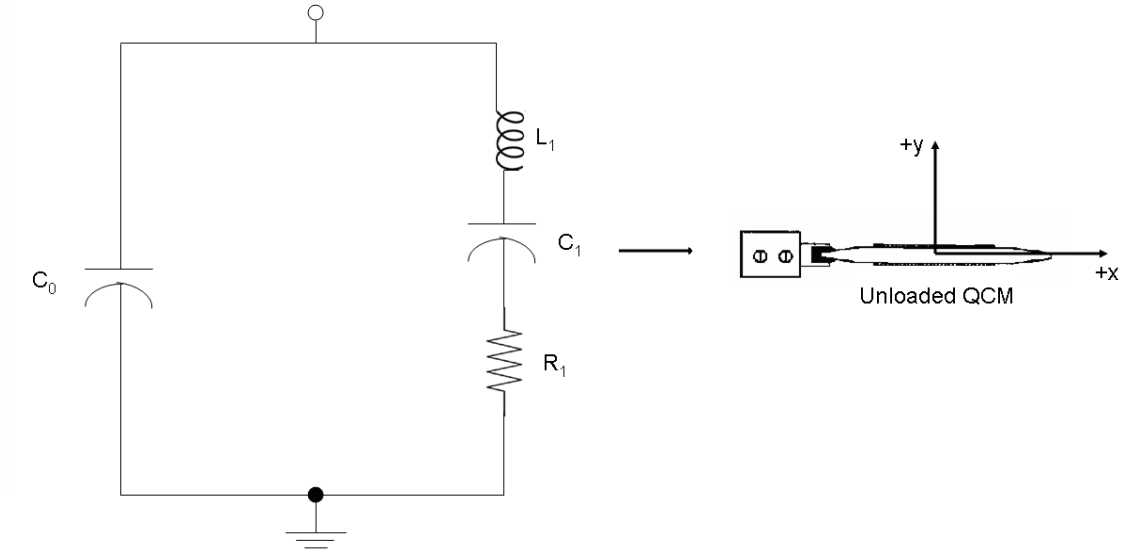

Figure 3.4 - Butterworth-Van Dyke equivalent circuit for unloaded QCM.

The term C_0 is the "shunt" capacitance and is a combination of the static capacitance between electrodes on both sides of the quartz and the "parasitic" capacitance that arises from external sources such as mounting. The right side of figure 3.4 is sometimes referred to as the "acoustic branch" and is composed of additional inductive, capacitive, and resistive (L_1, C_1, and R_1 respectively). The terms from the acoustic branch arise from electric coupling to the shear mechanical displacement resulting from oscillation. When a QCM is loaded by some external means (film deposition, liquid loading, microspheres deposited on surface, etc.) the system experiences additional impedance to its motion and is interpreted in the BVD model as load components. These components are pictured in figure 3.5.

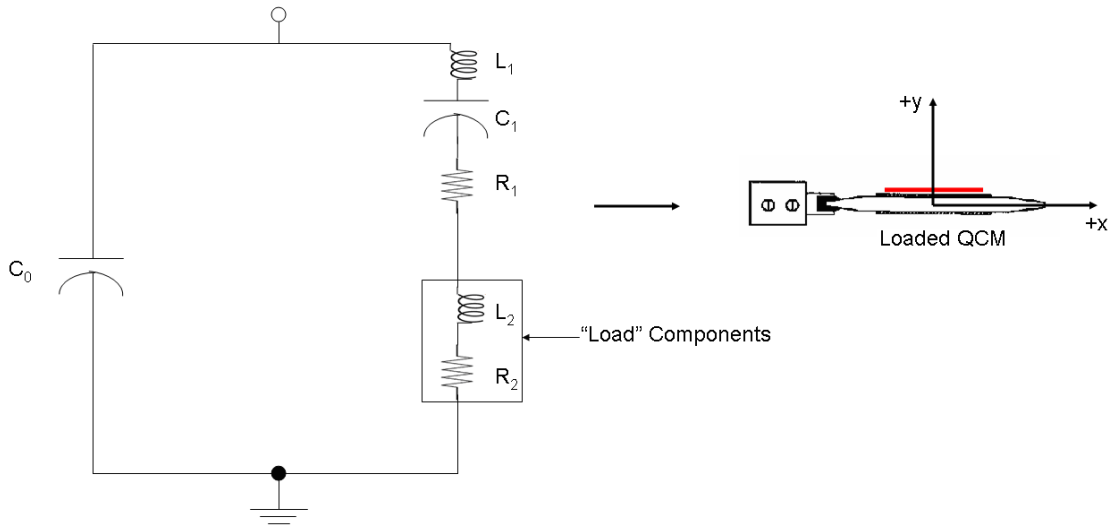

Figure 3.5 - Butterworth-Van Dyke equivalent circuit for loaded QCM.

For an unloaded QCM the components of the BVD circuit (figure 3.4) are commonly found by plotting the systems admittance (ratio of current flow to applied voltage) against the frequency (Y vs. f). Once this plot is made components C_0, L_1, C_1, and R_1 are determined by fitting them to equation (3.33). The admittance is related to the frequency by the following equation(s):

$$Y(f) = i\omega C_0 + \frac{1}{Z_a} \qquad (3.33)$$

where Z_a is the "acoustic" impedance for the unloaded QCM

$$Z_a = R_1 + i\omega L_1 + \frac{1}{i\omega C_1} \qquad (3.34)$$

when the QCM is under a load as shown in figure 3.5 equation (3.34) becomes

$$Z_a = R_1 + i\omega L_1 + \frac{1}{i\omega C_1} + Z_e \qquad (3.35)$$

where Z_e is the electrical load impedance and is written as

$$Z_e = R_2 + i\omega L_2 \qquad (3.36)$$

The electrical load impedance is directly proportional to the load impedance Z_L that results from the contact between the load material and the QCM surface. When $|Z_L|$ is small compared to the shear wave impedance of quartz, $Z_q = \sqrt{\mu_q \rho_q}$, it has been shown[8] that

$$Z_e = \frac{N\pi}{4K^2\omega_0 C_0}\left(\frac{Z_L}{Z_q}\right) \qquad (3.37)$$

where N is the overtone order (N=1,3,5,…), $\omega_0 = 2\pi f_0$ where f_0 is the undamped resonant frequency of the QCM and K^2 is the AT-cut quartz electromechanical coupling factor and is equal to 7.74×10^{-3} according to Ballato[9]. The load impedance Z_L is defined by the ratio of the shear stress of the loading material to the shear velocity of the load at the QCM boundary.

$$Z_L = \left.\frac{\sigma_{xy}}{v_x}\right|_{y=0} \qquad (3.38)$$

where σ_{xy} is the shear stress (force per unit area in x-direction normal to y-direction see figure 3.5) to the load material from the oscillation of the QCM and v_x is the corresponding shear velocity of the load particles.

It is important to note that Z_L is a complex quantity and the real component $Re(Z_L)$ represents the mechanical power dissipation and corresponds to the stress component in phase with the particle velocity. The imaginary component $Im(Z_L)$ is the stress component 90 degrees out of phase with the particle velocity and corresponds to the mechanical energy

storage at the surface. If it is possible to find (3.38) then the "load" components from (3.36) can be found. Combining (3.36) and (3.37) gives:

$$R_2 = \frac{N\pi}{4K^2\omega_0 C_0}\frac{\mathrm{Re}(Z_L)}{Z_q} \qquad (3.39a)$$

$$L_2 = \frac{N\pi}{4K^2\omega_0^2 C_0}\frac{\mathrm{Im}(Z_L)}{Z_q} \qquad (3.39b)$$

From equations (3.39a) and (3.39b) we observe that knowledge of the load impedance gives all the information required to calculate the electrical impedance Z_e of the loaded QCM. Information from these components are used to interpret interfacial properties of the system such as adhesion and friction [3]. It is useful to write out expressions for changes in frequency and bandwidth in terms of Z_L as we will see later on. To do so we begin by writing the series resonant frequency f_s in terms of the acoustic and load components.

$$f_s = \frac{1}{2\pi\sqrt{(L_1 + L_2)C_0}} \qquad (3.40)$$

Changes in L_2 lead to changes in f_s thus the change in frequency Δf can be approximated as:

$$\Delta f = \frac{-L_2 f_0}{2L_1} \qquad (3.41)$$

I will now write out the expressions for the unloaded "acoustic" components L_1, C_1, and R_1 as shown by Martin et al [10].

$$L_1 = \frac{(N\pi)^2}{8K^2\omega_0^2 C_0} \qquad (3.42a)$$

$$C_1 = \frac{8K^2 C_0}{(N\pi^2)} \qquad (3.42b)$$

$$R_1 = \frac{(N\pi)^2}{8K^2 C_0}\frac{\eta_q}{\mu_q} \qquad (3.42c)$$

In equations (3.42a-c) the term η_q is the viscosity of quartz and the term C_0 varies from the term in figures 3.4 and 3.5 in that it does not take into consideration the "parasitic" capacitance from external sources and is purely the capacitance between the electrode plates such that $C_0 = \frac{\varepsilon_q A_0}{h_q}$ where ε_q is the permittivity of quartz, A_0 is the active region of the electrode, and h_q is the thickness of quartz. Substituting (3.39b) and (3.42a) into equation (3.41) we obtain the frequency shift in terms of the load impedance Z_L.

$$\Delta f = -\frac{f_0}{N\pi}\frac{\mathrm{Im}(Z_L)}{Z_q} \qquad (3.43)$$

where equation (3.43) represents the frequency shift for one side of the QCM.

3.5 LIQUID QCM EXPERIMENT

In some applications mass adsorption on the QCM is performed in liquid medium. When a QCM is submerged in a fluid it experiences additional changes in its amplitude and frequency that must be subtracted from the effects adsorption. The frequency shift from resonance of a QCM taken from air and submerged into a Newtonian liquid was derived in 1985 by Kanazawa and Gordon [11].

The liquid decay length for a critically damped shear wave originating from the QCM's oscillating surface and migrating into the contacting layer of a Newtonian liquid is given by the following equation [2].

$$\delta = \left(\frac{2\eta_l}{\omega_0 \rho_l} \right)^{1/2} \qquad (3.44)$$

where η_l is the viscosity of the surrounding liquid, ρ_l is the density of the surrounding liquid, and $\omega_0 = 2\pi f_0$ is the angular resonant frequency of the QCM. If we assume that the thickness of the liquid layer coupled to the motion of the QCM is δ/2, and apply the following substitutions (3.45) to the Sauerbrey equation (3.1)

$$\begin{aligned} &(\rho_l)\frac{\delta}{2} \rightarrow \left(\frac{m_f}{A} \right) \\ &\mu_q = \rho_q v_s^2 \end{aligned} \qquad (3.45)$$

we obtain the following expression:

$$\delta f = \frac{-f_0^{3/2}}{\rho_q v_s} \left(\frac{\rho_l \eta_l}{\pi} \right)^{1/2} = -f_0^{3/2} \left(\frac{\rho_l \eta_l}{\pi \rho_q \mu_q} \right)^{1/2} \qquad (3.46)$$

Equation (3.46) is known as the Kanazawa-Gordon relation where ρ_l and η_l are the density and viscosity of the surrounding liquid. The values in the denominator of equation (3.46) are intrinsic properties of AT- cut quartz density ρ_q=2.651 g/cm^3 and shear stiffness μ_q= 2.947×10^{11} dyn/cm^2. Equation (3.46) can also be found using the BVD circuit model described in the previous section. The velocity field from the QCM generated into a semi infinite Newtonian fluid is [2]

$$v_x(y) = v_{x0} \exp\left(\frac{(1+i)}{\delta} y \right). \qquad (3.47)$$

From (3.47) the shear stress σ_{xy} for this system is

$$\sigma_{xy} = -\eta \left. \frac{\partial v_x}{\partial y} \right|_{y=0} = \frac{\eta v_{x0}}{\delta}(1+j) \qquad (3.48)$$

using thickness equal to δ/2 and plugging $(48) \rightarrow (38) \rightarrow (43)$ we obtain the Kanazawa-Gordon equation (3.46).

3.6 THE FLANIGAN EXPERIMENT

Another example of how a QCM can be used to probe contact mechanics is an experiment performed by Flanigan et. al. in the year 2000. In this experiment they used a QCM in conjunction with an axisymmetric adhesion test apparatus to obtain calibrations between the frequency change of the crystal and the corresponding contact area of a viscoelastic gel cap pressed against the crystal surface [12]. Their analysis was a combination of the JKR contact mechanics model [13] along with the previously mentioned Kanazawa-Gordon and Sauerbrey equations. Their overall goal was to show how a QCM along with a displacement sensor can be used to measure adhesion energy according to the JKR contact mechanics model. They demonstrated how a QCM can be used to acquire contact area directly without monitoring the contact area between the gel and electrode surface [12]. They found a linear relationship between the QCMs resonant frequency and the gel/electrode contact area. This is true provided that the contact area is confined to the central portion of the QCM where the amplitude and sensitivity is largest [8].

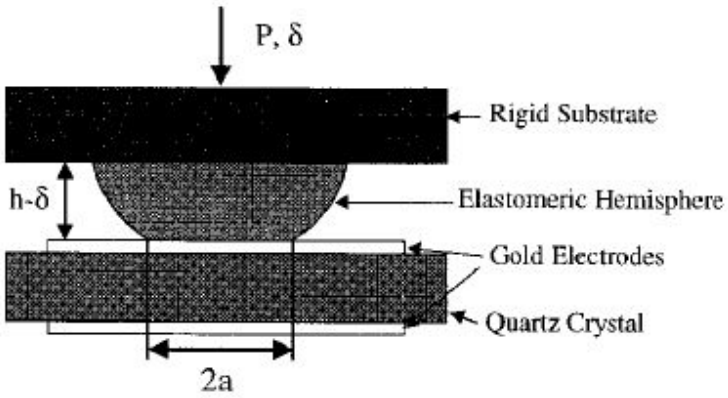

Figure 3.6 - Flanigan and associates experimental setup[12].

Substituting $\mu_q = \rho_q v_s^2$ into equation (3.1) we obtain the following expression for the Sauerbrey relation

$$\delta f = \frac{-2}{\sqrt{\rho_q \mu_q}} \left(\frac{m_f}{A} \right) f_0^2 . \qquad (3.49)$$

Similar to the Kanazawa-Gordon case a shear wave decay length must be found for their experimental set-up. The Kanazawa-Gordon equation assumes that the resonator is in direct contact with a Newtonian liquid which differs from the Flanigan experiment. In their experiment the QCM was in direct contact with a viscoelastic gel cap and as a result of this they had to calculate a decay length that was proportional to the shear modulus of the gel cap. The shear decay length for a plane wave emanating from the QCM and passing through a viscoelasic gel cap is

$$d = \frac{\left(|G| / \rho_g \right)^{1/2}}{\omega_0 \sin(\delta / 2)} . \qquad (3.50)$$

where ρ_g is the density of the gel cap, $|G|$ is the magnitude of the complex shear modulus of the gel, and the complex shear modulus is $G^* = G' + iG'' = |G|e^{i\delta}$. When $\delta = \pi/2 = 90^\circ$ is plugged into the complex shear modulus the entire contribution is from $G'' = \omega_0 \eta_g$ and equation (3.50) reduces to the decay length for a Newtonian liquid (3.44) where η_g is the viscosity of the gel but, for the case of $\delta = \pi/2 = 90^\circ$ it reduces to the viscosity of a Newtonian liquid. Substitution of $\frac{d(\delta = 90^\circ)}{2}\rho_g \rightarrow \left(\frac{m_f}{A}\right)$ in equation (3.49) results in (3.46) as expected from the previous section. Flanigan and coworkers applied this method for phase angles (δ) less than 90° to approximate the effects of viscoelasticity. Using equation (3.50) for d and applying $\frac{d(\delta < 90^\circ)}{2}\rho_g \rightarrow \left(\frac{m_f}{A}\right)$ in equation (3.49) gives:

$$\delta f = \frac{-f_0}{2\pi \sin(\delta/2)}\left(\frac{|G|\rho_g}{\rho_q \mu_q}\right)^{1/2}. \qquad (3.51)$$

The researchers realized that their work was not yet done since equation (3.51) assumes that the gel is in contact with the entire electrode. To address this issue they inserted a sensitivity factor into equation (3.51) and showed results for the two extreme cases.

$$\delta f = \frac{-f_0 K(A/A_0)}{2\pi \sin(\delta/2)}\left(\frac{|G|\rho_g}{\rho_q \mu_q}\right)^{1/2}\left(\frac{A}{A_0}\right). \qquad (3.52)$$

A in equation (3.52) is the "active area" or the area of the gel in direct contact with the QCM electrode. A_0 is the area of the entire electrode and $K(A/A_0)$ is the sensitivity factor. The first extreme case is $K(1) = 1$ which is in accordance with equation (3.51) the next extreme

case is where a very small amount of the gel is in contact with the electrode. This case was worked out by Lin et. al. [14] and the sensitivity factor is $K(0) \approx 2$. Plugging this result into (3.52) gives:

$$\frac{\delta f}{A} = \frac{-K_g |G|^{1/2}}{\sin(\delta/2)} \qquad (3.53)$$

where

$$K_g = \frac{-f_0}{\pi A_0}\left(\frac{\rho_g}{\rho_q \mu_q}\right)^{1/2} \qquad (3.54)$$

Equation (3.53) represents the slope of frequency shift from resonance plotted against the contact area of the gel cap. This theoretical model is supported by figure 3.7.

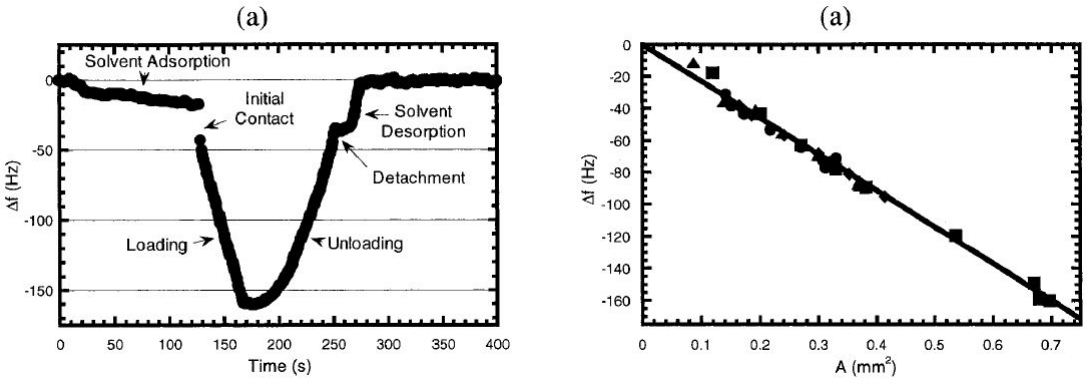

Figure 3.7 - Experimental results of Flanigan et. al. Plots show a linear relationship between frequency shift and contact area of the viscoelastic gel cap[12].

3.7 NEGATIVE SHIFTS, POSITIVE SHIFTS, AND CONTACT AREA

Figure 3.8 outlines the overall effect loading a QCM in a particular way has on the resonant frequency. One of three things happens to the resonant frequency of a QCM when an

object(s) interacts with its surface, the frequency either: decreases, increases, or remains the same.

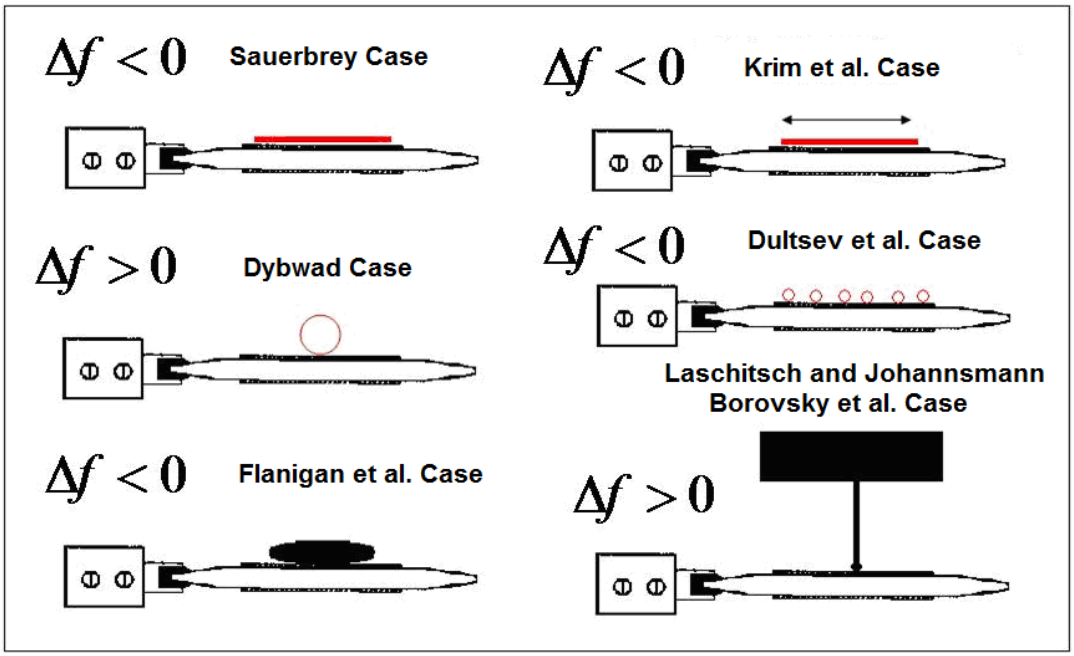

Figure 3.8 - A brief summary of QCM frequency shifts for varying load geometries.

From figure 3.8 we see that cases a, b, d, and e are geometries that result in a negative shift from resonance. Negative shifts in frequency are well understood when the QCM is modeled with plane waves. We first encountered this in Chapter 2 when working out the QCM's frequency dependence to the thickness of the cut. We assumed that "sound" moved through the QCM in a transverse shear mode as a plane wave, this was also the case for liquid loading (Kanazawa-Gordon) and viscoelastic materials (Flanigan). Generally speaking large contacts (uniform thin films and "soft" viscoelastic materials) result in negative shifts in frequency whereas small contacts result in positive shifts from resonance. A contact is considered small when the actual radius of the contact (r_c) is much smaller than the local

radius of contact (R) and the wavelength of sound (λ) [4]. When this is the case there is a stress concentration at the point of contact and it is assumed [15] that a spherical wave is emitted into the QCM that increases the "stiffness" ("k" value) of the oscillator. It is also possible for there to be no change in frequency, this is usually the case for purely elastic materials. In section 3.3 I rigorously worked out the result of Dybwad which shows the possibility of measuring a positive shift from resonance when a single particle is "lightly" coupled to the active area of the QCM. Dybwad's experiment is a classic example of how point contacts affect the resonant frequency of a QCM and his result can be replicated by using the BVD model discussed in section 3.7.

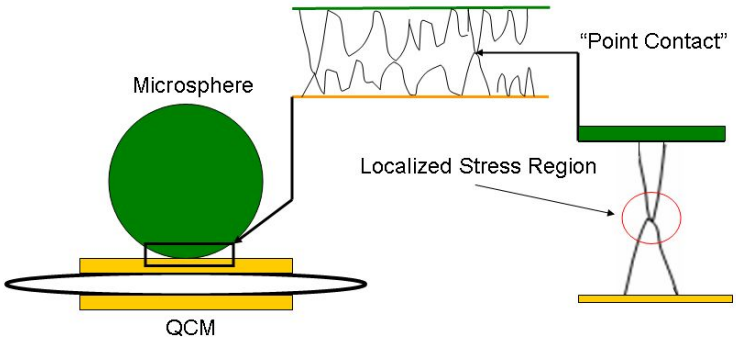

Figure 3.9 - Lightly coupled sphere on a QCM electrode. The buried contact is magnified to show that only a few regions or "asperities" are in actual contact. These contact asperities are highly localized stress regions.

Researchers Laschitsch and Johannsmann pointed out that if the size or radius r_c of the contact pictured in figure 3.9 is much smaller than the wavelength of sound λ then the wave transmitted into the sphere can be approximated as spherical[15]. Knowing the form of wave emitted into the sphere provides a starting point for evaluating the expected shift in frequency from this type of load geometry. Assuming that there is just one elastic modulus

for the sphere K and that transverse shear waves travel the same speed as longitudinal waves the position of the emitted spherical wave from the QCM electrode into the coupled sphere through a single asperity is:

$$u(r,t) = u_0 \frac{r_c}{r + r_c} \exp\left[i(\omega t - kr)\right] \qquad (3.55)$$

where r_c is the radius of the contacting asperity or the "true" contact radius, k is the wave number, u_0 is the amplitude, and r is the radial coordinate originating from the point of contact. The stress at the point of contact is approximated in equation (3.56) as

$$\sigma \approx K\nabla u\big|_{r=0} \approx K\frac{\partial u}{\partial r}\bigg|_{r=0} \approx \frac{Ku_0}{r_c}(1 + ikr_c). \qquad (3.56)$$

From equation (3.38) we find that the load impedance can be written as

$$Z_L = \frac{\sigma}{\partial u / \partial t}\bigg|_{r=0} = \frac{K}{\omega r_c}(kr_c - i) \qquad (3.57a)$$

$$Z_L = \frac{\sigma}{\partial u / \partial t}\bigg|_{r=0} = \frac{K}{\omega r_c}(kr_c - i) \approx \left(\frac{r_c^2}{r_e^2}\right)\frac{K}{\omega r_c}(kr_c - i) \qquad (3.57b)$$

where in equation (3.57b) a sensitivity factor $\frac{r_c^2}{r_e^2}$ is added to account for the finite nature of the contact. The term r_e in the sensitivity factor is active radius of the QCM electrode which for all practical purposes is the radius of the entire electrode. As previously mentioned this model assumes that the load the true contacting asperities experience is uniform throughout the apparent contact. Plugging this result into $\Delta f = -\frac{f_0}{\pi}\frac{\mathrm{Im}(Z_L)}{Z_q}$ (we have chosen the fundamental mode N=1 in equation (3.43)) gives

$$\Delta f = \frac{1}{r_e^2}\frac{f_0}{\pi Z_q \omega} K r_c \qquad (3.58)$$

We see that equation (3.58) is in agreement with Dybwad's result in that the shift in frequency is positive for small contacts ("light coupling"). To obtain information regarding the dissipation of this geometry we introduce a complex frequency shift.

$$\Delta f^* = \Delta f + i\Delta\Gamma \qquad (3.59)$$

where $\delta\Gamma$ is the shift in bandwidth (full width half max) and is directly proportional to energy dissipation D such that

$$D = \frac{2\Gamma}{f}. \qquad (3.60)$$

The components of (3.59) are

$$\Delta f = -\frac{f_0}{\pi}\frac{\mathrm{Im}(Z_L)}{Z_q} \qquad (3.61a)$$

$$\Delta\Gamma = \frac{f_0}{\pi}\frac{\mathrm{Re}(Z_L)}{Z_q} \qquad (3.61b)$$

Plugging (3.57b) into (3.61a-b) we obtain expressions for frequency shift (already solved for see (3.58)) and shift in bandwidth from a lightly loaded single sphere.

$$\Delta f = \frac{1}{r_e^2}\frac{f_0}{\pi Z_q \omega} K r_c \qquad (3.62a)$$

$$\Delta\Gamma = \frac{1}{r_e^2}\frac{f_0}{\pi Z_q \omega} k K r_c^2 \qquad (3.62b)$$

The frequency and bandwidth results from (3.62a-b) are referred to as the "small load" approximation (SLA)[4] and can be expanded to multiple load particles (spheres).

For completeness I will briefly mention the work of D'Amour et al who modified Dybwad's model to analyze the results from their study with glass microspheres and capillary aging[16].

To the Dybwad coupled oscillator model (section 3.3) they introduced a complex spring constant $\kappa^* = \kappa + i\omega\xi$ where κ is the elastic constant between the single sphere and QCM electrode and ξ is the drag coefficient that represents the energy dissipation from the QCM. They write the equation of motion as

$$m_s \frac{d^2 w}{dt^2} = -\kappa(w-u) - \xi \frac{d}{dt}(w-u) \qquad (3.63)$$

where $w = We^{i\omega t}$ and $u = Ue^{i\omega t}$ are the displacements of the sphere and QCM respectively and m_s is the mass of the loading sphere. Upon analyzing the forces at the contact and solving (3.63) the authors found the following expression for the complex frequency shift

$$\frac{\Delta f + i\Delta\Gamma}{f_0} = \frac{m_s \omega}{\pi Z_q} \frac{\omega^2 + i\omega\gamma}{(\omega^2 - \omega_s^2 - i\omega\gamma)}. \qquad (3.64)$$

In equation (3.64) $\omega_s = \sqrt{\frac{\kappa}{m_s}}$ and $\gamma = \xi / m_s$ are the resonant frequency and damping coefficient for the sphere. When $\omega << \omega_s$ the sphere is in phase with the QCM and effectively "clamped" onto the surface and therefore (3.64) reduces to the Sauerbrey relation $\Delta f = -f_0 m_s \omega / \pi Z_q$, this is a reasonable result since one can imagine that when an object is driven (relatively) slow that it will have no problem tracking the motion of the driver. This can be demonstrated easily by attaching a string to an object and very slowly driving it. In the opposing limit $\omega >> \omega_s$ (3.64) becomes

$$\Delta f = f_0 \frac{m_s}{\pi Z_q \omega} \omega_s{}^2 = \frac{f_0}{\pi Z_q \omega} \kappa \qquad (3.65a)$$

$$\Delta \Gamma = f_0 \frac{m_s}{\pi Z_q \omega} \omega \gamma = \frac{f_0}{\pi Z_q} \gamma \qquad (3.65b)$$

these equations are equivalent to the expressions worked out using the BVD model equations (3.62a-b) where $\kappa \propto Kr_c$. Equations (3.65a-b) are reasonable since they are in the limit where the loading particle is unable to track the extreme oscillation of the driver and therefore is not "detected" by the resonator. This condition is exactly that of light coupling (Dybwad) and leads to positive shifts in frequency. In figure 3.8 the geometry of an SFM (surface force microscopy) probe[15, 17] interacting with a QCM pictured in (f) is well described in the SLA approximation. In the next section I will review an article[18] that uses the SLA equations (3.62a-b) and (3.65a-b) as its main form of analysis. The geometry of this experiment is closely related to the work reported in this thesis. Another experiment closely related to the topic of this thesis is that of Dultsev et al[19]. This geometry is pictured in figure 3.8 (d) and labeled beside it is a negative shift in frequency. This shift was true for the experiment performed by the authors however, positive shifts have been observed as well for the geometry shown in figure 3.8 (d)[16, 18]. Geometries involving microspheres of varying sizes and distributions on a QCM have shown varied shifts in resonant frequency when initially placed on the QCM[6, 16, 18] which suggest that the initial conditions of the deposition procedure are important. We have seen from the various forms of the Dybwad model that the contact area and overall adhesion or (coupling constant) dictate which way the frequency will go once the particles are deposited. The variation in behavior suggest that differences in the environment (dry or wet) during the deposition procedure as well as the roughness of the

particles can have a major affect on the initial contact area and adhesion of the particles to the QCM surface.

3.8 REVIEW OF "STUDYING MECHANICAL MICROCONTACTS OF FINE PARTICLES WITH QUARTZ CRYSTAL MICROBALANCE" [32]

The aim of the research reported in this article was to analyze the adhesion of glass microspherical particles, in particular how the adhesion is affected by QCM experiments. The researchers studied three different particle diameters (5μm, 10μm, and 20μm) in order to vary the inertial and contact forces. The particles were deposited on a thin polystyrene (PS) layer that was spin coated on the surface of the electrode. Particle adhesion was increased by annealing the PS layer at $150^{\circ}C$ which formed a PS meniscus. Experiments were performed by tracking changes in the frequency and bandwidth of the QCM as the oscillation amplitude was increased. Initial runs were performed on QCM's with the PS layer alone to test the range of oscillation amplitudes allowed to perform the experiment. If the oscillation amplitude was too high the polystyrene film would decouple and slip (see section 3.2) on the surface which would distort the researcher's data. To prevent this they performed their experiments well below this limit. The entire process was observed via optical spectroscopy as shown in figure 3.10.

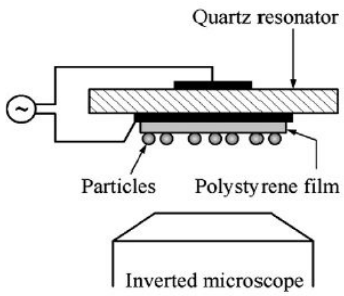

Figure 3.10 - Diagram of the experimental setup.

A semi-quantitative analysis was performed by applying the Dybwad model (3.64) to multiple contacts and using SLA equations (3.65a-b). Particles where placed in one of two categories “strong” or “weak” coupling. Strange behavior in their results was explained by the particles being in the intermediate coupling regime where behavior is hard to predict as shown by figure 3.11.

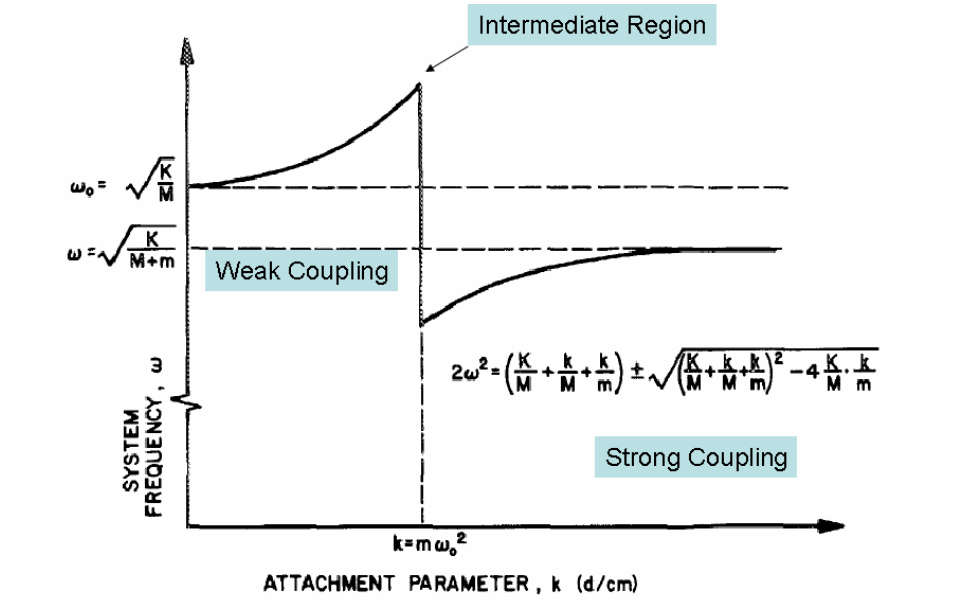

Figure 3.11 - System frequency ω as a function of attachment parameter k.[6]

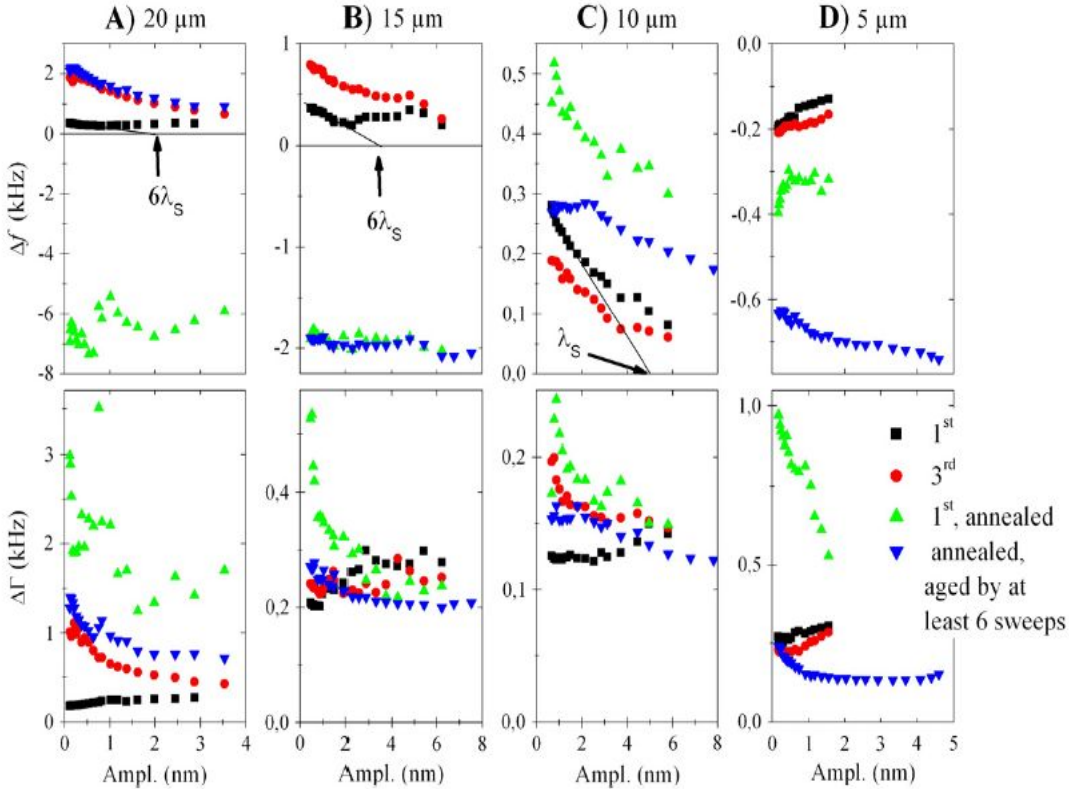

Figure 3.12 - selected QCM experimental results (Fig 6 taken from Ref.18). Drive voltage was increased to cause a corresponding increase in the oscillation amplitude of the QCM. Changes in frequency and bandwidth were tracked as the amplitude was increased. The effects of annealing were monitored in each experiment for the initial annealing and after a period of time (aged contacts). The experiment was performed for all size particles.

The black λ_s ("slip length") lines aligned with the zero on the Δf axis of figure 3.12 are scaling factors that take into consideration the partial slip ("Mindlin Slip")[20] spheres may experience before actually breaking contact with the surface. These partial slip lengths are written in terms of the normal load and coupling constant in the following way

$$\lambda_s = \frac{\mu_s F_\perp}{k}. \qquad (3.66)$$

In equation (3.66) μ_s is the coefficient of static friction and $F_\perp$ is the normal load where the authors assume the normal load or (adhesive force) of the spheres on the PS surface is caused purely from van der Waals interactions. For a PS-air-silica contact corresponding van der Waals force is

$$F_{vdw} = F_\perp = \frac{A_H R}{6D^2} \qquad (3.67)$$

where $A_H = 2\times10^{-20}$ J is the Hamaker constant for PS-air-silica, R is the radius of the particle, and D is the distance between the sphere and planar surface. The researchers found $F_{vdw} \approx 1.1\mu N$ for a 20 micron diameter particle. Using this value along with the data in figure 3.12 they calculated an average coupling constant k for a number of particles determined from optical spectroscopy. This coupling constant was calculated using the SLA applied to multiple spheres observed in the optical region. The addition of the "particle number density" $\left(N / A_Q\right)$ to the SLA gives the following result

$$\frac{\Delta f}{f_F} = \frac{f - f_0}{f_F} = \left(\frac{N}{A_Q}\right)\frac{1}{\pi Z_q}\frac{k}{\omega_0}. \qquad (3.68)$$

In equation (3.68) N is the number of particles and A_Q is the active area of the electrode. For the 20 micron diameter spheres data displayed in figure 3.12 the authors measured an increase in frequency of $\Delta f \approx 350 Hz$ which meant they were in the "weak" coupling regime. Using optical spectroscopy they estimated the number density $\left(N / A_Q\right)$ to be 30 particles/mm^2. Their experiments were performed using a 6 MHz QCM. Plugging

these values into equation (3.68) gave what they considered to be an extremely high value for the average coupling constant k which was equal to approximately 6000 N/m. They compared this result to an analysis using Hertz theory.

$$k = G^* a \qquad (3.69)$$

In equation (3.69) a is equal to the radius at the contact and G^* is equal to the effective modulus such that

$$\frac{1}{G^*} = \frac{1}{8}\left(\frac{2-\nu_1}{G_1} + \frac{2-\nu_2}{G_2} \right) \qquad (3.70)$$

where 1 and 2 represent the PS layer and the glass (silica) sphere respectively. In equation (3.70) G is a shear modulus and ν is Poisson's number. In equation (3.69) the contact radius is found using Hertz theory (neglecting roughness and assuming semi-infinite substrate) and is

$$a = \left(\frac{F_\perp R}{E^*} \right)^{1/3}. \qquad (3.71)$$

where

$$\frac{1}{E^*} = \frac{3}{4}\left(\frac{1-\nu_1^2}{E_1} + \frac{1-\nu_2^2}{E_2} \right) \qquad (3.72)$$

The reduced Youngs' modulus is E^* and the Youngs' modulus is E. Since glass spheres are much stiffer than the PS layer the terms E_2 and G_2 are approximately equal to infinity. Using $\nu_1 \approx 1/3$ the authors found a spring constant k=1000 N/m which is a factor of 6 smaller than their experimental value. The authors argue that discrepancies like the one above from theory (Hertz) and experimental results have been observed in the past by other

and these high k values may be explained (qualitatively) by the existence of multi asperity contacts.

3.8.1 - 20 MICRON SPHERE SUMMARY

Next the authors began with their interpretation of the results from figure 3.12. For the 20 micrometer spheres they observed an initial increase in frequency after deposition. After annealing the surface (increasing the contact area) they observed a decrease in frequency below resonance which they explained as the system crossing over from the weak coupling regime to the strong coupling regime in figure 3.9. Using the Sauerbrey equation and comparing it to optical microscopy they found that 80% of the spheres must be “tightly” bound to the surface. They however did mention that an alternate explanation was that the system could reside in the intermediate range of figure 3.11 with k slightly above the resonance value. The changed the surface properties by performing several (at least 6) sweeps on the annealed sample. They found that the frequency of the system jumped up to the starting values above resonance. They explained this by arguing the effects of annealing where nullified by the contacts breaking during successive sweeps which lowered the mean k value and brought the system back into the weak coupling regime.

3.8.2 - 15 MICRON SPHERE SUMMARY

Similar to the 20 micron spheres the authors observed an increase in frequency after initial deposition. After annealing the surface they also observed a decrease in frequency below resonance however, when they performed additional sweeps the frequency did not jump back to the weak coupling regime (above resonance) as it did with the 20 micron spheres in fact it did not change at all. They explained their results by stating that the

particles were so strongly attached to the surface that they did not decouple. They also suggested that since the particles were smaller than the 20 micron particles moving them would be more difficult because of the radial dependence of the peak force of the oscillation. They applied the Sauerbrey equation to these particles and found that their result was off by a factor of five. They attribute this error to the fact that the system for these size particles is in the intermediate coupling range of figure 3.9 where analysis is extremely difficult.

3.8.3 - 10 MICRON SPHERE SUMMARY

When the particles where initially deposited and increase in frequency was observed as with all previous cases. However, additionally runs after the deposition caused the frequency to decrease (still above resonance) which is not in agreement with the previous two particle sizes were the frequency further increased. After annealing the system frequency increased above the values measured previous to the annealing. This result also varied from the previous two cases where the frequency decreased upon annealing. The authors explain this behavior by stating that the annealing process was not enough to move the system into the strong coupling regime instead it only brought the mean k value closer to the resonance condition which would explain the observed increase.

3.8.4 - 5 MICRON SPHERE SUMMARY

When these particles were deposited on the QCM a negative shift in frequency was observed. The frequency did not change upon successive sweeps of the voltage. After annealing the sample the frequency further decreased and after aging set in and more sweeps were performed the frequency further decreased. The authors concluded that the spheres were in the strong coupling regime.

The authors concluded by making some general statements about consistent behavior found in all the experiments. One particular example was the bandwidth's dependence on QCM amplitude before and after the annealing process. Before annealing the authors found that the bandwidth increased with the amplitude which is in agreement with their Mindlin slip model (added dissipation from in place rocking). However, after annealing they observed a decrease in bandwidth with increasing amplitude which is not an obvious result. They argue that such a dependence could be explained by Coulomb friction. The authors do however state that measurements of bandwidth alone are not sufficient to understand the detailed mechanisms. The authors then briefly discuss optical data where surface damage was observed after QCM experiments in the PS layer. They used these images to estimate a particle velocity for the displaced sphere. They calculated the velocity in two different ways. The first way took into consideration only one component (v_x) of the velocity which yielded a higher value then the second method that added a vertical component to their calculation. In their concluding marks the authors summarized the results of their experiments by stating that observed shifts in frequency are understood as a balance between the coupling and inertial forces. Individual spheres have varying coupling constants (k) through out the active region of the QCM. As a result measured coupling constants are interpreted as average values over an approximate Gaussian distribution of spheres. A fully quantitative determination of forces between the particles and QCM doesn't seem possible since a measured shift in frequency can be the result of varying coupling constants.

3.9 USING A QCM TO DETERMINE THE FRICTION LAW OF LOADING PARTICLES

In 1993 researchers Sokoloff, Krim, and Widom pioneered a method[21] for determining the frictional force law of strongly coupled atomistic thin films on the surface of a QCM. The astonishing thing about this method is that it is independent of the samples actual friction law. This at first seems contradictory because in section 3.2 I discussed how a QCM probes "viscous" friction or friction that obeys Stoke's law

$$F_f = -\eta v^1 . \qquad (3.73)$$

Where F_f is the force of friction, η is the drag or "viscous" coefficient, and v is the velocity. This apparent contradiction is removed when using a more general frictional force law

$$F_f = -\eta |v|^n \operatorname{sgn}(v) \qquad (3.74)$$

where $|v|^n = |v_2 - v_1|^n$ is the magnitude of the relative velocity between the QCM velocity

$$v_1 = v_0 \cos(\omega t) \qquad (3.75)$$

(the term v_0 is the magnitude of the QCM velocity and ω resonant angular frequency of the QCM) and the strongly coupled slipping particles v_2. To account for the oscillating substrate of a QCM the term sgn(v) is added on to account for the constant sign change of the force. The term of interest in equation (3.74) is the power law n. The value of n determines the type of frictional force the adsorbed particles experience while slipping on the surface.

Displayed below are figures which show the dependence of frictional force to velocity for varying friction laws.

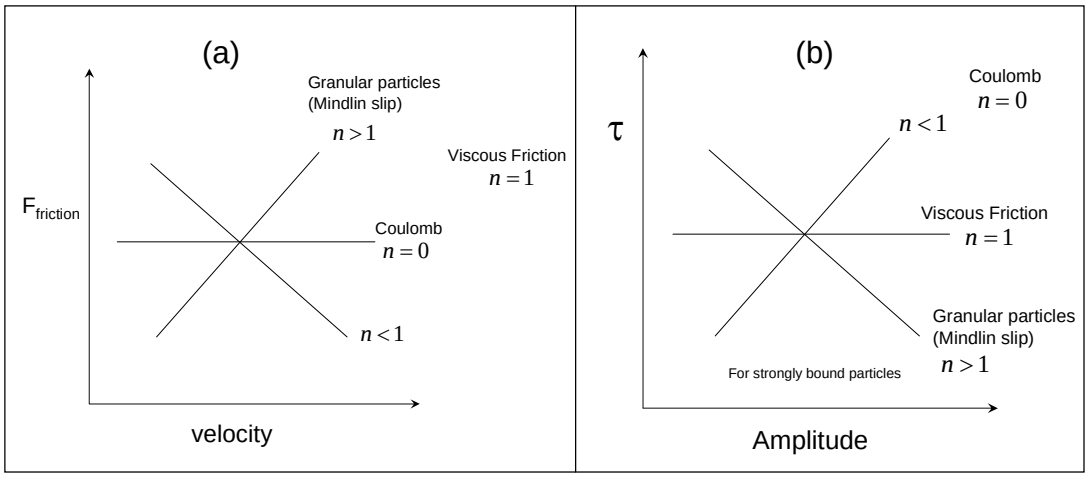

Figure 3.13 – 3.13a shows the velocity dependence of various frictional force laws (n). 3.13b shows the QCM amplitude (velocity) dependence of the slip times (calculated using n=1) of adsorbed particles (strongly coupled regime) on a QCM.

The slipping velocity of the adsorbed particles v_2 can be solved for exactly for the n=1 case of viscous friction. This is achieved by first rewriting (3.74) as

$$\dot{v}_2 + \frac{\eta}{m} v_2 = \frac{\eta}{m} v_0 \cos(\omega t) \qquad (3.76)$$

where m is the mass of the adsorbed particles. Equation (3.76) is a first order differential equation and is solved by multiplying both sides by the "integrating factor" $e^{\frac{\eta}{m}t}$ and integrating. Applying this to equation (3.76) gives

$$v_2 e^{\frac{\eta}{m}t} = \frac{\eta v_0}{m} \int e^{\frac{\eta}{m}t} \cos(\omega t) dt \,. \qquad (3.77)$$

Using integration by parts twice on the right hand side of (3.77) allows one to solve for the velocity which is

$$v_2 = (\omega^2 m^2 + \eta^2)^{-1}\left[\eta^2 v_0 \cos(\omega t) + \eta m v_0 \omega \sin(\omega t)\right]. \quad (3.78)$$

Using the result found from (3.78) along with the relation

$$v_1 = -A\omega\cos(\omega t) \quad (3.79)$$

where A is the amplitude of particle slippage, the relative slipping distance of the particles can be computed. Now returning to the original discussion, I stated earlier that the quantity of interest in our friction analysis is n, so the question that remains is how the QCM is used to measure this quantity. The methods discussed earlier in section 3.2 developed by Krim and Widom that particle slip times can be calculated from the shifts in QCM frequency Δf (3.20) and shifts in inverse quality factor $\Delta(1/Q)$ (3.19). The experiments reported in this thesis use (3.20) to compute slip time values. A main result of the Sokoloff et. al article[21] was the dependence of the inverse quality factor to the amplitude

$$Q^{-1} \approx A^{-(1-1/n)}. \quad (3.80)$$

Using (3.19) and (3.80) the particle slip time can be written in terms of the oscillation amplitude and force law "n"

$$\tau \sim A^{-(1-1/n)}. \quad (3.81)$$

Using equation (3.81) the force law "n" can be determined fro m the slope of the line created from a log-log plot ($\ln(\tau)$ vs. $\ln(A)$).

3.10 SLIDING FRICTION AND VELOCITY DEPENDENCE

As discussed in sections 3.2 and 3.10 a QCM can be used to probe sliding friction or to be more specific, systems that follow Stoke's law (3.73). In the previous section it was shown how a QCM could be used to probe a wide variety of friction laws using Stoke's law as a baseline. These friction laws are velocity dependent and can be interpreted in the same way as setting an object (the block shown in figure 3.14) at an initial velocity v_0 and observing the amount of time it takes for it to come to a complete stop.

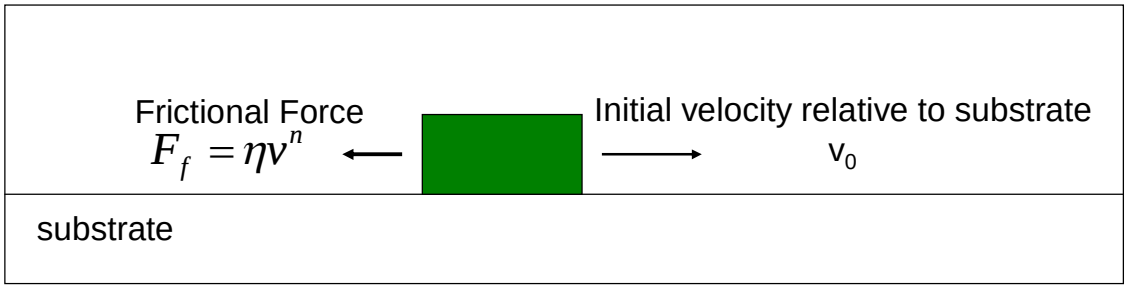

Figure 3.14 An illustration of an object set at an initial speed that is subject to a constant resistive damping force of friction that is velocity dependent. The object shown in this figure will eventually reach a final velocity of zero as a result of the damping force. The amount of time the object takes to reach this terminal velocity is dependent on the damping coefficient and the power law "n" of the damping force.

In order to visualize the time it takes for an object to reach its terminal velocity on a QCM I have created a theoretical plot (figure 3.16) that shows the decay of a particle's initial velocity over a period of time with the particle experiencing various velocity dependent damping forces. The plot shown in figure 3.16 was constructed by first finding the expression of the particle velocity as a function of time and then computing the characteristic slip time of a particle as derived using Stoke's law as a base line. In mathematical terms the velocity as a function of time or $v(t)$ was found by solving the following equation

$$F_f = m\dot{v} \qquad (3.82)$$

where

$$F_f \propto v^n . \qquad (3.83)$$

For the vast majority of "n" values equation (3.82) was in the form of a Bernoulli equation (first order differential equation) and could be readily solved. Expressions for slip time were computed using the following equation

$$F_f = -cons\tan t * v^n = -\frac{m}{\tau}v_0 . \qquad (3.84)$$

Results for a few sample values of n are displayed below in table 3.1.

Table 3.1 velocity and slip time values for various friction laws.

n	$v(t)$	τ
0	$v(t) = v_0 - \frac{\mu F_N}{m}t$	$\tau = \frac{mv_0}{\mu F_N}$
1	$v(t) = v_0 e^{-(b/m)t}$	$\tau = \frac{m}{b}$
2	$v(t) = \frac{v_0}{1 + \frac{cv_0}{m}t}$	$\tau = \frac{m}{cv_0}$
$-\frac{1}{2}$	$v(t) = \left(v_0^{3/2} - \frac{3d}{2m}t \right)^{2/3}$	$\tau = \frac{m}{d}v_0^{3/2}$

The slip time shown for the n=1 case or "Stoke's law" is independent of velocity which supports what was shown earlier in figure 3.13b. Table 3.1 along with additional values for n

were used to create the graph shown below in figure 3.15.

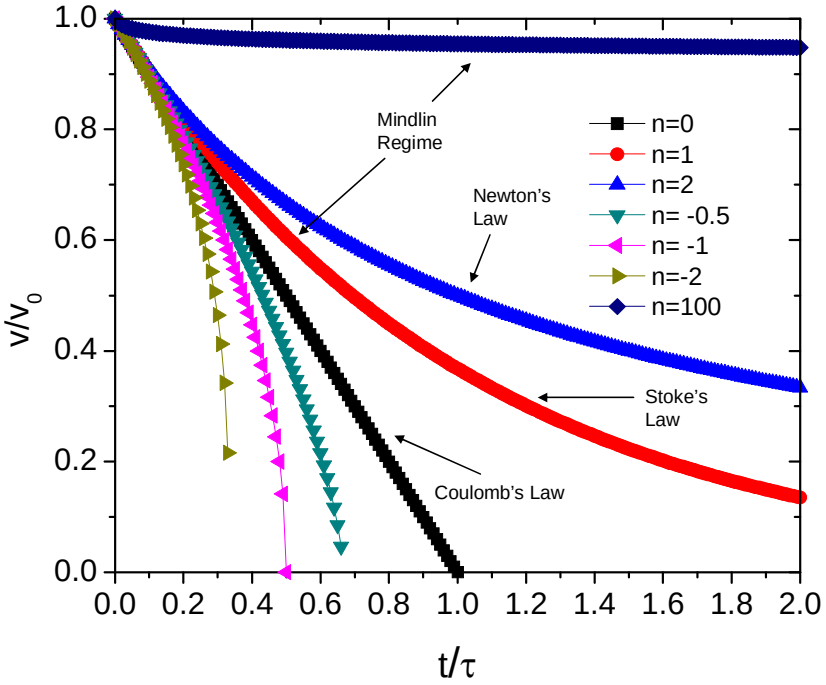

Figure 3.15 terminal velocity as a function of slip time for various friction laws.

Values of n above 1 in figure 3.15 are representative in granular systems are known to follow "Mindlin" friction behavior. The value of n=2 is known as Newton's law of friction, where as stated earlier n=1 is Stoke's law and n=0 is Coulomb's or Amonton's law of friction. From figure 3.15 it is shown that a system under going Coulomb friction reaches terminal velocity in a period of exactly one slip time. For negative values of n terminal velocity is reached before a complete slip time increment is reached. When n is larger than 0 terminal velocities are reached at values above a single slip time.

3.10 REFERENCES

1. Vogt, B. D.; Lin, E. K.; Wu, W.-l.; White, C. C., Effect of Film Thickness on the Validity of the Sauerbrey Equation for Hydrated Polyelectrolyte Films. *The Journal of Physical Chemistry B* 2004, *108* (34), 12685-12690.

2. White, F. M., *Viscous Fluid Flow*. McGraw-Hill New York, 1974.

3. Widom, A.; Krim, J., Q factors of quartz oscillator modes as a probe of submonolayer-film dynamics. *Physical Review B* 1986, *34* (2), 1403-1403.

4. Johannsmann, D., Viscoelastic, mechanical, and dielectric measurements on complex samples with the quartz crystal microbalance. *Physical Chemistry Chemical Physics* 2008, *10* (31), 4516-4516.

5. Stockbridge, C. D., *Vacuum Microbalance Techniques*. Plenum: New York, 1966; Vol. 5.

6. Dybwad, G. L., A sensitive new method for the determination of adhesive bonding between a particle and a substrate. *Journal of Applied Physics* 1985, *58* (7), 2789-2789.

7. Martin, S. J.; Frye, G. C.; Ricco, A. J.; Senturia, S. D., Effect of surface roughness on the response of thickness-shear mode resonators in liquids. *Analytical Chemistry* 1993, *65* (20), 2910-2922.

8. Seah, P. J. C. a. M. P., The quartz crystal microbalance; radial/polar dependence of mass sensitivity both on and off the electrodes. *Measurement Science and Technology* 1990, *1* (7), 544-555.

9. Ballato, A., FREQUENCY-TEMPERATURE-LOAD CAPACITANCE BEHAVIOR OF RESONATORS FOR TCXO APPLICATION. *IEEE Transactions on Sonics and Ultrasonics* 1978, *SU-25* (4), 185-191

10. Martin, S. J.; Granstaff, V. E.; Frye, G. C., Characterization of a quartz crystal microbalance with simultaneous mass and liquid loading. *Analytical Chemistry* 1991, *63* (20), 2272-2281.

11. Kanazawa, K. K.; Gordon, J. G., Frequency of a quartz microbalance in contact with liquid. *Analytical Chemistry* 1985, *57* (8), 1770-1771.

12. Flanigan, C. M.; Desai, M.; Shull, K. R., Contact Mechanics Studies with the Quartz Crystal Microbalance. *Langmuir* 2000, *16* (25), 9825-9829.

13. Johnson, K. L.; Kendall, K.; Roberts, A. D., Surface Energy and the Contact of Elastic Solids. *Proceedings of the Royal Society of London. A. Mathematical and Physical Sciences* 1971, *324* (1558), 301-313.

14. Lin, Z.; Hill, R. M.; Davis, H. T.; Ward, M. D., Determination of Wetting Velocities of Surfactant Superspreaders with the Quartz Crystal Microbalance. *Langmuir* 1994, *10* (11), 4060-4068.

15. Laschitsch, A.; Johannsmann, D., High frequency tribological investigations on quartz resonator surfaces. *Journal of Applied Physics* 1999, *85* (7), 3759-3759.

16. D'Amour, J. N.; Stålgren, J. J. R.; Kanazawa, K. K.; Frank, C. W.; Rodahl, M.; Johannsmann, D., Capillary Aging of the Contacts between Glass Spheres and a Quartz Resonator Surface. *Physical Review Letters* 2006, *96* (5), 058301-058301.

17. Borovsky, B.; Krim, J.; Syed Asif, S. A.; Wahl, K. J., Measuring nanomechanical properties of a dynamic contact using an indenter probe and quartz crystal microbalance. *Journal of Applied Physics* 2001, *90* (12), 6391-6391.

18. Vittorias, E.; Kappl, M.; Butt, H.-J.; Johannsmann, D., Studying mechanical microcontacts of fine particles with the quartz crystal microbalance. *Powder Technology* 2010, *203* (3), 489-502.

19. Dultsev, F. N.; Ostanin, V. P.; Klenerman, D., “Hearing” Bond Breakage. Measurement of Bond Rupture Forces Using a Quartz Crystal Microbalance. *Langmuir* 2000, *16* (11), 5036-5040.

20. Deresiewicz, R. D. M. a. H., Elastic spheres in contact under varying oblique forces. *Journal of Applied Mechanics* 1953, *20*, 327-344.

21. Sokoloff, J. B.; Krim, J.; Widom, A., Determination of an atomic-scale frictional force law through quartz-crystal microbalance measurements. *Physical Review B* **1993,** *48* (12), 9134-9134.

CHAPTER 4 - SPHERE ON FLAT CONTACT MECHANICS

4.1 INTRODUCTION

Understanding the fundamental nature of a contact is essential for any tribological study. The importance only increases as one enters the microscale, where the force of friction becomes extremely sensitive to both the nature of the contact and the area of contact. An essential geometry characteristic for the topic of this thesis is the analysis of a sphere interacting with a flat surface. This chapter will cover this geometry for both dry and humid (wet) environments.

4.2 DRY CONTACTS

Simply put, a dry contact is one in which the contact behavior or adhesion between the adjoining surfaces is purely dependent on the surface energies and loading forces of the two contacts in the absence of external influences such as capillaries forming at the rim of the contact as a result of a humid environment.

4.2.1 HERTZIAN CONTACT

One of the most basic and useful approximations for the contact area between a sphere and flat geometry was worked out by Hertz[1] in 1882. This geometry is displayed below in figure 1 where the contact radius, radius of the particle, and the distance resulting from elastic deformation is represented as a, R and z respectively. The Hertz model is used

to describe an elastic contact with the surface which suggests that the process of loading and unloading is a reversible process. The contact radius a Hertzian Contact predicts is

$$a = \left(\frac{3RL}{4E_c} \right)^{1/3} \qquad (4.1)$$

where $\frac{1}{E_c} = \frac{1-\upsilon_2^2}{E_1} + \frac{1-\nu_2^2}{E_2}$ is the elastic modulus of the two surfaces in contact, R is the radius of the sphere and L is the applied load. The "real" contact area associated with this contact geometry is

$$A = \pi a^2 = \pi \left(\frac{3RL}{4E_c} \right)^{2/3} \qquad (4.2)$$

If the loading force is known, then the pressure associated from a Hertzean contact can be calculated by dividing the loading force by (4.2)

$$P_m = \frac{1}{\pi} \left(\frac{4E_c}{3R} \right)^{2/3} L^{1/3} \qquad (4.3)$$

Equation (4.3) is an expression for the average (mean) pressure exerted at the contact area however the pressure is not uniform though out. The pressure distribution is given by

$$p = p_0 \left\{ 1 - \left(\frac{r}{a} \right)^2 \right\}^{1/2} \qquad (4.4)$$

The deformation distance associated with a Hertzean contact is

$$\Delta z = \frac{a^2}{R} = \left(\frac{9L^2}{16RE_c^2} \right)^{1/3} \qquad (4.5)$$

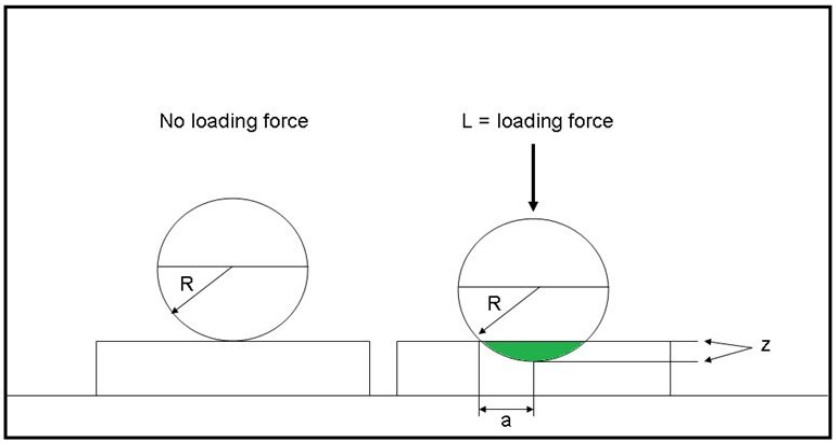

Figure 4.1 - Sphere flat geometry under elastic Hertzean contact.

The Herzian model is a first approach to estimating contact area, but does not incorporate the impact of adhesive forces on the size of the contact area.

4.2.3 THE DERJAGUIN APPROXIMATION

The Derjaguin approximation[2] is an extension of the Hertzian contact model that takes into account the effects of adhesive forces. It relates the force of adhesion F_{adh} (the main quantity of interest) between contacting surfaces to the interaction energy $W(D)$ associated with their bond. This useful approximation is based on the assumption that the radius of curvature between the two surfaces in contact is much greater than the separation distance D and the range at which the adhesive force acts. This assumption is generally applicable for the QCM experiments described in this thesis. The sphere on flat geometry, which is of great importance for this thesis, is derived from an expression for the force of adhesion between two contacting spheres given by[3]

$$F(D)_{sphere-sphere} = 2\pi\left(\frac{R_1 R_2}{R_1 + R_2}\right)W(D) \qquad (4.6)$$

where R_1, R_2, and $W(D)$ are the radius of curvature for the first sphere, radius of curvature for the second sphere, and the interaction energy per unit area as a function of separation distance D respectively. Equation (4.6) has relevance for the conditions in our experiments, in particular when microspheres adsorbed on the surface of our QCM are in direct contact and/or on top of each other. The sphere on flat geometry is the special case of equation (6) where $R_1 = R$ (the radius of the sphere) and $R_2 = \infty$ (the flat or in our case QCM electrode). Substituting these conditions into (4.6), one obtains:

$$F(D)_{sphere-flat} = 2\pi R W(D). \qquad (4.7)$$

When surfaces come in contact with each other, the force of adhesion between them is thus dependent on the corresponding surface energies between the interacting objects (sphere and flat). The interaction energy $W(D)$ is generally expressed as the surface energy γ_s which is an intrinsic property dependent on the materials intermolecular actions. When the sphere and flat are made from the same material $(\gamma_s = \gamma_1 = \gamma_2 \Rightarrow W_{12}(D) = 2\gamma_s)$ equation (4.7) reduces to

$$F_{adh} = 4\pi R \gamma_s \qquad (4.8)$$

Whenever the surfaces are comprised of different materials, $(\gamma_1 \neq \gamma_2)$, then the combined surface energy γ_s is approximated using the Good-Girifalco method[4]

$$\gamma_s = 2\phi\sqrt{\gamma_1 \gamma_2} \qquad (4.9)$$

The term ϕ is a correction factor usually in the range[5] of 0.5 to 1 to account for a the varying intermolecular interactions.

4.2.2 JKR MODEL

The Johnson–Kendall-Roberts[1] or (JKR) is an extension of the Hertz contact geometry described in section 4.2.1. In the Hertz model the contact between the two surfaces was assumed to be an elastic interaction with no energy lost from forming the contact. The JKR model takes into consideration inelastic (irreversible) interactions between the contact resulting from surface energy induced adhesive forces. The Hertz contact model only takes into consideration the compressive loads associated with elastic contact which in most real situation underestimates the real area of contact "a" shown in figure 1. To the Hertz pressure distribution (4.4) the JKR model adds an additional "tensile" term to the Hertz pressure that is compressive in nature. Equation (4.4) becomes

$$p(r) = p_0\left(1-\frac{r^2}{a^2}\right)^{1/2} + p_o'\left(1-\frac{r^2}{a^2}\right)^{-1/2} \qquad (4.10)$$

where p_0' is negative and represents the tensile stress component that is induced from the sphere adhering to the flat from surface energy. The form of equation (4.10) suggests that the closer r is to the center, the contribution is mainly a result of compression. However, as r moves closer to the edge of the contact, the pressure contribution is mainly tensile as indicated by $p(r)$ diverging when $r = a$. This divergence occurs because the JKR model assumes that the adhesion forces only act over the exact region in which contact is made. This is an artificial condition. The divergence can be removed[6] by substituting a real surface interaction such as Van der Waals in place of the artificial condition. The increased tensile energy causes the loaded sphere to elastically deform which causes the contact radius (a) to increase beyond the value predicted by the Hertz model (a_H). The JKR model includes a

contribution of a possible external loading force in addition to the load present from the surface energies (W_{12}) of the contacting objects (adhesion). The relationship between the contact radius and load is

$$\left(F_{ext} - \frac{4E_c a^3}{3R}\right)^2 = 8\pi W_{12} E_c a^3 \qquad (4.11)$$

where F_{ext} is the external loading force, a is the contact radius, W_{12} is the adhesion energy between the two surface, and E_c is the composite elastic modulus associated with the loading (deformed) sphere. When no external load ($F_{ext} = 0$) is present the contact radius under JKR theory becomes a constant value a_0 that has the form

$$a_0 = \left(\frac{9\pi W_{12} R^2}{E_c}\right)^{1/3}. \qquad (4.12)$$

In the presence of a loading force solving (4.11) for the contact radius gives

$$a^3 = \frac{3R}{4E_c}\left(F_{ext} + 3\pi R W_{12} + \sqrt{6\pi R W_{12} F_{ext} + \left(3\pi R W_{12}\right)^2}\right). \qquad (4.13)$$

The JKR model can be used to predict an adhesion force in the absence of an external load. This is done by equating the negative external loading force or "pull off force" to the elastic restoring force of the sphere at the point of separation this is adhesion force is

$$F_{adh} = \frac{3}{2}\pi W_{12} R \qquad (4.14)$$

The contact radius at separation a_s predicted by JKR is

$$a_s = \frac{a_0}{4^{1/3}}. \qquad (4.15)$$

The JKR model assumes perfectly smooth surfaces, which is clearly not the case for many applications. However, this model does prove useful for materials such as rubber[5] with low elastic modulus where the rough contacting asperities flatten out at the contact.

4.3 CONTACT MECHANICS IN WET ENVIRONMENTS

In many experimental situations (such as the experiments examined in this thesis) the JKR model can not be readily applied since the contacting asperities do not necessarily flatten out from adhesive forces to form a perfectly smooth surface. When contacts are unable to flatten out, separation gaps are present in between contacting asperities. These gaps easily become filled with a mobile fluid (such as water) in the nearby vicinity. The addition of this fluid has dramatic effects on the contact mechanics between interacting surfaces. Since the experiments performed in this thesis compare humid and dry conditions, we also examine the effect water has on the nature of the contact between the sphere and flat geometry.

4.3.1 CAPILLARY PRESSURE

The capillary pressure P_{cap} originally derived by Young and Laplace[7] in 1805 provides an expression for computing the pressure difference between arbitrary curved surfaces that are present when liquids such as water attempt minimize surface energy by forming a sphere.

$$P_{cap} = \gamma_l \left(\frac{1}{r_1} + \frac{1}{r_2} \right) \tag{4.16}$$

where γ_l, r_1, and r_2 are the surface tension of the liquid and the radius of curvatures shown in figure 4.2 respectively. The sign of r_1 and r_2 can be positive or negative depending on if the meniscus is bending outwardly (+) or inwardly (-). For the geometry shown in figure 4.2 which is a good representation of experiments described in this thesis equation (4.16) becomes

$$P_{cap} = \gamma\left(\frac{1}{r_2} - \frac{\cos\theta}{d/2}\right) \approx -\frac{2\gamma\cos\theta}{d}. \qquad (4.17)$$

The approximation is a result of the condition that $r_2 >> r_1$ which is usually the case for most situations. Equation (4.17) demonstrates the dependence of capillary pressure has on the separation distance between the sphere and the flat. This dependence is an important observation for the data recorded in this thesis.

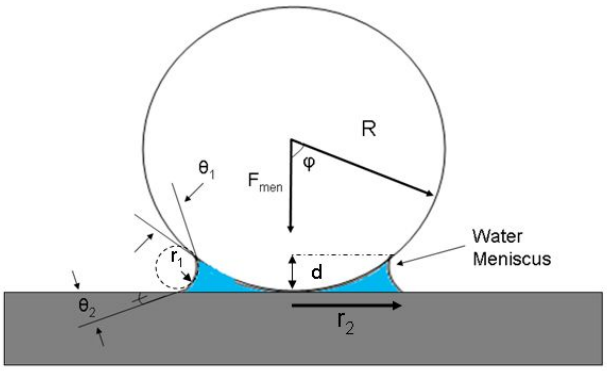

Figure 4.2 - Sphere on flat geometry in the presence of water

4.3.2 CAPILLARY CONDENSATION AND FORCES

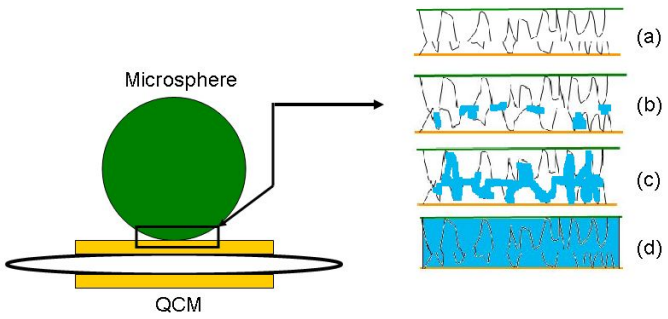

Figure 4.3 - Zoomed in image of a microsphere and QCM surface in contact at varying levels of humidity.

Figure 4.3 is a visual interpretation of how capillaries from water vapor may be distributed within the contact region of a sphere flat geometry. Since vapor pressure is curvature dependent, it is possible for water vapor to condense at these asperity contacts at lower vapor pressures then what is expected normally. This is the scenario illustrated from (a) to (b) where (a) is a perfectly dry contact and (b) represents early water condensation. As the humidity increases so does the amount of water trapped in the contacts (b). At some point of extremely high humidity the contacts become completely filled as illustrated in (d). The force of adhesion as a result of the presence of capillaries is a sum[5] of the tensile and compressive components of associated with the formation of a meniscus.

$$F_{men} = F_{ten} + F_{cap} \qquad (4.18)$$

where F_{men}, F_{ten}, and F_{cap} are the meniscus force, tensile of "tension" component of force, and the "compressive" force normal to the surface capillary. In most cases the tensile component

is much smaller than the contribution from the capillary interaction thus $F_{men} \approx F_{cap}$. The capillary force is directly proportional to the capillary pressure (4.17) such that $F_{cap} = P_{cap} \times A$ where A is area of the meniscus parallel to the surface. For cases where φ (figure 4.2) is small and the water wets both surfaces, the meniscus force becomes

$$F_{men} = F_{adh} \approx 4\pi R\gamma_l . \qquad (4.19)$$

This equation has the same form as equation (4.8) which approximated the adhesion force for a dry contact.

4.4 REFERENCES

1. Johnson, K. L.; Kendall, K.; Roberts, A. D., Surface Energy and the Contact of Elastic Solids. *Proceedings of the Royal Society of London. A. Mathematical and Physical Sciences* **1971,** *324* (1558), 301-313.

2. Derjaguin, B.,
Untersuchungen über die Reibung und Adhäsion, IV - Theorie des Anhaftens kleiner Teilchen. *Kolloid-Zeitschrift* **1934,** *69* (2), 155-164.

3. Israelachvili, J., *Intermolecular and Surface Forces*. Elsevier: (1985-2004); Vol. 2.

4. Girifalco, L. A. a. G., R. J., A theory for the estimation of surface and interfacial energies. . *Journal of Physical Chemistry* **1957,** *64*, 904-909.

5. Mate, C. M., *Tribology on the small scale a bottom up approach to friction,lubrication, and wear*. Oxford University Press: New York, 2008; Vol. 1, p 333.

6. Muller, V. M.; Derjaguin, B. V.; Toporov, Y. P., On two methods of calculation of the force of sticking of an elastic sphere to a rigid plane. *Colloids and Surfaces* **1983,** *7* (3), 251-259.

7. Adamson, A. W. a. G., A.P., *Physical Chemistry of Surfaces*. Wiley: New York, 1997.

CHAPTER 5: FRICTION ANALYSIS OF 5 MICRON POLYSTYRENE SPHERES DEPOSITED FROM AQUEOUS SOLUTION ON A QUARTZ CRYSTAL MICROBALANCE

I. Lynch, J. McNutt*, and J. Krim

Department of Physics North Carolina State University

*Department of Physics University North Carolina Asheville

In this study we have employed a Quartz Crystal Microbalance (QCM) in conjunction with optical techniques to analyze the frictions and adhesion of 5μm diameter polystyrene spheres physisorbed on an oscillating QCM electrode. Upon placing the particles on the surface, we observe a negative shift in frequency, indicating that the particles are in a strong coupling regime of adhesion[1]. In this regime, the Sauerbrey equation should be sufficient to estimate the mass loading of the microspheres. An optical count of the microspheres on the electrode confirmed this assumption, if corrections for slipping are taken into account. Optical observations also reveal that the particle motion depends on the oscillation direction and surface topology of the QCM. To explore the nature of the decoupling (small amplitude in-place oscillatory motion, rupture and reattachment, rupture and complete particle removal, etc) the QCM frequency response was monitored while the drive level was increased and decreased. The resulting "decoupling curve" is reflective of the nature of the particle adhesion to the QCM surface as well as the friction law governing it. For the case of particles "slipping in place" it is possible to calculate an average slip time τ associated with the QCMs frequency response to the effective decrease in massloading. We found that the slip time values are of the same order as slip times previously recorded in the literature [2] for

physisorbed sytems, including water. After an initial drying and run-in period, the particles exhibit frictional behavior that is nearly independent of vibrational amplitude, as would be the case for a system strictly governed by a viscous friction law. The behavior may arise from the presence of physisorbed water at the interface, which is ubiquitous in air.

5.1 INTRODUCTION

The notion of transporting micro/nano objects has been of interest to the scientific community since the early days of nanotechnology. Progress in this area requires an understanding of the frictional behavior of these objects when they are in motion. Transport and manipulation of nano and micro devices is a necessary application of both nano/micro technology that is as intriguing as it is complex. Obtaining this control can lead to many exciting advancements that span from drug delivery in nanobiotechnology[3], micro particle sorting and grouping by mass[4], particle monitoring for toxicological studies as well and many more favorable applications that span multiple disciplines. However, before these applications can become a reality several questions must be addressed. What forces contribute to the friction between the device and surface? How strong are these forces? Can they be manipulated and if so how? At the micro/nano scale it has been observed in the literature [5] that particle dynamics are dramatically different than what is seen for the macro or meso length scales. This is due to the fact that intermolecular and capillary forces become increasingly important at these length scales.

We focus here on polystyrene microspheres, which are of growing interest due to their medical and textile applications. In particular microencapsulation of phase change materials (PCMs) using polystyrene microspheres, has potential applications toward medical

hot/cold therapy as well as manufacturing clothing to handle extreme weather conditions.[6] Dultsev and coworkers, in a pioneering 2000 publication [4], suggested that quartz crystal microbalances (QCM's) could have wide spread potential applications for separation, sorting, and sizing. In their experiment polystyrene microspheres were attached to the oscillating surface of a QCM by multiple interactions and detachment of the spheres from the QCM was achieved by varying the driving voltage of the QCM. The sample was oriented horizontally with the spheres deposited on the top side of the electrode. The detachment was inferred by measuring the "sound" the spheres emit upon detaching with respect to the voltage at which the crystal was being driven.

The experimenters also measured the change in the resonant frequency of the QCM as a function of the driving voltage. They attributed the changes in frequency of the QCM to be a result of the spheres detaching from the surface and eventually rolling off the edge of the QCM causing the mass to decrease which results in a frequency change in the QCM. This explanation is theoretically sound however, a similar shift in frequency can be observed when a portion of spheres no longer track the motion of the resonator as a result of surface decoupling from slipping, sliding, and/or rocking in place in a bound region. Sokoloff[7] explored this possibility, by theoretically examining the form of a QCM response to sliding adsorbed layers whose friction laws were of the form:

$$\vec{F}_{friction} = -\frac{m_{film}}{\tau}\vec{v}^{\,n} \qquad (5.1)$$

where m_{film} is the mass of the film, v is the sliding velocity, and τ is a slip time characteristic of the particle-substrate friction[2]. For the case of tightly bound films, Sokoloff reported that

slip time measurements recorded as a function of the amplitude of vibration of the QCM would reveal the form of the friction law, according to:

$$\partial(Q^{-1}) \propto \tau \approx A^{-(1-1/n)} \qquad (5.2)$$

We report here measurements of sliding friction analysis, and images to document the nature of decoupling observed. In our experiment the particles in our optical region did not roll off the surface. However, for a small percentage of the particles in the optical region motion was observed. The observed motion was dependent on the oscillation direction and surface topology of the QCM. Before we address the details of our experiment we will begin with a review of prior work outlining QCM response due to various load configurations.

We found that the slip time values are of the same order as slip times previously recorded in the literature [2] for physisorbed sytems, including water. After an initial drying and run-in period, the particles exhibit frictional behavior that is nearly independent of vibrational amplitude, as would be the case for a system strictly governed by a viscous friction law. The behavior may arise from the presence of physisorbed water at the interface, which is ubiquitous in air.

5.2 QCM RESPONSE TO LOAD CONFIGURATION AND BEHAVIOR

In what follows we will discuss the results of previous QCM experiments in which depending on the nature of the experiment, the QCM experiences a shift either in the positive or negative direction from natural resonance. First we will discuss is the Sauerbrey case which deals with molecularly thin films that are rigidly attached to the QCM (figure 1a). In 1959 Sauerbrey [8] showed that the mass absorbed on the electrode of a QCM is directly proportional to the measured frequency shift (5.3).

$$\delta f_{film} = -2\frac{(m_{film}/A)}{\rho_q v_q} f_0^2 \qquad (5.3)$$

where m_{film} is the mass of a loading film rigidly attached to the motion of the QCM, A is the area of the electrode, ρ_q is the density of quartz, v_q is the velocity of sound through quartz, and f_0 is the resonant frequency of the QCM**.** This equation corresponds to negative shifts in frequency and works well when the loading mass is rigidly attached to the QCM's motion. Next we will discuss what we denote as the Krim et. al. case[9]. This case describes the frequency response of a QCM coated with a molecularly thin film whose bond with the surface is strong, but not completely attached to the QCM's motion as a result of surface slippage (figure 5.1b). The sliding film is assumed to obey the viscous friction law which means the force of friction is velocity dependent (no static friction) as shown in the following equation.

$$\vec{F}_{friction} = -\frac{m_{film}}{\tau}\vec{v} \qquad (5.4)$$

In this equation τ represents the slip time of the film which by definition is the time it takes for the film sliding velocity to diminish to 1/e of its original value and $\vec{v}$ represents the average film sliding speed. The frequency response to this type of behavior is described by equation (5.5) below

$$\delta f_{measured} = \frac{\delta f_{film}}{1 + (\omega\tau)^2} \qquad (5.5)$$

where ω is the angular resonant frequency of the crystal. When there is no film slippage ($\tau = 0$) (5.3) reduces to (5.1). The Krim et. al. case along with the previously mentioned Sauerbrey case result in a negative shift from resonance of the unloaded QCM frequency.

The difference is that the shift for the Krim et. al. case is smaller by a factor of $\frac{1}{1+(\omega\tau)^2}$ which is shown in (5.5). The next case we will discuss (figure 5.1c) gives rise to a positive shift in QCM frequency, this is the Dybwad case[10]. In this experiment large (compared to the two previous cases which were on atomistic length scales) spherical gold particle between 10-50 μm were loosely attached to the surface of a QCM and the resulting frequency shift from resonance was positive. Dybwad constructed a coupled oscillator model that accurately predicted the observed behavior. This model has since been modified by the addition of a complex spring constant to extract additional information concerning the added dissipation to the QCM upon interaction with surface particles[1, 11]. According to the Dybwad model a QCM's frequency shift is dependent on the bond strength between the load particle(s) and QCM surface. It is difficult to employ the Dybwad model to predict the response of a QCM as a result of bond strength when the data lies near the transition from positive to negative shifts[12].

The next case which we denote as the Laschitsch and Johannsmann/Borovsky et. al. case[13] (figure 1d) deals with the QCM's response to point or "asperity" contacts. To simulate this geometry they pressed a probe tip into the surface of the QCM, which resulted in an increase in the QCM's frequency proportional to the contact area between the tip and electrode surface. This increase was interpreted as an added stiffness to the QCM resulting from spherical waves emitted from the probe point contact. The observation of a positive frequency shift is not limited the single sphere geometry of the Dybwad experiment nor the

previously mentioned probe tip geometry but, can easily be realized using sub-monolayer and monolayer coverages.

For example, in an experiment performed to study the effects of capillary adhesion to glass microspheres (45-700 μm) deposited on the surface of a QCM with a gold electrode[11]. The researchers observed a positive shift from resonance when a monolayer of spheres was deposited, that further increased once the bonds where tightened due to capillary forces further stiffing the surface. This observation agrees with the combined results of the Dybwad and the Laschitsch and Johannsmann/Borovsky et. al. cases. The last configuration we will discuss is the Flanigan et. al. case (figure 5.1e) and it results in a negative shift in QCM frequency. When a viscoelastic medium such as a gel cap is placed on the surface of a QCM the resulting shift in frequency is negative.

In contrast to the previous case, Flanigan et al. found that by increasing the contact area between the gel cap and QCM surface the frequency decreased approximately in direct proportion[14]. Combining the Flanigan and Johannsmann/Borovsky et. al. cases gives implications about the effect a melting surface would have on the frequency of a QCM. Currently experiments[15] are being conducted where an STM tip is in contact with an oscillating QCM coated with a thin film. It has been shown[15] that frictional heat generated from the STM/QCM interaction can cause a detectable phase change in the thin film. This phase change can be monitored by recording the changes in QCM frequency.

When the STM tip is initially in contact with the QCM the Laschitsch and Johannsmann/Borovsky case applies and one observes a positive shift in frequency. However, when the film undergoes a solid to liquid phase change the resulting shift in

frequency is negative and is best explained using the Flanigan et. al. case. In summary a QCM experiences a negative shift from the Sauerbrey case which describes the affect a rigidly attached film has on the natural frequency a QCM. The next case is the Krim et. al. which results in a negative shift from resonance that is smaller then the shift from the Sauerbrey case due to surface decoupling and slippage effects. We employ the latter approach here to infer particle slip times, as we are able to infer mass loading from both an optical count of the particles, and from the frequency shift associated with mass loading.

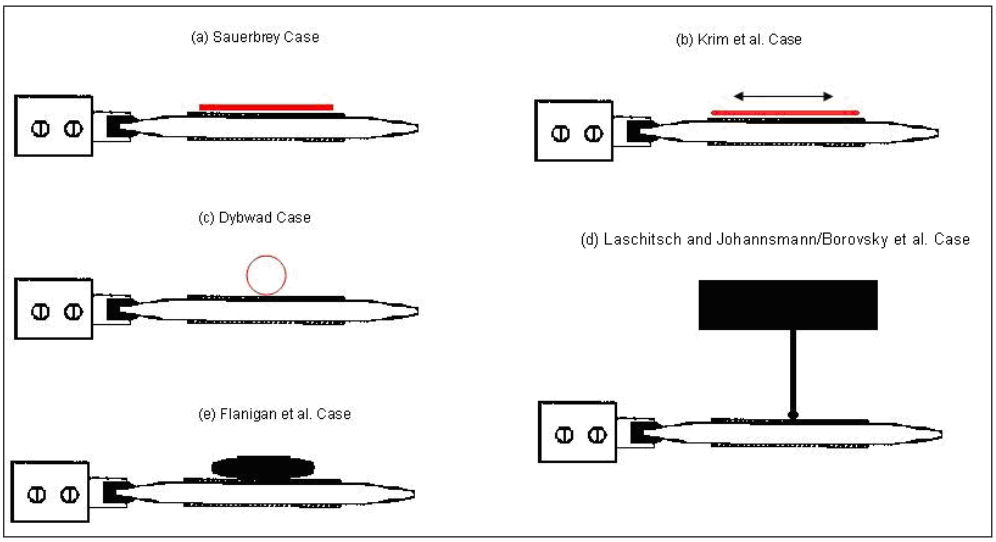

Figure 5.1 - Depiction of previously studied load geometries of QCM experiments.

5.3 EXPERIMENTAL SETUP

In our experiment we depositied a sub monolayer (1-10%) of polystyrene microspherical particles on the top electrode of a QCM. We initially observed a negative shift in resonant frequency which suggested that the particles where in the strong coupling regime according to the small load approximation [16] and agreed with Sauerbrey's prediction. . We suspected that as a result of the oscillatory nature of the QCM it was possible that a

fraction of the spheres deposited on the surface could be loosely attached or "decoupled" and as a result increase the initial negative frequency shift caused by the majority particles that were rigidly attached to the surface. To test this we increased the drive voltage of our QCM and recorded the frequency response against crystal amplitude. We then decreased the drive voltage to its starting value to track the frequency response in both directions. We assigned the name "decoupling curve" to this particular measurement. This type of measurement has been performed before in the literature in the forward direction alone.[4, 12]We believed that by steadily increasing the drive voltage of the QCM we would create more decoupling events which would be sensed by the crystal and recorded as a relative increase in frequency. When decreasing the drive voltage back to the original value we observed some interesting hysteresis behavior. This hysteresis raised further questions about the actual dynamics and behavior of the particles on the surface. Our main goal for this experiment was to obtain information regarding the frictional force at this micron scale which is currently not well understood[11]. Interestingly enough probing friction at the atomistic scale is a much easier feat when implementing techniques developed by the Krim group[9, 17]. As mentioned in the previous section when a thin uniform film deposited on the electrode of a QCM begins to slip as a result of the oscillatory motion, frictional properties (in particular the slip time) can be probed from changes in both the quality factor Q and resonate frequency of the QCM. Current analytical models (Sauerbrey[8], Kanazawa-Gordon[18], and Krim group[9, 17]) describe properties of uniformly distributed thin films on a QCM. However, our experiments do not fit the conditions of these models. Spring models such as the Dybwad and Johannsmann/Borovsky et. al. cases are the most appropriate to describe surface behavior in

our experiments. When analyzed with a spring interpretation decoupling curves in principle describe changes in coupling and stiffness between the particles and surface as the amplitude of oscillation is increased and then decreased to the original value. This information can be used to infer surface dynamics as the amplitude of oscillation is swept forward and backward. Since we are not aware of any existing model that can accurately describe frictional behavior for our experimental configuration, we used the previously mentioned methods developed by the Krim group that describes sliding molecularly thin films as our baseline theory for this undeveloped configuration to calculate particle slip times during initial deposition and the forward sweep of our decoupling curve. This method assumes that the microspheres obey a velocity dependent friction law which may or may not be the case for the microscale.

5.4 METHODS AND MATERIALS

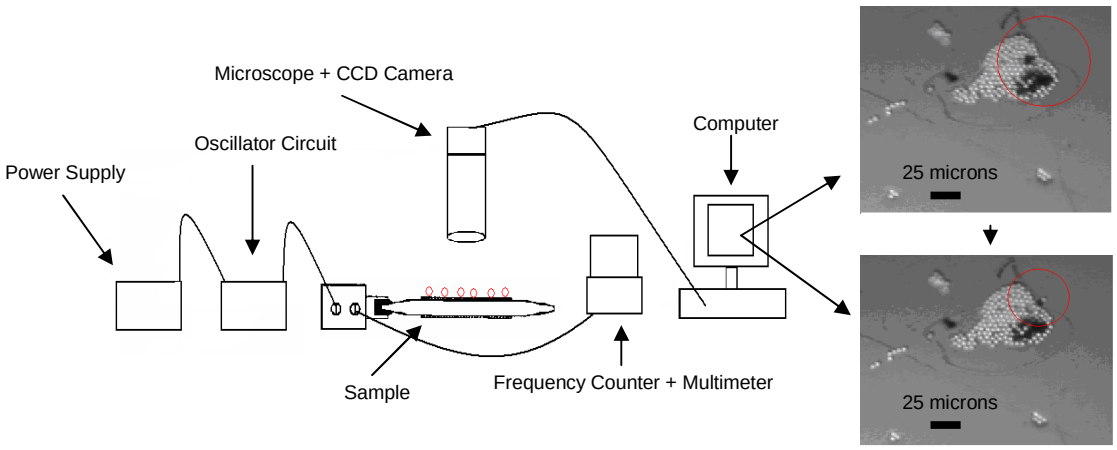

Figure 5.2 - Sketch of experimental apparatus.

Our QCM's (Laptech Precision, Inc.) were AT cut at 35˚ and the diameter was 0.375 inches with a 0.01 inch flat on the –x axis and were used directly out of the package. The

crystals oscillated with a fundamental mode of 8 MHz and had an optical polished finish. The electrode was keyhole design with a diameter of 0.250 inches and it was made from gold deposited atop a thin chrome layer. The QCM was driven by a Pierce oscillator circuit whose output signal was mixed using a 0.5 to 500 MHz frequency mixer (Mini-Circuits®) with a reference signal supplied by an 8 MHz can crystal (Crystek, Inc.) oscillator driven by a different Pierce oscillator circuit. The mixed output ran through a low pass filter and was detected using a Hewlett Packard 5384A frequency counter. The crystal amplitude was measured using a Keithley 2000 multimeter. Each pierce oscillator circuit was powered by an Elenco Precision model XP-15 regulated variable power supply. We applied 5 μm diameter polystyrene microspheres from aqueous solution (Bangs Laboratories, Inc.) to the center of the electrode where maximum amplitude occurs on one side of the QCM covering approximately 1-10% of the electrode. The surface was then dried with helium flow and the sample was left over night to air dry. Particle motion was analyzed using an Edmund optics Proximity Series Infinitube microscope with a Mitutoyo 10X/0.28 lens illuminated by an Edmund Industrial Optics model 21AC illuminator. Attached to the microscope was a B/W CCD camera (Industrial Vision Source) whose video output was sent to the computer program Flash Point 3D and a Toshiba DVD recorder to record movies of particle motion during experiments.

5.5 RESULTS AND DISCUSSION

Using the Krim et. al. methods as a baseline theory we estimated the slip time of the decoupled spheres on the QCM surface with the following equation. Solving equation (5.3) for τ gives

$$\tau = \frac{1}{\omega}\sqrt{\frac{\Delta f_{massloading}}{\Delta f_{film}} - 1} \qquad (5.4)$$

which shows that the slip time of the particles is proportional to the frequency shift of the QCM due solely to particle loading. Here the frequency shift of the film represents the shift in frequency from decoupled spheres when the amplitude of oscillation is increased. We understood that it was possible that a fraction of spheres may have been decoupled during the initial oscillation of the crystal which would lead to an underestimated value for the frequency shift due to mass loading. To correct for this we scanned and imaged the entire electrode surface and counted the individual spheres on each image. We took this value and compared it to the amount of spheres predicted by applying the Sauerbrey equation from the extended Dybwad model (for one side of the QCM) to our initial frequency shift. The difference in these values corresponded to the amount of decoupled spheres. Applying the Sauerbrey equation once more we calculated the amount of frequency shift the decoupled spheres would cause if they were not decoupled. We then added this value to the initial measured frequency shift to obtain an estimated value for the true mass loading frequency shift. The modified Sauerbrey equation [1, 11] (equivalent to equation (5.1)) is written as

$$\Delta f_{massloading} = -N\frac{m_s \omega}{\pi Z_q} f_0 \qquad (5.5)$$

where N is the number per unit area of microspheres, m_s is the mass of a single microsphere, $Z_q = \rho_q v_q = 8.8\times10^6 kgm^{-2}s^{-1}$ is the impedance of quartz, and $\omega = 2\pi f_0$ is the angular frequency of the unloaded QCM. On the electrode surface we counted a total of 6,353 spheres.

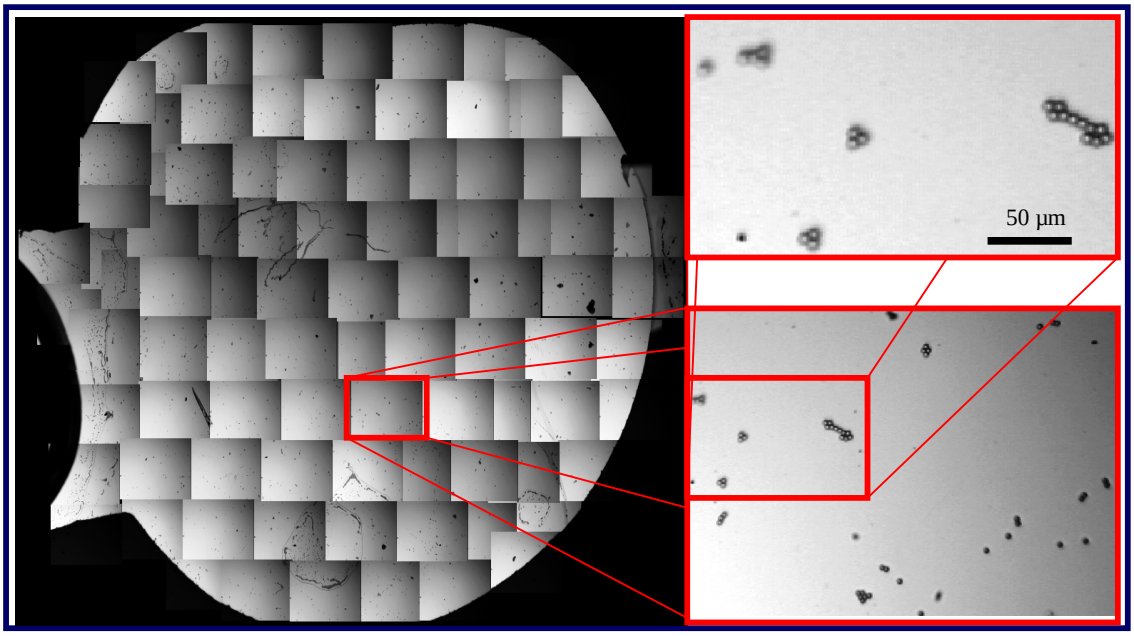

Figure 5.3 - The image above is a reconstruction of the QCM used in which the initial slip time was estimated by counting the spheres on the electrode surface before first oscillation. Each tile is an image with the dimensions of our optical region when adjusting the resolution to illuminate the spheres on the surface. Scratches were intentionally placed on the surface to provide a reference point when analyzing the distance from one image to another when spheres move on the surface.

After depositing the spheres we observed a negative initial mass loading frequency shift of 207 ± 0.1 Hz. We calculated from equation (5.5) that this corresponded to a total of 6140 ± 4 spheres a value less than what was initially counted on the surface. Taking the difference of the observed and predicted sphere values we estimated that a total of 213 ± 4 spheres initially decoupled from the surface at the lowest drive voltage. The decoupled spheres amounted to about 3% of the total electrode coverage. Applying equation (5.5) once more we found that if stationary (not decoupled) these spheres would cause the QCM frequency to shift by approximately 7 ± 0.1 Hz. Adding this to our original 207 Hz shift we obtained an estimated true mass loading frequency shift of 214 ± 0.2 Hz. We then calculated the slip times of the

decoupled particles by applying equation (5.4) to the forward sweep of the initial decoupling curve using our corrected mass loading frequency shift as a baseline. Our results are displayed in the following table.

Table 5.1 - Calculated slip times from forward decoupling curve run.

Drive Voltage(V)	Crystal Amplitude (mV)	Frequency Shift of Film(Hz)	Slip Time (ns)
8.53	64.8	207	3.7 ± 0.06
9.58	74.9	199	5.5 ± 0.06
10.5	81.6	195	6.2 ± 0.07
11.57	89	186	7.7 ± 0.07
12.56	95.7	183	8.2 ± 0.07
13.53	100.9	179	8.8 ± 0.07
14.57	105.1	176	9.2 ± 0.07
15.57	108.1	170	10.1 ± 0.08

Given the slip times calculated in table 1 we were interested to see what the approximate amplitude of sphere slippage was relative to the substrate. Keeping with our assumption of a linear velocity dependent viscous friction law (5.2) we use the equation of motion derived by Sokoloff et al [7] (5.6) of the velocity of a slipping film (in our case microspheres) as a function of the relative velocity between the moving QCM substrate and slipping film.

$$m\dot{v}_2 = -\gamma|v_2 - v_1|\,\mathrm{sgn}(v_2 - v_1) \qquad (5.6)$$

Where $\gamma = m_s / \tau$ is the damping coefficient from (5.2), v_2 is the velocity of the slipping film, and $v_1 = v_0 \cos(\omega t)$ is the velocity of the QCM at a given amplitude. Equation (5.6) can be solved exactly for v_2

$$v_2 = (\omega^2 m^2 + \gamma^2)^{-1}\left[\gamma^2 v_0 \cos(\omega t) + \gamma m v_0 \omega \sin(\omega t)\right]. \qquad (5.7)$$

Using vector addition on v_1 and equation (5.7) we solved for the relative velocity between the sphere and substrate. From the angular frequency and the calculated relative velocity we obtained results for the approximate relative amplitude of particle slippage as shown in figure 5.4.

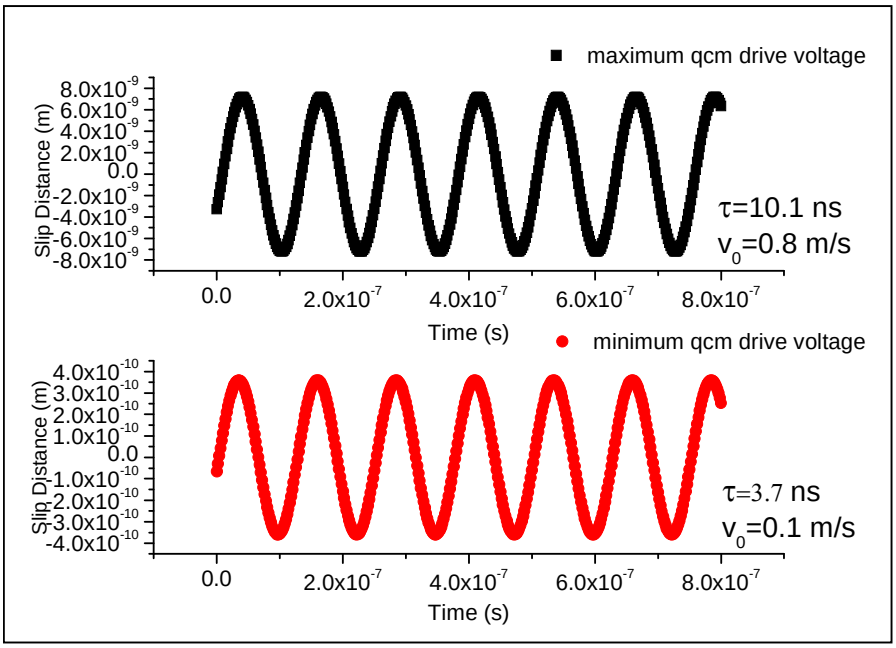

Figure 5.4 -Results above were calculated from the slip time values displayed in Table 5.1 for the initial (minimum) drive level and the final (maximum) drive level.

We assumed typical[15] QCM velocities of 0.1 m/s and 0.8 m/s for the minimum and maximum drive levels respectively. Figure 5.4 suggest that the surface particles slosh back and forth at atomist dimensions for the weakest drive level displaying a relative amplitude range an order of magnitude lower than the estimated 2 nm amplitude of vibration of the QCM. At the strongest drive level the particles move at comparable distances with the estimated amplitude of QCM vibration which was approximately 15nm for a substrate velocity of 0.8 m/s.

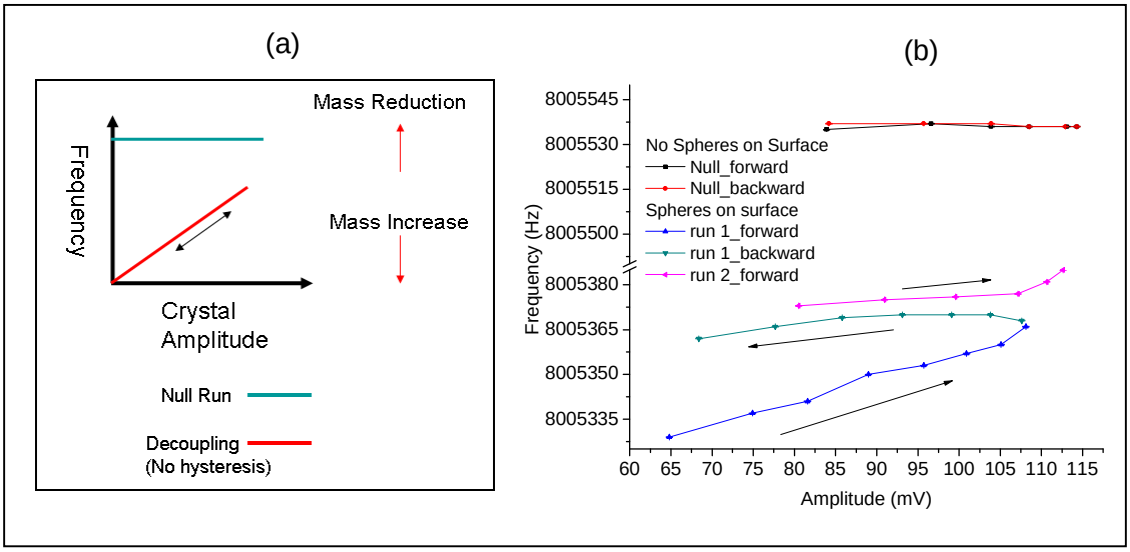

Figure 5.5 - (a) in this figure represents an idealized depiction of the QCMs response to in place particle decoupling or "decoupling curve" in the strong coupling regime of the Dybwad model. The graph shows no hysteresis because it assumes that particles return to initial state once crystal amplitude decreases to original drive level. The graph to the right (b) is the actual experimental data that table 1 is based on.

From figure 5.5(b) it is evident that particles are in the strong coupling regime of Dybwad model as shown by the initial negative shift in frequency from the null curve and the initial decoupling curve (run 1 forward). As the crystal amplitude increased in run 1 we observed (roughly) a linear increase in frequency which agreed with figure 5.5(a). However, when decreasing the drive voltage back to the original level which in turn decreased the crystal amplitude we observed hysteresis. This hysteresis indicates that even though these drive levels were insufficient to eject particles from the surface or even cause noticeable motion in the optical region changes in coupling deep within the buried contact between the microspheres and the gold electrode were detected by the QCM. The increase in frequency observed during the decreasing sweep of the decoupling curve in run 1 indicates that the

average coupling of the spheres on the surface has decreased. In figure 5.6 the behavior between runs 1 and 2 are magnified to show the difference in decoupling behavior. Initially the slope in the increasing decoupling curve for run 2 is less than that for run 2 until some critical amplitude around 105 mV is reached to further weaken even more bonds on the surface as indicated by the sharp increase in slope shown in figure 5.6.

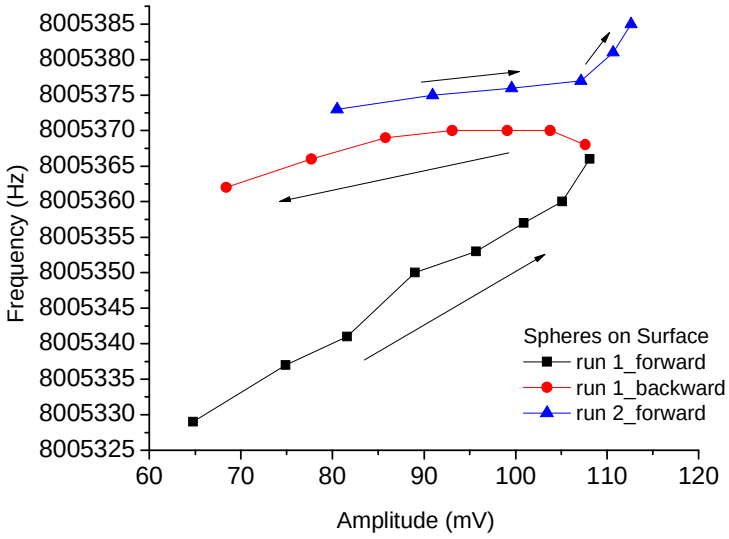

Figure 5.6 - Magnification of runs 1 and 2 from figure 5.5(b)

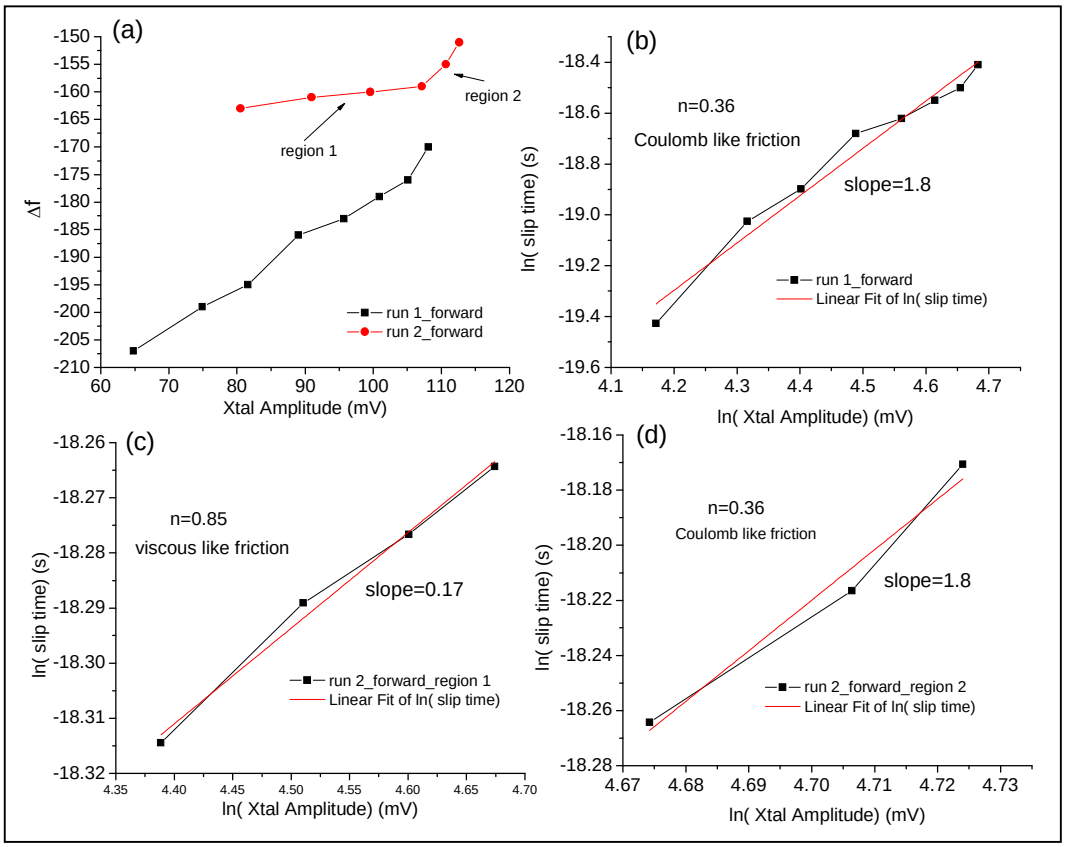

Figure 5.7 - Friction analysis of Figure 5.6 decoupling curves. Figure 5.7 (a) is a plot of the change in frequency from QCM resonance plotted against the crystal amplitude. Run 2 in (a) has been divided into two regions to analyze the change in frictional behavior associated with the transition between regions. The values of n displayed in (b), (c), and (d) correspond with the particle friction law as shown in equation (5.1). These n values were calculated by applying equation (5.2).

Optical data was recorded for both the long and short run decoupling curves in the horizontal orientation and we observed no gross movement of the surface particles when viewing the center of the electrode where the QCM amplitude is a maximum. However, our data suggest that the particles are not completely idle. The decoupling curve results from figures 5.5 and 5.6 suggest that these particles are undergoing some sort of behavior (rocking, sliding, slipping, reordering, depinning, etc…) that reduces the average coupling

between the particles and substrate. In figure 5.7 (a) we see that our frequency shift "Δf" against crystal amplitude agrees with the trend one would expect to see for particles undergoing Coulomb like friction as worked out by Vittorias et al.[12] This result is favorable since we observed no loss in particles but still saw an obvious shift in frequency. Using methods developed by the Krim group we simplified the decoupling mechanism to be in place slipping in which frictional results can be worked out. We found under this assumption that our 5 micron diameter polystyrene microspheres adsorbed from aqueous solution behave like ordinary physisorbed films previously studied in the literature.[2]

This observation was in the opposite direction of the initial shift observed by D'Amour et. al in their study of capillary adhesion[11] however, agreed with the experiment performed by Dultsev and coworkers. The discrepancy may be a result of the differences in the deposition as well as the size (ours were smaller) and/or composition (glass vs. polystyrene) of the particles. D'Amour et. al found that particles with diameters smaller than 40μm did not agree with small load approximation theory for weak coupled particles [11] which is in agreement with the work presented here. In our experiment spheres were deposited from aqueous solution where capillary bridges form between the spheres and QCM surface, these bridges clamp the spheres in place allowing them to track the motion of the QCM**.** In their experiment the spheres were deposited from a dry state where the rms roughness of the spheres was an order of magnitude larger than their QCM surface [11] which increases the possibility of point contacts upon deposition as well as the chance for their experiment to fall into the weak coupling regime. In conclusion we found that when QCM experiments (decoupling curves) were performed on our polystyrene particles experienced

initially a “Coulomb like” friction as they underwent some decoupling process that effectively decreased the average adhesion to the surface. When decreasing the crystal amplitude to the original value we observed hysteresis in frequency indicated by the observed increase in frequency from the initial value before the experiment was performed. This suggested that the overall coupling

strength of particles to the surface has decreased as a result of the initial sweep forward.

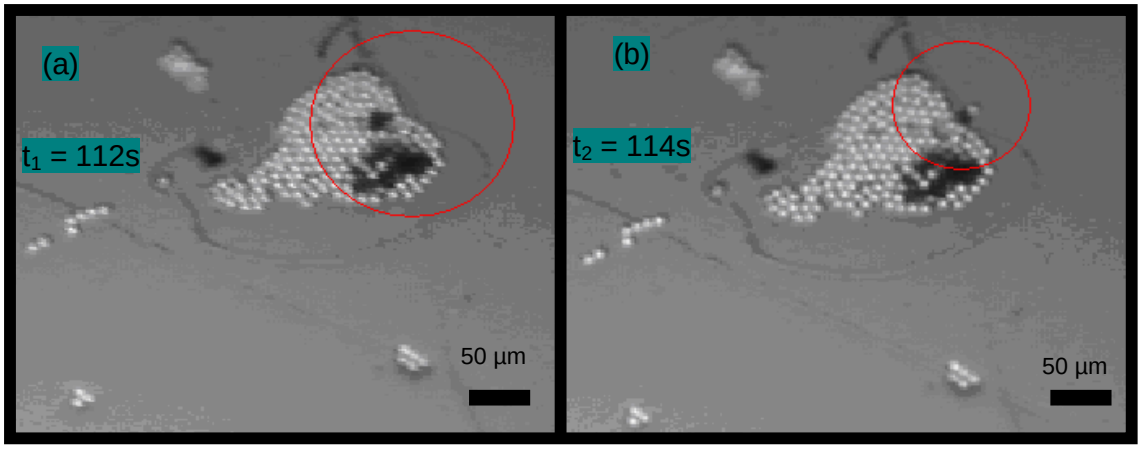

Figure 5.8 - Particle motion observed after rapidly varying the driving voltage. Figures (a) and (b) serve to illustrate a reordering mechanism that may occur during QCM experiments. These figures were performed on a different sample in which we observed top layer spheres transition to the surface of the QCM. This motion suggests the sphere-sphere bond is weaker than the spheres-electrode bond.

When performing the experiment a second time we found that the particles experienced a viscous like friction law similar to that of a physisorbed monolayer until some critical crystal amplitude value above what was previously tested was reached to induce particle decoupling which placed particles in a Coulomb like friction regime identical in value to what was observed initially. This suggest that the particles are essentially “picking up where they left off” from the initial decoupling run. For a completely viscous friction law we would expect to calculate a value of 1 for n however, as shown in figure 5.7(c) we

calculated n=0.87 which is viscous like but suggest other mechanisms are at work on the surface that hinder a completely viscous friction law. These mechanisms as mentioned earlier include decoupling, depinning, and reordering of the surface during the QCM experiment. In figures 5.8 (a) and 5.8 (b) we show one possible reordering mechanism that may contribute to moving the system away from a completely viscous friction law. Although we did not observe any movement or behavior in the optical region it is not fair to assume that all of the particles on the entire surface are experiencing the same inactivity.

5.6 REFERENCES

1. Johannsmann, D., Viscoelastic, mechanical, and dielectric measurements on complex samples with the quartz crystal microbalance. *Physical Chemistry Chemical Physics* **2008,** *10* (31), 4516-4516.

2. Krim, J.; Watts, E. T.; Digel, J., Slippage of simple liquid films adsorbed on silver and gold substrates. *Journal of Vacuum Science & Technology A: Vacuum, Surfaces, and Films* **1990,** *8* (4), 3417-3420.

3. Medvedeva, N. V. I., O.M.; Ivanov, Yu. D.; Drozhzhin, A.I.; Archakov, A.I., Nanobiotechnology and nanomedicine. *Biomeditsinskaya Khimiya* **2006,** *52* (6), 529-546.

4. Dultsev, F. N.; Ostanin, V. P.; Klenerman, D., "Hearing" Bond Breakage. Measurement of Bond Rupture Forces Using a Quartz Crystal Microbalance. *Langmuir* **2000,** *16* (11), 5036-5040.

5. Peri, M. D. M.; Cetinkaya, C., Rotational motion of microsphere packs on acoustically excited surfaces. *Applied Physics Letters* **2005,** *86* (19), 194103-194103.

6. Sánchez, L.; Sánchez, P.; Lucas, A.; Carmona, M.; Rodríguez, J. F., Microencapsulation of PCMs with a polystyrene shell. *Colloid and Polymer Science* **2007,** *285* (12), 1377-1385.

7. Sokoloff, J. B.; Krim, J.; Widom, A., Determination of an atomic-scale frictional force law through quartz-crystal microbalance measurements. *Physical Review B* **1993,** *48* (12), 9134-9134.

8. Sauerbrey, G., Verwendung von Schwingquarzen zur Wägung dünner Schichten und zur Mikrowägung. *Zeitschrift für Physik* **1959,** *155* (2), 206-222.

9. Krim, J.; Widom, A., Damping of a crystal oscillator by an adsorbed monolayer and its relation to interfacial viscosity. *Physical Review B* **1988,** *38* (17), 12184-12184.

10. Dybwad, G. L., A sensitive new method for the determination of adhesive bonding between a particle and a substrate. *Journal of Applied Physics* **1985,** *58* (7), 2789-2789.

11. D'Amour, J. N.; Stålgren, J. J. R.; Kanazawa, K. K.; Frank, C. W.; Rodahl, M.; Johannsmann, D., Capillary Aging of the Contacts between Glass Spheres and a Quartz Resonator Surface. *Physical Review Letters* **2006,** *96* (5), 058301-058301.

12. Vittorias, E.; Kappl, M.; Butt, H.-J.; Johannsmann, D., Studying mechanical microcontacts of fine particles with the quartz crystal microbalance. *Powder Technology* **2010,** *203* (3), 489-502.

13. (a) Laschitsch, A.; Johannsmann, D., High frequency tribological investigations on quartz resonator surfaces. *Journal of Applied Physics* **1999,** *85* (7), 3759-3759; (b) Borovsky, B.; Krim, J.; Syed Asif, S. A.; Wahl, K. J., Measuring nanomechanical properties of a dynamic contact using an indenter probe and quartz crystal microbalance. *Journal of Applied Physics* **2001,** *90* (12), 6391-6391.

14. Flanigan, C. M.; Desai, M.; Shull, K. R., Contact Mechanics Studies with the Quartz Crystal Microbalance. *Langmuir* **2000,** *16* (25), 9825-9829.

15. Dawson, B. D.; Lee, S. M.; Krim, J., Tribo-Induced Melting Transition at a Sliding Asperity Contact. *Physical Review Letters* **2009,** *103* (20), 205502-205502.

16. (a) Buttry, D. A.; Ward, M. D., Measurement of interfacial processes at electrode surfaces with the electrochemical quartz crystal microbalance. *Chemical Reviews* **1992,** *92* (6), 1355-1379; (b) Seah, P. J. C. a. M. P., The quartz crystal microbalance; radial/polar dependence of mass sensitivity both on and off the electrodes. *Measurement Science and Technology* **1990,** *1* (7), 544-555.

17. Widom, A.; Krim, J., Q factors of quartz oscillator modes as a probe of submonolayer-film dynamics. *Physical Review B* **1986,** *34* (2), 1403-1403.

18. Kanazawa, K. K.; Gordon, J. G., Frequency of a quartz microbalance in contact with liquid. *Analytical Chemistry* **1985,** *57* (8), 1770-1771.

CHAPTER 6: REDUCING THE EFFECT OF CAPILLARY ADHESION IN QCM EXPERIMENTS THROUGH IN SITU MICROPARTICAL TRANSFER AND THE ENVIRONMENTAL DEPENDENCE OF SURFACE DYNAMICS OF POLYSTYRENE MICROSPHERES ON A QUARTZ CRYSTAL MICROBALANCE

I. Lynch, A. Brown*, Ben Keller, and J. Krim

Department of Physics North Carolina State University

*Department of Mechanical Engineering Arizona State University

6.1 INTRODUCTION

Recent applications involving the use of the quartz crystal microbalance (QCM) are of growing interest in the biosensor community.[1,2] The QCM provides several advantages in terms of particle detection. The QCM is low cost and relatively low maintenance in terms of operation and most importantly is extremely sensitive (can easily detect mass changes on the order of micrograms) to surface changes which makes it ideal for gaining information regarding contact mechanics[3,4] in a non destructive way. One key advantage the QCM brings to the biosensor community is its ability to easily distinguish between the weak "non-specific" surface interactions from the stronger "specific" bonds of study particularly in complex serums such as blood.[1] The use of a QCM also eliminates the need for tedious labeling procedures during bond rupture scans[2]. It has been observed in the literature[5] that varying surface and environmental conditions in particular water layers from the presence of

humidity or deposition can lead to drastic changes in the binding energy of the particles of study. It has also been suggested within the biosensing community that the presence of water can result in unwanted additional effects rising from changes in the acoustic coupling of the adsorbed liquid layer (interfacial slip) which would cause difficulties during interpretation of data.[6] Sensing is not the only issue that is affected by the presence of capillaries from water vapor, the prospect of micro-sorting via QCM experiments[7] would be a cumbersome task in the presence of water vapor for various reasons. At the microscale inertial loading has little to no influence on the particles attachment to the surface which means that the particles adherence to the surface arises primarily from other means such as the Van der Waals interaction and capillary adhesion. It has been observed[8] that during QCM experiments surface particles distributed on the electrode experience non uniform binding energies even when all surface particles are of the same size and material and deposited under the same conditions. It is also known[9] that the oscillation amplitude of the QCM decreases radially from the center of the electrode which would have an affect on bond rupture. As a result of these factors it is not guaranteed that adsorbed particles of varying size will sort according to size alone. In this article we analyzed (separately) particle dynamics of 5 and 15 micron polystyrene microspheres deposited on an 8 MHz gold QCM electrode as we increased (and later decreased to the original value) the amplitude of oscillation of the crystal and monitored the corresponding shift in resonant frequency, we call this graph a “decoupling curve” which describes the surface behavior (effective decrease in the adhesion between the attached particle and substrate) during the forward sweep of our data runs. When the circuitry used during decoupling curves was insufficient in generating particle motion we connected our

sample to a separate stronger power source to induce particle motion which was then analyzed via optical microscopy coupled with video recording. We perform these experiments under varying experimental environments including air, vacuum, and dry nitrogen. We introduce a new method for reducing the unwanted affect of capillary adhesion during QCM experiments and provide results after applying this method.

6.2 METHODS AND MATERIALS

Our QCMs were AT cut at 35˚ and the diameter was 0.375 inches with a 0.01 inch flat on the –x axis. The crystals oscillated with a fundamental mode of 8 MHz and had an optical polished finish. The electrode was keyhole design with a diameter of 0.250 inches and it was made from gold deposited atop a thin chrome layer. The QCM was driven by a pierce oscillator circuit whose output signal was mixed using a 0.5 to 500 MHz frequency mixer with a reference signal supplied by an 8 MHz can crystal oscillator driven by a different Pierce oscillator circuits. The mixed output ran through a low pass filter and was detected using a Hewlett Packard 5384A frequency counter. The crystal amplitude was measured using a Keithley 2000 multimeter. The reference "can" QCM was powered by an Elenco Precision model XP-15 regulated variable power supply and the experimental 8 MHz QCM was driven with a Keithley 2400 digital source meter. A second Keithley 2400 digital source meter was used to drive a 5 MHz QCM in experiments where both the 8 MHz and 5MHz crystal were oscillating simultaneously in close range. We chose different valued frequency QCMs for these experiments to eliminate "cross talk" from beat frequencies. These source meters are extremely low noise instruments which allowed us to make accurate measurements while varying the drive voltage of one of the crystals. We applied the 5 and

15 μm diameter polystyrene microspheres from aqueous solution to the center of the electrode where maximum amplitude occurs on one side of the QCM covering approximately 1-10% of the electrode. The surface was then dried with helium flow and the sample was either used immediately or left over night to air dry depending on the experiment. The majority of experiments were performed in a vacuum chamber customized to rotate approximately 270 degrees in order to perform experiments in both vertical and horizontal orientations along with all angles in between. The horizontal and vertical experiments were both performed in the following environments: air, vacuum, and dry nitrogen. Particle motion was analyzed using an Edmund optics Proximity Series Infinitube microscope with a Mitutoyo 10X/0.28 lens illuminated by an Edmund Industrial Optics model 21AC illuminator. Attached to the microscope was a B/W Panasonic CCD camera whose video output was sent to the computer program Flash Point 3D and a Toshiba DVD recorder to record movies of surface motion.

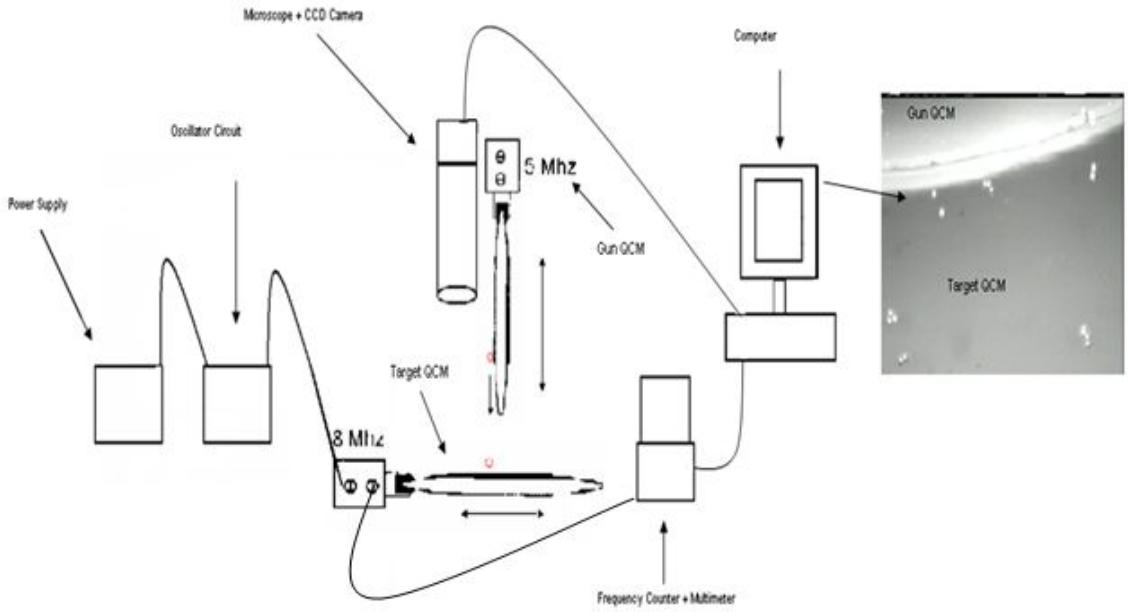

Figure 6.1 - Schematic of sphere transfer experiment used to reduce the affect of capillary adhesion from water existing in the buried contact between the QCM electrode and adsorbed microsphere. In the experiment the 5 MHz or "gun" QCM ejects particles originally adsorbed from aqueous solution onto the experimental "target" 8 MHz QCM where data is collected. We chose the 8 MHz QCM as our target due to its higher sensitivity.[9]

6.3 PROBING CONTACT MECHANICS WITH A QCM

The QCM traditionally is used to monitor mass uptake during thin film deposition. This is done by monitoring the change in frequency from resonance as mass adsorbs on the surface layer by layer. This relation is given by the Sauerbrey relation In 1959 Sauerbrey[10] showed that the mass absorbed on the electrode of a QCM is directly proportional to the measured frequency shift (6.1).

$$\delta f_{film} = -2\frac{(m_{film}/A)}{\rho_q v_q} f_0^2 \qquad (6.1)$$

where m_{film} is the mass of a loading film rigidly attached to the motion of the QCM, A is the area of the electrode, ρ_q is the density of quartz, v_q is the velocity of sound through quartz, and f_0 is the resonant frequency of the QCM. This equation corresponds to negative shifts in frequency and works well when the loading mass is rigidly attached to the QCM's motion. This equation however, does not apply strictly to the load geometry of a non uniform distribution of microspheres. To understand how this load geometry can be probed by a QCM one has to visit the Dybwad experiment[3] which is the foundation for interpreting the complex contact behavior associated with this configuration. In 1985 Dybwad performed an experiment where he placed a single gold microsphere on the center portion of an oscillating QCM. He observed a positive shift in frequency which at first glance appears contradictory to the Sauerbrey equation. Similar to the authors from section 3.2 Dybwad decided to view the QCM as a mechanical system. He explained his result by modeling the single sphere QCM geometry as a coupled mechanical oscillator. By doing so he justified the possibility of measuring a positive shift in frequency when a single particle is "lightly" coupled to the electrode of the QCM. This experiment was one of the first examples of how a QCM could be used to probe particle adhesion. His model predicts the "coupled" systems frequency response to the attachment parameter k thus probing contact mechanics. The result is shown in equation (6.2) below

$$2\omega^2 = \left(\frac{K}{M}+\frac{k}{M}+\frac{k}{m}\right) \pm \left[\left(\frac{K}{M}+\frac{k}{M}+\frac{k}{m}\right)^2 - 4\frac{K}{M}\frac{k}{m}\right]^{1/2}. \qquad (6.2)$$

where M is the mass associated with the QCM, m is the mass of the sphere, K is the spring constant associated with the QCM, and k is the spring constant of the sphere which is also

referred to as the “attachment parameter” a value that describes the bond strength between the sphere and QCM surface. Plotting the system frequency ω as a function of the attachment parameter k, Dybwad showed the idealized behavior of the coupled system. This plot is asymptotic and displays two main regimes the frequency of the system falls in as a function of the attachment parameter they are the “strong” and “weak” coupling cases. In the strong region (large k values) the plot shows negative values for the frequency in accordance with equation (6.1). Conversely in the weak region (small k values) the plot shows that when the sphere is “loosely” attached to the QCM positive shifts in frequency are possible. This is a result of the additional “stiffness” the system experiences from the bond. In other words the bond is not strong enough for the sphere to track the motion of the QCM so the resonator does not detect its mass (inertial loading) however, it can sense the added stiffness from the sphere-electrode bond. The Dybwad model has since been extended[5, 11] to include multiple spheres adsorbed on the surface assuming the loads are small. The details of the SLA or “small load approximation” have been rigorously shown[5, 8] for both strong and weak coupling regimes. The results are displayed below in the following equations (6.3) and (6.4). In the weak coupling regime or $\omega >> \omega_s$ such that the loading particles are unable to track the extreme oscillation of the driver are therefore not “detected” by the resonator. This condition is exactly that of light coupling (Dybwad) and leads to positive shifts in frequency given by equation (6.3). The corresponding shift in bandwidth or “dissipation” from the interaction is also predicted from this model however is not considered in this paper.

$$\Delta f = f_0 \frac{m_s}{\pi Z_q \omega} \omega_s^{\,2} = \frac{f_0}{\pi Z_q \omega} \kappa \qquad (6.3)$$

In equation (6.3) Z_q is the shear wave impedance of quartz, $\omega_s = \sqrt{\frac{\kappa}{m_s}}$ is the resonant frequency of the sphere where κ is the elastic constant between the single sphere and QCM electrode. When $\omega << \omega_s$ or the strong coupling regime the sphere is in phase with the QCM and effectively "clamped" onto the surface and therefore reduces to the Sauerbrey relation

$$\Delta f = -f_0 m_s \omega / \pi Z_q . \qquad (6.4)$$

Equation (6.4) which pertains to microparticles is equivalent in form to (6.1), this is a reasonable result since one can imagine that when an object is driven (relatively) slow that it will have no problem tracking the motion of the driver. This can be demonstrated easily by attaching a string to an object and very slowly driving it.

6.4 USING DECOUPLING CURVES TO INTERPRET AVERAGE SURFACE BEHAVIOR

QCM studies[7-8, 12] in particular "bond rupture scans" have reported curves of the change in frequency against drive voltage in the forward direction alone. The purpose of performing these scans was to induce bond rupture of the adsorbed particles in such a way that the weaker "non-specific" bonds would break at lower drive voltage values (smaller oscillation amplitude) and thus be dissociated from the bonds of interest which require a larger amplitude to free them from the surface. During bond rupture scanning it has been observed[1, 7, 12] that for particles adsorbed on the surface in the strong coupling regime an increase in drive voltage (crystal amplitude as well) results in an increase in QCM frequency from the deposition level. During bond rupture scans the "noise" emitted[7, 12] from surface

particles as there bonds are broken is measured and plotted under the frequency vs. drive voltage curve. These experiments show that a relative increase in frequency corresponds to a spike in the noise spectrum analysis indicating bond breakage during that frequency shift. The drive levels during bond rupture scans are relatively high and usually result in the majority of the surface particles rolling, sliding, or hopping off the surface. A relative increase in frequency does not strictly imply that the surface particles are leaving the surface. It has been observed[8] for particles in the strong coupling regime that relative changes in frequency during rupture scans did result in the removal of particles from the surface. This result suggest that the QCM is sensitive to the changes in the average coupling of particles adhered to the surface as suggested by the SLA and Dybwad model discussed earlier. In our experiments we ramp the drive voltage in a linear fashion first up to some maximum value and back down to the starting position and record the frequency response. We call this measurement a decoupling curve because it provides a qualitative interpretation of the average bond strength of the particles adsorbed on the surface as they decouple from changes in oscillation amplitude.

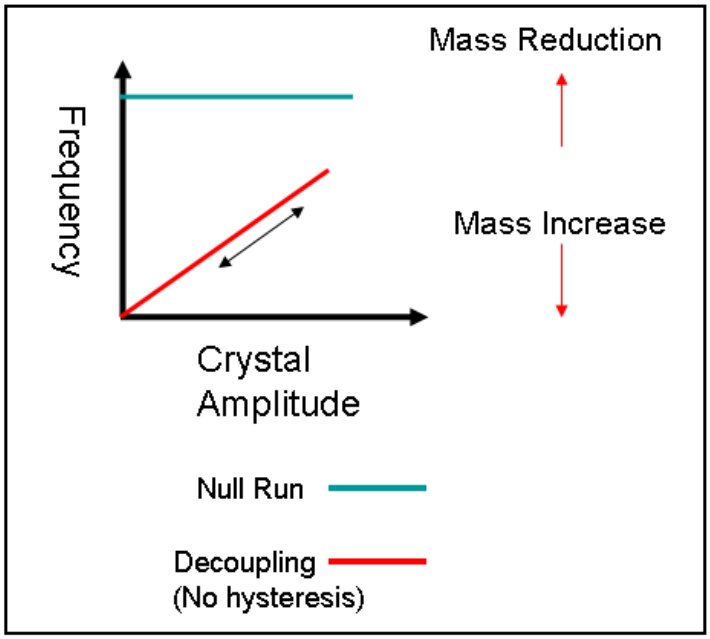

Figure 6.2 - describes the ideal (artificial) situation of decoupling in the strong coupling regime where a negative shift from fundamental is observed when spheres are initially applied from mass loading in accordance with the Sauerbrey equation. As the crystal amplitude is incrementally raised by increasing the drive voltage the frequency increases as well as a result of effective mass reduction due to sphere decoupling.

Decoupling is very much an irreversible process meaning the bonds that were disrupted during the increasing sweep in voltage do not (on average) return to there initial state when decreasing the voltage back to the initial value. This hysteresis has been observed for all our experiments thus making the situation illustrated in figure 6.2 to be highly unrealistic. The shape of a decoupling curve is dependent on several factors including: the initial bond regime (strong or weak) of particles after deposition (deposition procedure), environment, cleanliness of surface, time in between multiple scans, and surface roughness. All of these factors are intimately related to contact conditions that affect the bond strength between the adsorbed particles and the surface.

6.5 RESULTS AND DISCUSSION

Under the Derjaguin approximation[13] for a sphere-on-sphere contacting geometry (6.5)

$$F_{adh} = 2\pi R\gamma_{polystyrene} \qquad (6.5)$$

in dry conditions where F_{adh} is the adhesive force between the spheres, R is the radius of a sphere, and $\gamma_{polystyrene}$ is the surface energy of polystyrene we found that the force between two 5 micron diameter and two 15 micron diameter spheres was $0.5\mu N$ and $1.5\mu N$ respectively. Since the majority of our samples were deposited in air from aqueous solution on samples on samples used directly from the package we assumed the force of adhesion between the spheres electrode surface to be a combination of capillary adhesion from water coupled with extra surface energy from contamination (hydrocarbons). Assuming the meniscus force is the dominating factor for particle adhesion and arises mainly from the capillary pressure we approximate the force of adhesion as

$$F_{adh}^{wet} \approx 4\pi R\gamma_{total} \qquad (6.6)$$

where R is the radius of microsphere and

$$\gamma_{total} = 2\phi\sqrt{\gamma_{water}\gamma_{hydrocarbon}} \ . \qquad (6.7)$$

Equation (6.7) is the Good-Girifalco method[14] which estimates the surface energy at the contact. We are assuming that under these humid conditions as stated previously arises from capillaries forming at the buried contacts between the sphere and electrode. Taking into account the fact that the crystals were used as is we included the surface energy associated

with contamination ($\gamma_{hydrocarbon}$). The ϕ term or "correction factor" was set to 0.5 to take into account the mismatch in intermolecular interactions of water and hydrocarbons. We found for $\gamma_{water} = 73\frac{mN}{m}$ and $\gamma_{hydrocarbon} \approx 23\frac{mN}{m}$ that the force of adhesion F_{adh}^{wet} was equal to approximately $2\mu N$ and $6\mu N$ for the 5 micron and 15 micron diameter spheres respectively.

These estimated forces are approximately 3 times the force which was calculated for the interaction between microspheres. This implies that any spheres lying on top of spheres that were directly adsorbed on the surface of the electrode (second order spheres) would in principle move easier than the spheres attached to the surface (first order spheres). This behavior was observed during an experiment performed in humid air (34% r.h.) for a sample of $5\mu m$ diameter spheres deposited from aqueous solution on an 8 MHz QCM. This sample was allowed to air dry over night before experiments were performed. We then performed 2 decoupling curve runs in the horizontal orientation where we observed no motion in the optical region. Following immediately after the second horizontal decoupling curve run we moved the sample to the vertical orientation and performed an additional decoupling curve run where we again observed no motion in the optical region. We knew from previous experiments that the spheres responded to abrupt changes in crystal amplitude. As a result of this we performed our next experiment by rapidly and randomly varying the drive voltage to induce particle motion. Before performing an experiment rapidly varying the QCM amplitude we performed an additional decoupling curve figure 3a in the horizontal orientation to gain some qualitative insight as to the varied average coupling strength in response to changes in oscillation amplitude. We observed a negative shift in frequency

from natural resonance of 591 Hz which suggested that the particles were in the strong coupling regime and equation (6.4) could be used to interpret there behavior. Applying equation (6.4) we found approximately 17,550 where adsorbed on the surface. During the forward sweep of our decoupling curve run we observed a slope change in the decoupling curve around 110 mV indicating an increase in the average rate of particles decoupling. The observed hysteresis during the backward sweep indicates that the particles restored to a restored to a state of lower average coupling since the frequency at the return point has increased from its initial value. After this decoupling curve (as mentioned earlier) we wished to observe the particles dynamics since we were unable to do so during the decoupling scans. The sample was mounted horizontally under normal lab air environmental conditions. Images were taken in 2s intervals over a 10 minute period as we rapidly and randomly varied the drive voltage in the range of the voltages used during the decoupling curve runs. Results of this experiment are displayed in figures 6.4a and 6.4b where we observed a group of second order spheres moving onto the surface of the electrode during the experiment while no motion was observed during the entire experiment for first order spheres. This suggest that the force of adhesion between spheres is less than force of adhesion between the spheres and electrode as predicted earlier using equations (6.5), (6.6), and (6.7).

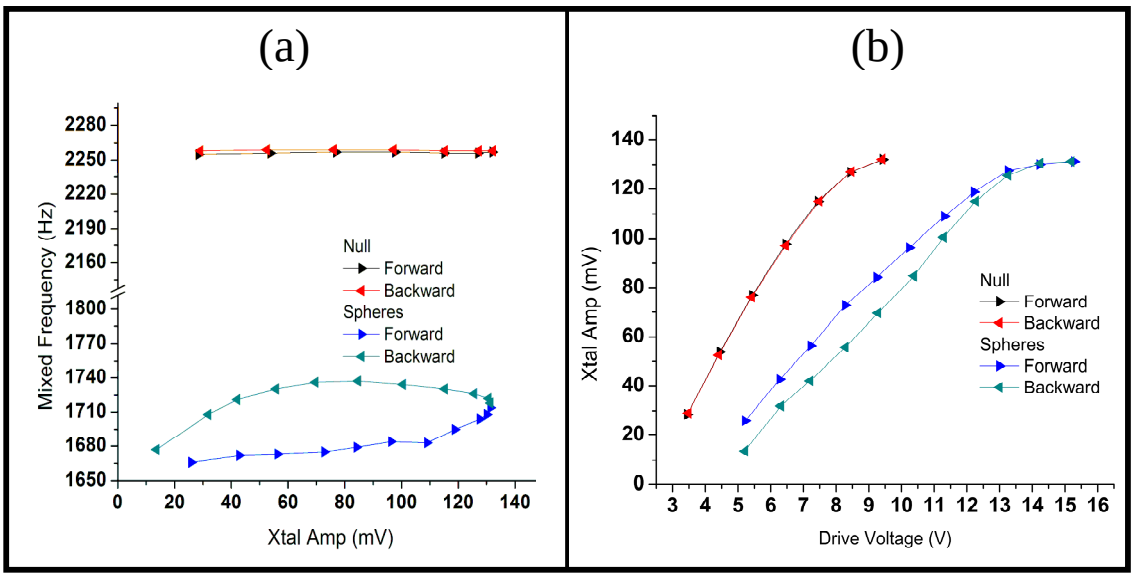

Figure 6.3 - a) displays the QCM response during a decoupling curve experiment, b)the dependence of crystal amplitude to drive voltage or "signal curve", and it is linear for the majority of the experiment.

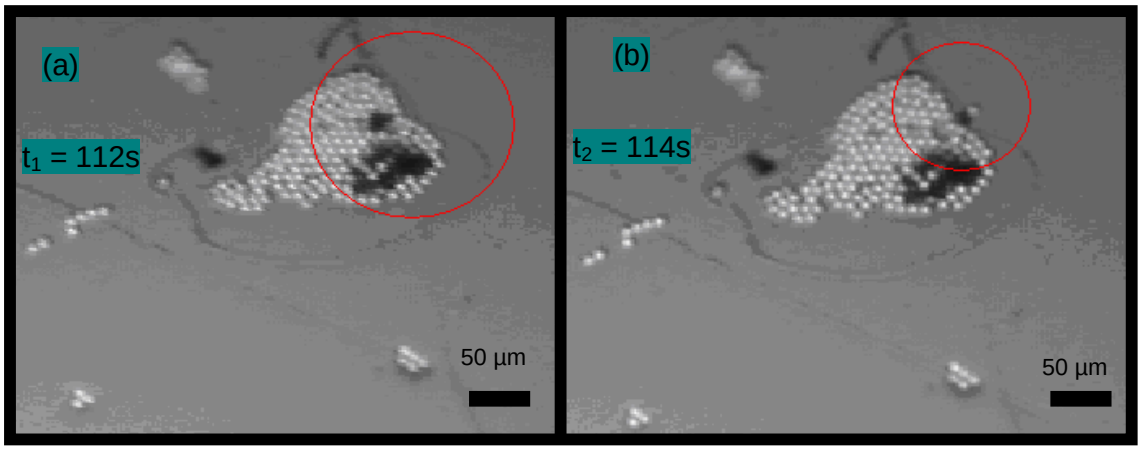

Figure 6.4 - Particle motion observed after rapidly varying the driving voltage. This motion suggests the bond between the spheres is less than the bond between the spheres and electrode.

6.5.1 DYNAMICS UNDER FLOODED CONDITIONS

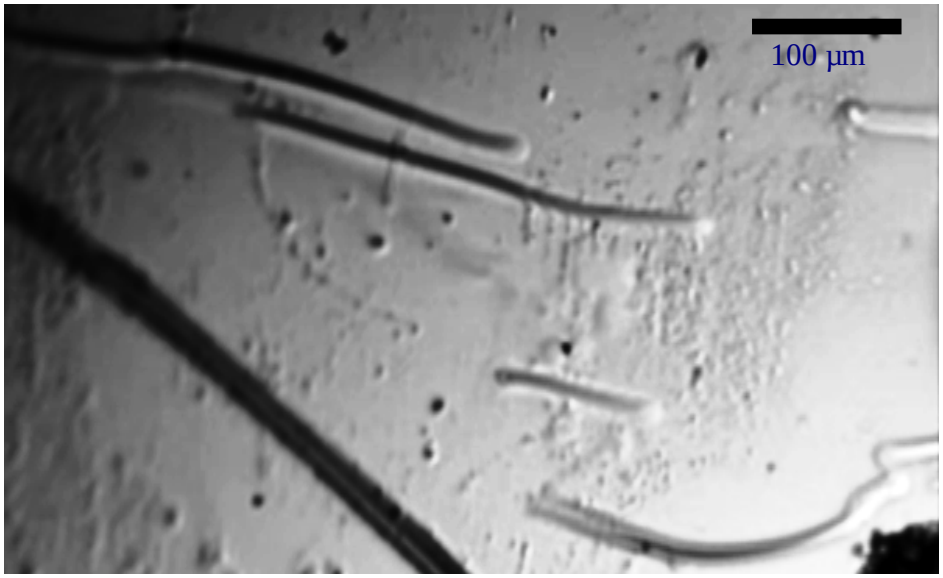

Figure 6.5 - Image of a QCM in 1 atm Nitrogen while rapidly varying the drive amplitude at large values to induce particle motion. This QCM had a substantial amount of water adsorbed onto the surface as a result of the deposition procedure (no drying time). As a result of the extreme shear forces produced by the QCM the adsorbed layer of water displayed an extreme amount of mobility.

Figure 6.2 describes the ideal situation of decoupling where a negative shift from fundamental is observed when spheres are initially applied from mass loading in accordance with the Sauerbrey equation. As the crystal amplitude is incrementally raised by increasing the drive voltage the frequency increases as well as a result of effective mass reduction due to sphere decoupling. Since sphere decoupling is energy dependent it is safe to suppose that under ideal conditions such as a relatively flat and dry surface, that the decoupling curve could in principle track itself during successive forward and backward runs within a drive range below that which would induce particle motion. It is our experience that this has not been the case. It was previously mentioned that the deposition conditions can have a profound affect on the shape of decoupling curve. This was indeed the case for the

decoupling curve shown in figure 6.6. This decoupling curve was performed in the horizontal orientation in laboratory air. For this particular sample we did not allow it to dry over night like the previously mentioned samples, meaning soon after the 5 micron diameter spheres were deposited from aqueous solution decoupling curves were performed. We observed an initial decrease in frequency after the spheres had been applied and for the most part saw a linear increase in frequency with increasing crystal amplitude. Then when tracing back to the original crystal amplitude we observed an interesting contradiction to the decoupling model above and measured an increase instead of a decrease in QCM frequency with decreasing amplitude. Upon repeating this run twice more we observed that the hysteresis was removed however, the trend of the decoupling curve was opposite of the model. These results imply that the surface behavior is more complex, and sphere decoupling is not the only mechanism at work. For this particular sample sphere movement was observed in the optical region at the higher amplitude values during the forward sweep. This observation was true for the successive decoupling curve runs however, the observed sphere motion decreased with additional runs.

This behavior is characteristic of the dynamics granular materials undergo experience when there contacts are flooded. When the buried region between two contacting materials (under capillary adhesion) becomes flooded the capillaries are broken thus weakening and increasing the mobility between the two objects. This explanation is supported by the fact we observed motion during decoupling curve runs for this experiment at lower crystal amplitude values then what was observed for the previously mentioned experiment where the sample was allowed to air dry over night. For the previously mentioned sample no motion

was observed during decoupling curve runs which suggest the bonds are much stronger between the spheres and electrode surface than this “wet” case. This result is expected since the process of drying results in capillary aging which in turn increases the contact area between the sphere and electrode surface thus increasing the bond strength.[5] The complexity in the interpretation of the decoupling curve displayed in figures arises from the QCMs sensitivity to the mass reduction resulting from the sample drying during data runs, particularly the initial data run. The data points for this experiment were taken in 3 min intervals resulting in the entire run lasting 30 minutes plenty of time for the sample to lose a substantial (60Hz which by applying equation (6.1) comes to 13 micrograms) amount of mass due to drying alone. We performed an experiment (data not shown) to test the affect a drop of pure (DI) water would have on the oscillation of a QCM. We found that the initial drop (once blown with helium flow to form a uniform layer) caused the QCM frequency to shift by -88Hz, over a period of about 30 minutes the shift from resonance frequency jumped to -35Hz below resonance where it remained for a long period of time (2 days). This suggested that the (positive) shift in frequency from water evaporating off the surface during the 30 minute period resulted in a shift of 53 Hz which corresponds to about 12 micrograms of water evaporated from the surface. This value is in agreement with the initial increase in frequency observed during the forward sweep in figure 6.6a.

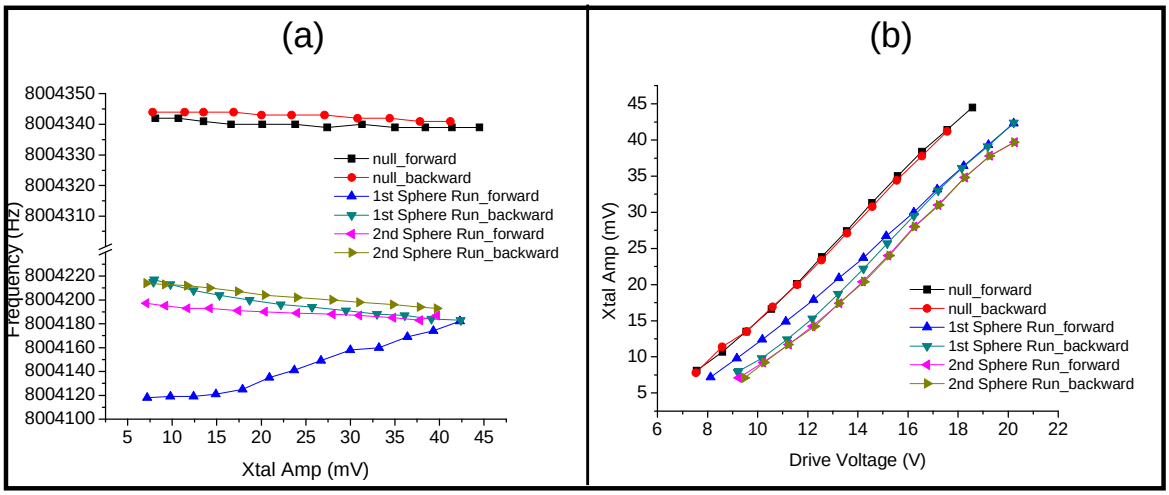

Figure 6.6 - (a) shows the behavior of the initial decoupling curve performed on this QCM as well a second decoupling curve followed soon after. The signal curves (b) are displayed for each data run and show that the oscillation amplitude depended linearly on the drive voltage from our power supply.

Motion was observed within the first ten minutes of the decoupling curve as shown in the figures 6.7a and 6.7b. No additional motion was observed until the maximum drive voltage was reached in which the motion on the surface was substantial. For the most part microspheres moved in the direction of oscillation however, as shown in the figures this was not the case for all of the mobile spheres on the surface.

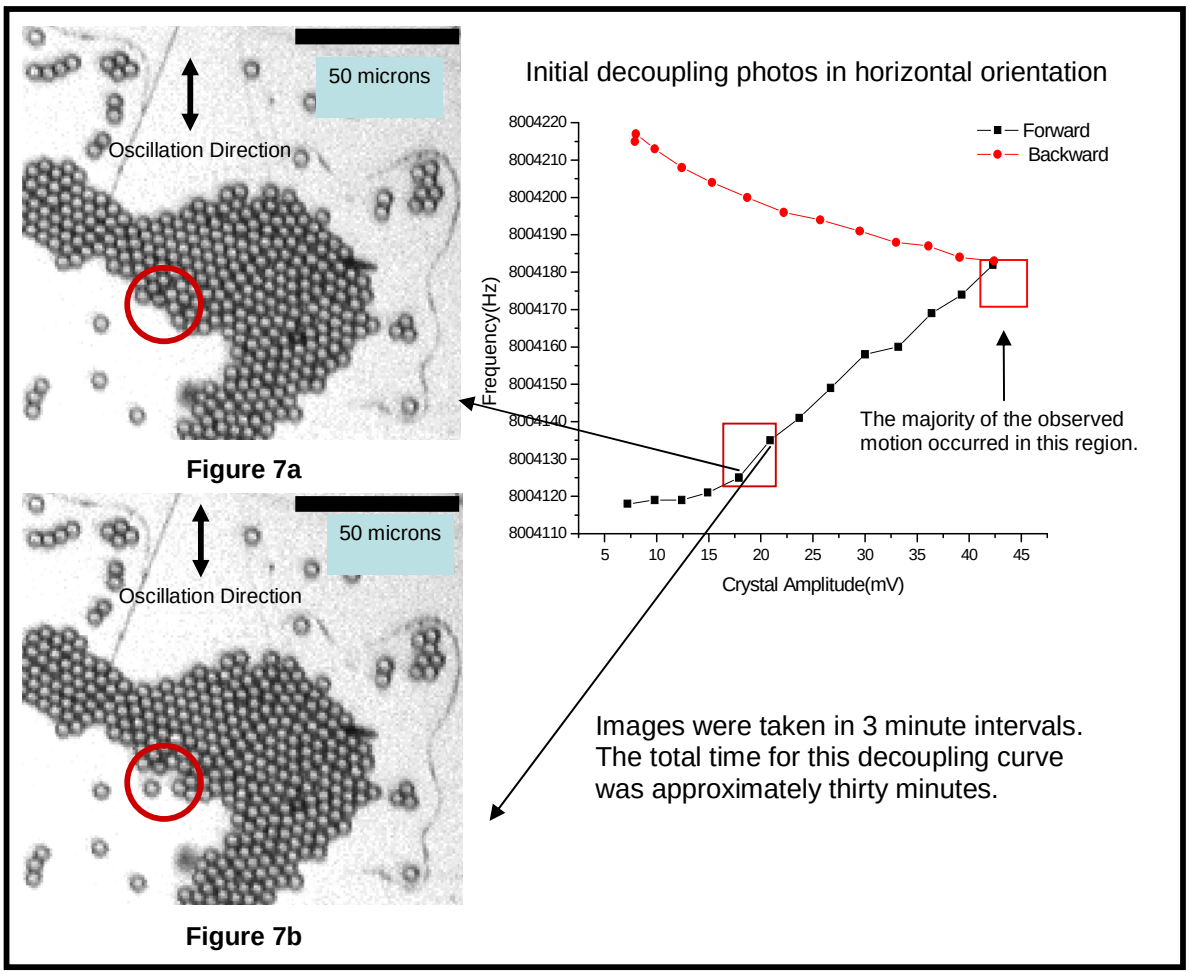

Figures 6.7 - a) and b) are images taken during the initial horizontal orientation decoupling curve run, these images were taken 3 minutes apart from each other and correspond in time to the boxed region of the decoupling curve. The increased energy from the rise in oscillation amplitude from figure 6.7a to 6.7b, aided in breaking the necessary bonds to translate the circled sphere from the cluster in which it belonged. The circled sphere is a "first order" or bottom layer sphere that moves roughly in the oscillation direction.

6.5.2 ENVIRONMENTAL INFLUENCE ON FRICTION

In a study[4] performed by Flanigan et. al. the researches demonstrated how a QCM could be used to probe contact mechanics. They found that the (negative) shift in resonate frequency of a QCM in response to a viscoelastic loading material (such as the spheres we used in our experiments they used gel caps) is linearly dependent with the (real) contact area

the material shares with the QCM electrode. In their experiment the authors varied the contact area of their sample by introducing an external loading force which flattened out compliant gel cap thus increasing the overall contact area between the gel cap and QCM electrode. This situation is similar to a study[8] performed by Vittorias et al. in which the authors increased the contact area of glass microspheres adsorbed on a QCM uniformly coated with a thin polystyrene layer by annealing the surface (via heat) to form a polystyrene meniscus around the spheres. The increased contact area from annealing was reflected in their frequency shift results in fact for their larger particles (larger than our 5 micrometer diameter spheres used for the data displayed in figures 6.9a and 6.9b but not exceeding 20 micrometers) the annealing was sufficient enough to change the coupling regime (within the SLA and Dybwad models) in which the particles resided initially. Both of these scenarios are indicative of a QCMs sensitivity to changes in coupling (adhesion) between its electrode and loading particles. At the microscale the force of adhesion is proportional to the contact area (or more precisely the separation distance) between the loading particles and the electrode. During QCM experiments such as bond rupture scans and decoupling curve runs the average separation distance between contacting particles and QCM electrode changes (usually) resulting in resulting in an altered force of adhesion interpreted as a frequency shift by the QCM. The specific details regarding the mechanism of bond breakage (or weakening) is not well understood, so it is best to analyze the overall affect of bond breakage, which is the altering of the particles average contact area and separation distance with its contacting surface. Figure 6.8 below summarizes the change in frequency during QCM experiments for particles undergoing a specific bond interaction whether it be that the particles are “resting”

in place experiencing constant contact (separation distance remains constant on average) throughout the entire experiment (6.8a and 6.8b) or that there contact area and perhaps the separation distance is changing throughout the experiment as a result of friction (6.8c and 6.8d). We assume that the force of adhesion at the scale of our experiments is dominated by two main forces Van der Waals and capillary respectively. These forces are both dependent on the separation distance at the contact and are[15]

$$F_{adh}^{vdw} = \frac{A_H R}{6D^2} \qquad (6.8)$$

$$F_{adh}^{cap} = A_{men} \frac{2\gamma_l}{D} \qquad (6.9)$$

where A_H ,R,D are the Hamaker constant, radius of particle, and separation distance respectively for equation (6.8). The terms A_{men} , γ_l , and D are the area of the flooded contact region, surface energy/tension of the liquid layer (in our case water), and the separation distance respectively. When analyzing the observed behavior for the wet environment associated for our experiments we expect that equation (6.9) provides the most relevant interpretation.

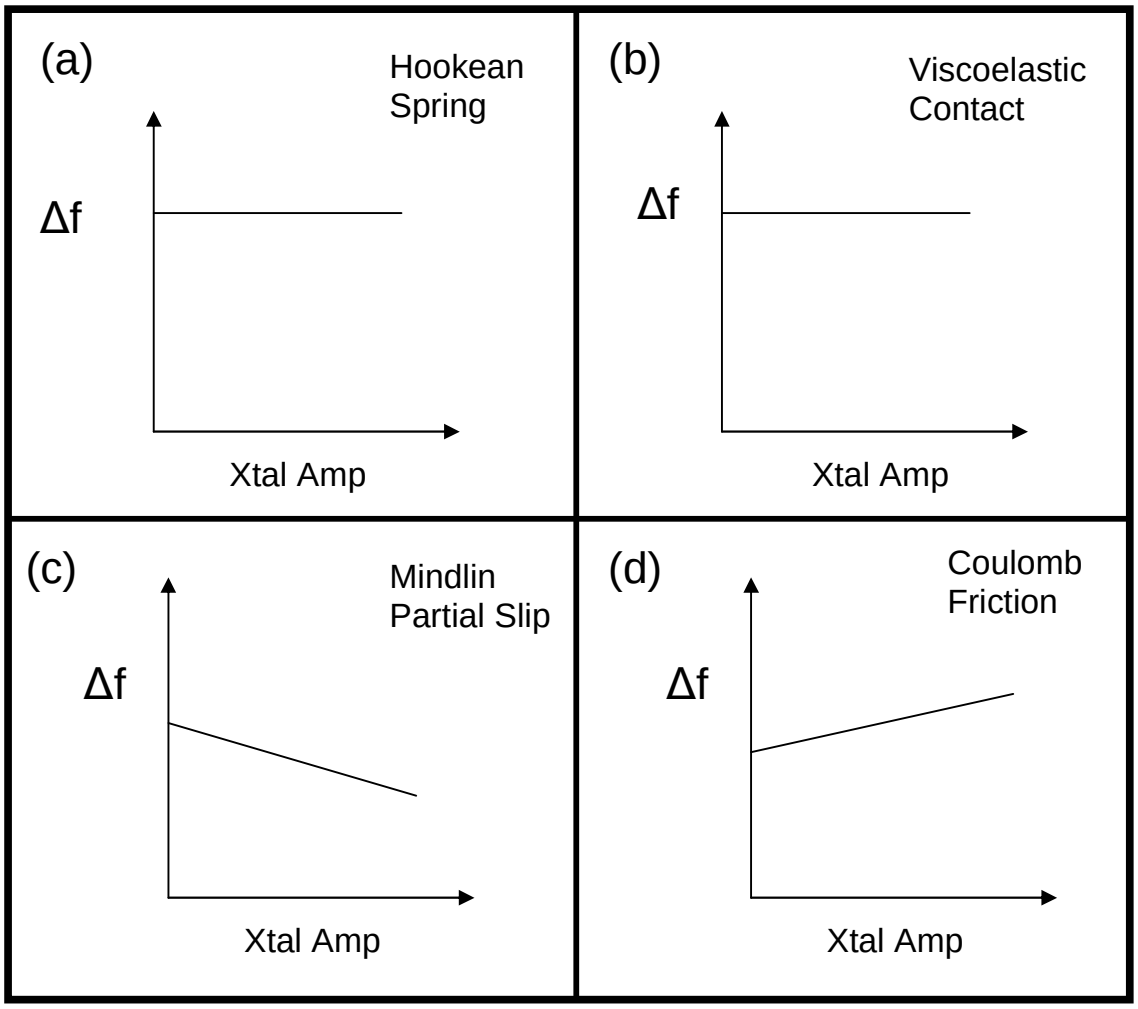

Figure 6.8 - describes the predicted response of the change in QCM frequency to oscillation amplitude when the adsorbed particles are undergoing a particular frictional interaction between its contact with the surface.

These scenarios have shown up in the literature before[8] with the added component of the change in bandwidth (dissipation) with oscillation amplitude.

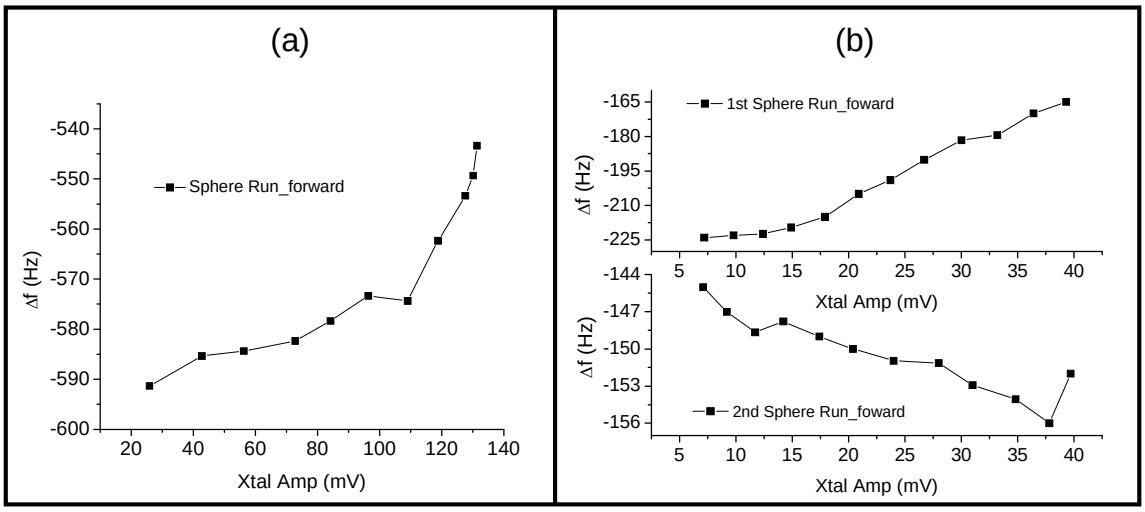

Figure 6.9 - (a) is the change in frequency with respect to crystal amplitude for the decoupling curve experiment shown in figure 3a. The to plots in (b) are the change in frequency with respect to crystal amplitude for the "wet" decoupling curve experiments displayed in figure 6a for the forward runs during the first and second sweeps.

According to figure 6.8 the trends displayed in both 6.9a and 6.9b are indicative of Coulomb type friction. This is quite possible for the experiment illustrated by plot 6.9a where the particles were clamped to the surface by capillary aging. This observation is similar to the situation described in the Vittorias et. al. study[8] for the case of annealed particles where they too observed Coulomb like friction behavior for clamped particles. For our experiments the environmental conditions along with the varying oscillation amplitude during decoupling curve runs influenced the contact area between our particles and the electrode. Even though the initial or "first sphere run" displayed in figure 6.9b suggest a Coulomb friction mechanism we realized that the majority of the observed behavior was a result of water drying on the surface due to the wet surface conditions which has little to do with the actual sphere decoupling friction mechanism. We therefore began our analysis of the observed sphere behavior at the "second sphere run" which according to 6.8c suggest a

"Mindlin[16] microslip" friction mechanism. However, after applying friction analysis mentioned in chapters 3 and 5 the frictrion law was primarily viscous (n=1.05). We illustrate in figure 10 an alternate mechanism that could result in the trend observed in figures 6.8c and 6.9b (run 2) for spheres in wet conditions (flooded contacts).

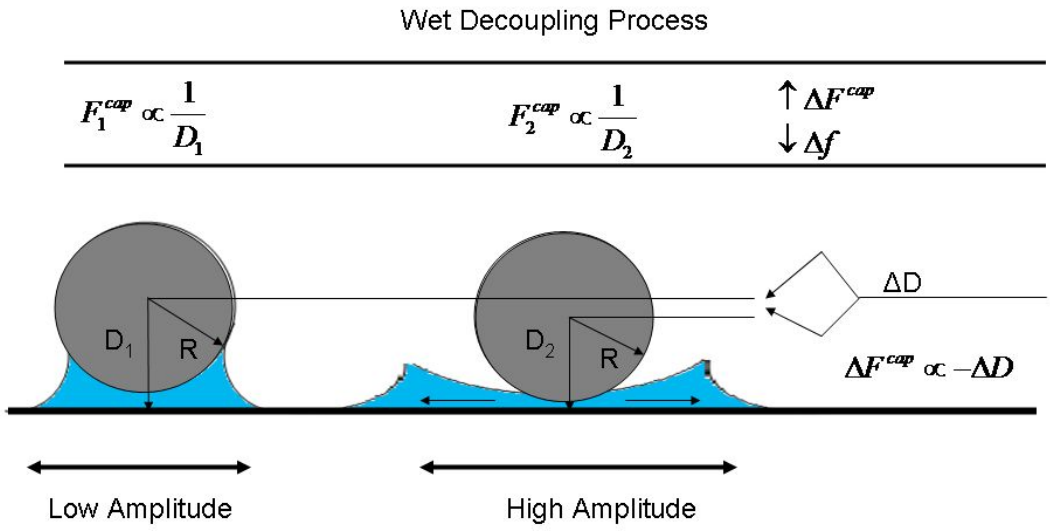

Figure 6.10 - Illustrates a mechanism that explains the trend displayed in figures 6.8c and 6.9b run 2 with out the presence of microslip. At increasing amplitude water in the flooded contact experiences an increase in mobility that draws the microsphere closer to the substrate increasing the loading force resulting in a negative shift in frequency.

The scenario shown in figure 10 is supported by the observed (figure 6.5) mobility of water on the surface of an oscillating QCM. Under these wet conditions it is reasonable to assume that the majority of the adsorbed spheres on the surface have there entire "buried" contact area flooded with water from the surface. At the lowest drive levels the water buried with in the contact has the lowest level of mobility and mainly serves to reduce the adhesive force with the surface (compared to when it is clamped down in solid-solid contact like the experiment shown in figure 6.9a) by increasing the separation distance between the sphere

and the QCM electrode which supports why we observed particle motion early in our decoupling curve (figure 6.7). As the oscillation amplitude is increased the buried water layer becomes more mobile as a result of the increase in shear force and therefore gains a sufficient amount of energy to escape the buried contact region which draws the particle closer to the surface as a result of the shear force exceeding the meniscus force as illustrated in Figure 6.10 above. One main implication of this mechanism is that the oscillation amplitude is sufficient to remove the water from the buried contact and induce mobility, we expect that as time increases and the contacts are able to dry this process becomes exceedingly difficult and will require larger drive levels to release the buried water. For some critical drying time this "wet decoupling process" will move shift to the strong coupling regime of the SLA and Dybwad models which was exactly what we observed for figures 6.3A and 6.9A.

6.5.3 DYNAMICS IN "DRY" CONDITIONS (TRANSFER EXPERIMENT)

In an effort to reduce the affect that capillaries have during QCM experiments and to analyze particle dynamics in a drier and thus more controlled environment we performed particle transfer experiments. In these experiments we deposited 15 micron diameter microspheres from aqueous solution in the usual manner on the electrode of a 5 MHz "gun" crystal. Our experimental 8 MHz "target" crystal was oriented below the gun to catch particles during the procedure. The transfer experiments were performed in a dry (approximately 1 atm of nitrogen gas) environment. After performing the experiment we observed particle motion during decoupling curve sweeps even though the majority of the particles landed in regions away from the center of the electrode where the oscillation

amplitude is highest. No such motion was observed for similar crystal amplitudes during experiments where the particles were left to air dry after deposition even though they were deposited at the center of the electrode. This observation supports that the transferred spheres from the “gun” QCM are landing on the target QCM and forming a weaker bond with the surface which is what is expected for a drier contact.

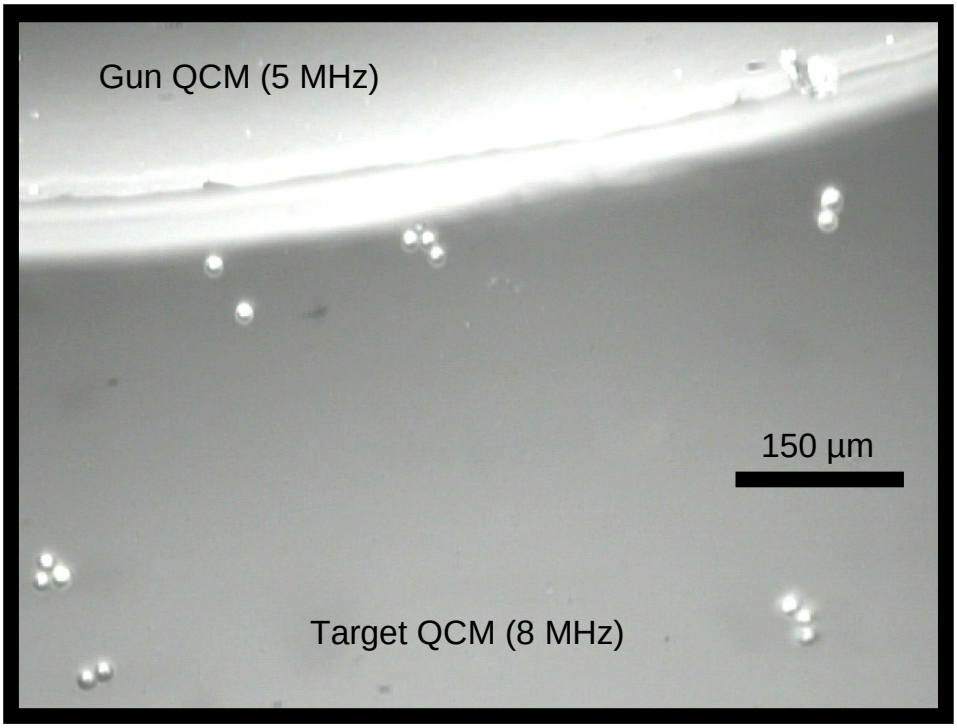

Figure 6.11 - Image taken after completing a successful transfer experiment.

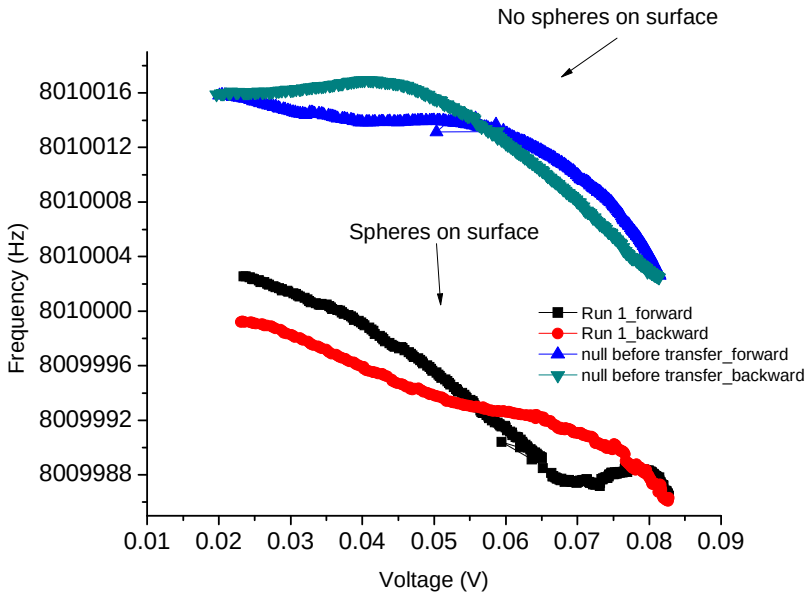

Figure 6.12 - Decoupling curves of the target QCM before and after the transfer experiment was performed.

The null run in figure 6.12 suggest that the target QCM was not clean and it was likely that a thin film of water along with containments were present on the sample. The trend suggest that the contamination particles were undergoing a wet decoupling friction mechanism. After successful transfer we observed a negative shift from resonance of 12 Hz which after applying equation (6.4) amounts to approximately 13 spheres on the electrode surface. After analyzing the surface via optical microscopy (figure 6.14) we counted a total of approximately 82 spheres which amounted to a considerable difference. This difference was of no surprise to us as a result of several factors. The first and possibly the most important factor is the fact that only a very small fraction of the spheres landed near the center of the QCM electrode where the sensitivity is a maximum[9] and falls off in a Gaussian manner radially outward. Another factor that influenced this difference was the fact that

particles of this size have been observed in the literature[8] to fall with in the intermediate range between strong and weak coupling where analysis is much more difficult. This transition was indeed observed in Figure 6.13 which shows an abrupt change in friction mechanism as a result of this newly formed contact from transfer. We compare these curves to a 15 micron decoupling curve experiment (Figure 6.14) performed under usual atmospheric conditions (lab air) and deposited from aqueous solution, the sample was then allowed a day to air dry.

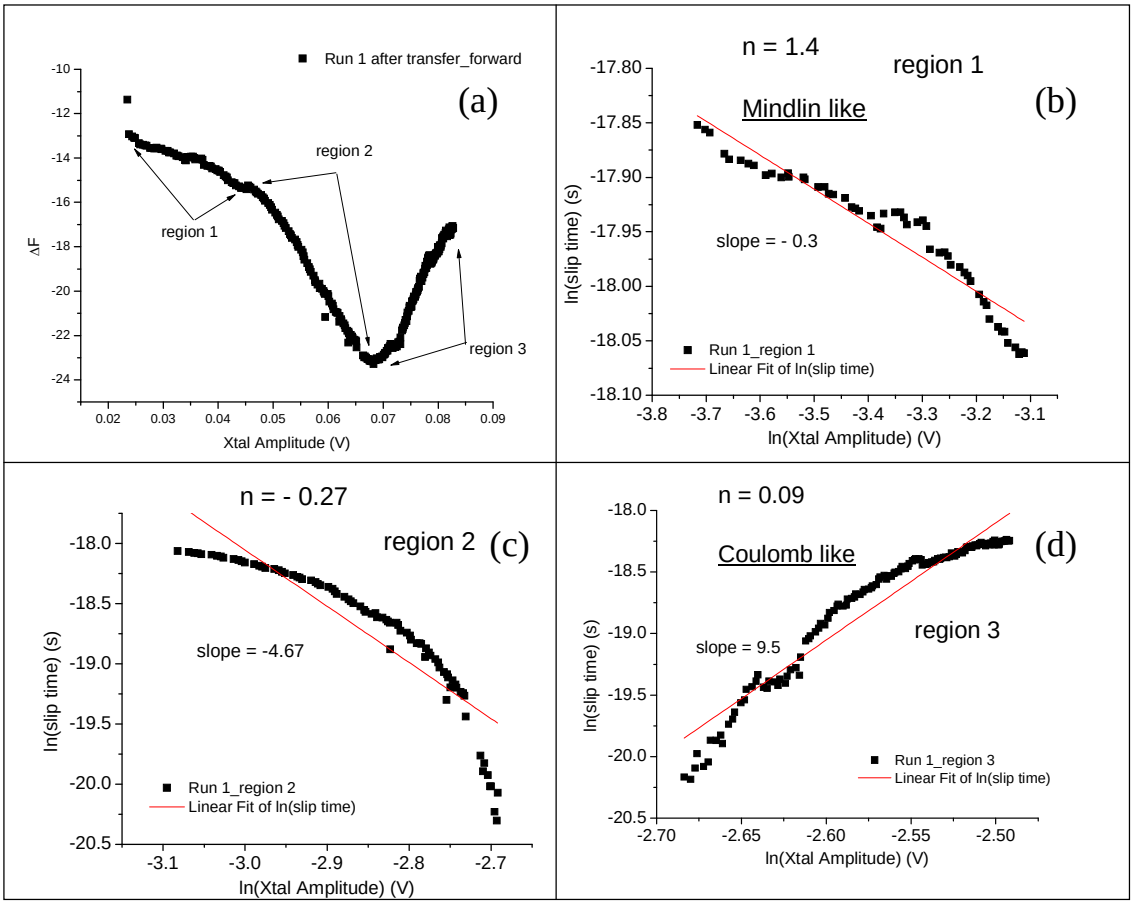

Figure 6.13 – Friction analysis of the target QCM after the transfer experiment was performed.

We observed particle motion (as indicated in figures 6.13a and 6.13b) spheres caught during the transfer experiment. This motion was first observed right around the time the friction mechanism changed as indicated by the varied trend in 6.13b. At the critical amplitude of 65 mV the particles experienced a Coulomb like friction law. This could be explained by the fact that the water layer the spheres are sliding on is very thin (perhaps even solid-like[17]) and as a result experiences a larger viscous force than would be expected normally (like in experiments displayed in 6.7a and 6.7b). If we think of it this way then when the oscillation amplitude is sufficient for supplying a shear force that overcomes the films viscosity (or yield stress if solid like) then the bond breaks and the interaction is the same as what was observed for particles in the strong coupling regime figure 6.3a.

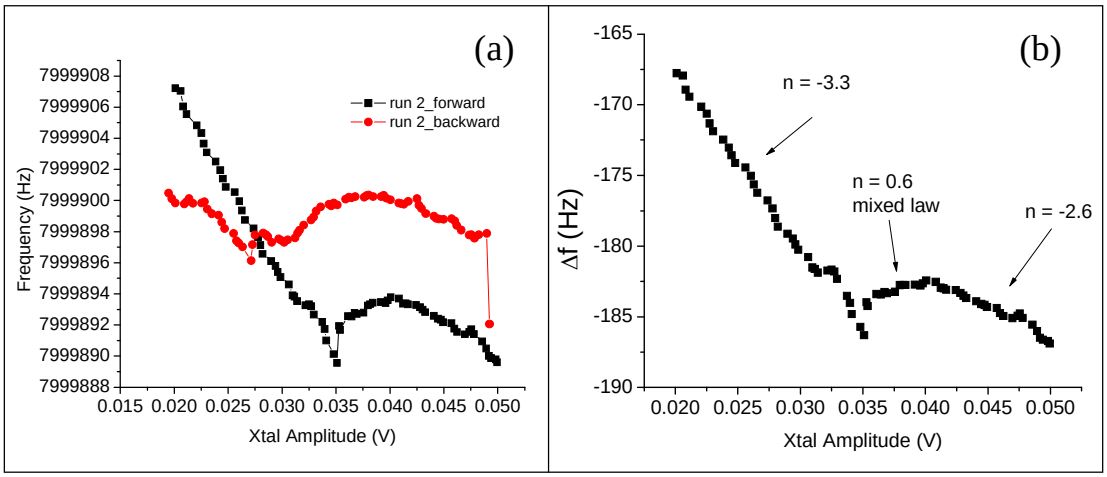

Figure 6.14 - Friction analysis of 15 micron microsphere sample deposited from aqueous solution. The sample was in the strong coupling regime of the Dybwad (SLA) model.

The decoupling curve shown in figure 6.14a exhibits a “stick-slip” like behavior as the amplitude increases to about 35 mV (the “mixed law” region). Figure 6.14b shows that the friction law transitions but does not change it’s inverse dependence on velocity. This lack of

alteration in friction mechanisms was the main difference between the dry and “semi-wet” (figure 6.14ab) experiments. Another difference is the appearance of Mindlin like partial slip in the dry experiment which is not present in the wet experiment.

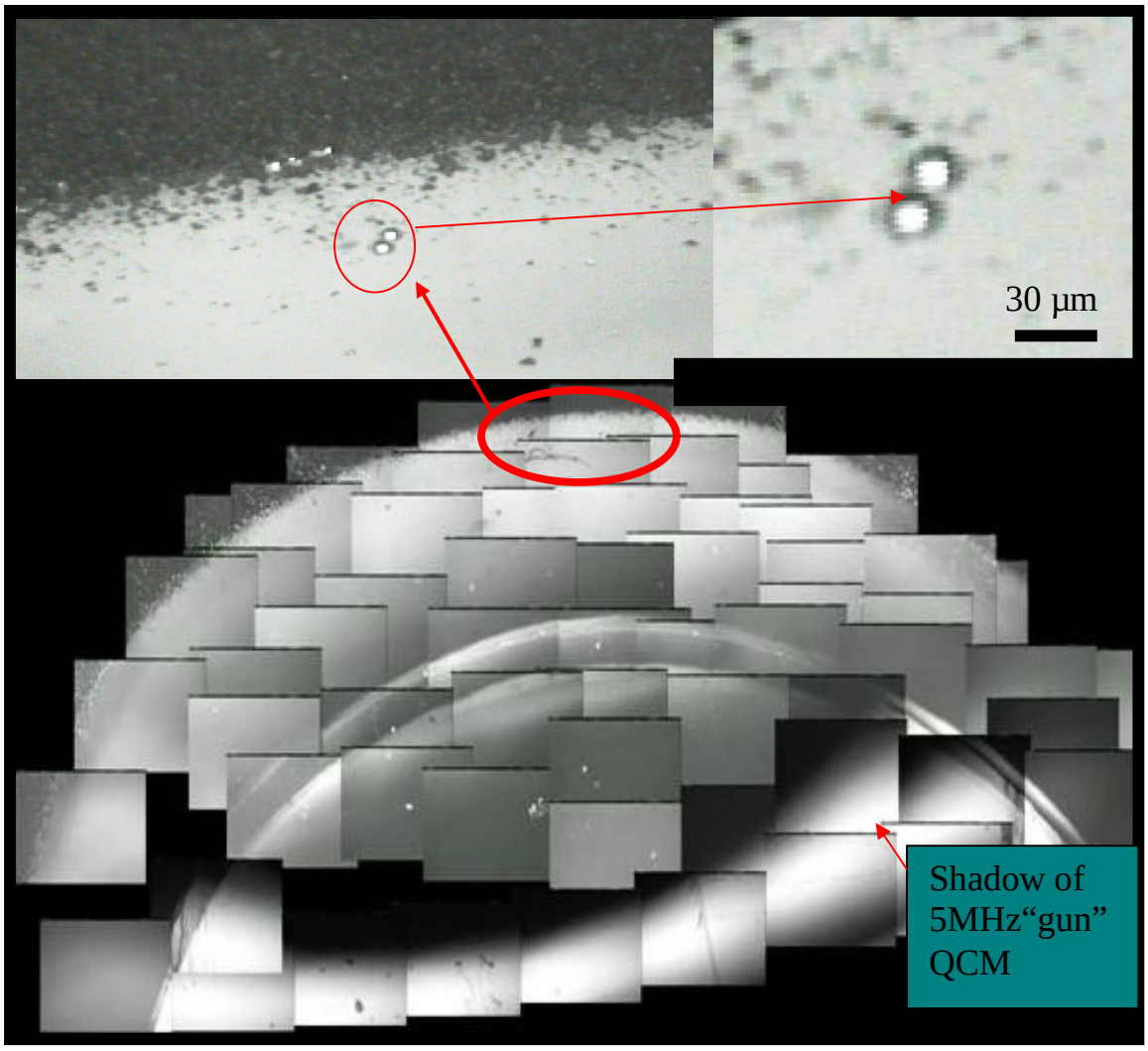

Figure 6.15 - The image above is a reconstruction of the QCMs used after the transfer experiment was performed. Each tile is an image with the dimensions of our optical region when adjusting the resolution to illuminate the spheres on the surface. Scratches were intentionally placed on the surface to provide a reference point when analyzing the distance from one image to another when spheres move on the surface. The highlight region is of a sphere caught near the edge of quartz where the QCM sensitivity would be minimal.

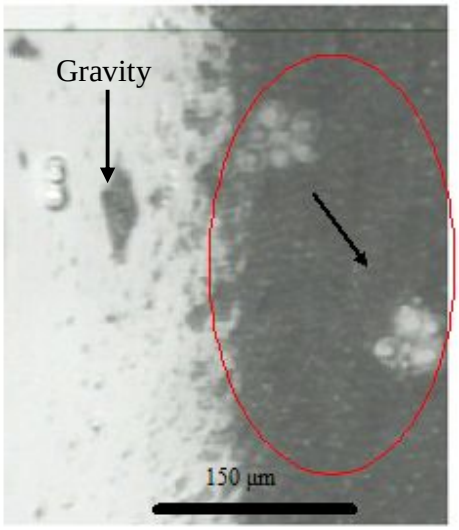

Figure 6.16 - The above photo consist of two images superimposed onto each other. The first image is of the surface oriented in the horizontal orientation and the second image is after the sample has been rotated in the vertical orientation where gravity has an affect. We observed particle motion on the rough (quartz) crystal side circled to the right due to gravity alone whereas no motion was observed for the particles that landed on the smoother polished gold electrode.

It was expected that the presence of microscale roughness greatly reduces the force of adhesion between two solids in contact. Figure 6.16 supports that the particles are indeed "drier" as indicated by the observed movement of a cluster of spheres on the rougher quartz region of the crystal from gravity alone. This observation supports the idea that roughness increases the separation distance between the particle and substrate which in turn weakens the force of adhesion (Van der Waals) which is inversely proportional to the square of the separation distance. If the particles on the quartz were wet at the contact the increased roughness of the quartz would have less of an effect on the force of adhesion which would be primarily a result of the liquid meniscus force. Since the landed particles are presumably drier there attraction to the surface would result from a Van der Waals interaction which is

sufficient to hold them on the surface (provided the separation distance between the particles and the surface is small enough).

6.5.4 DYNAMICS IN VARIED ENVIRONMENTAL CONDITIONS

Several decoupling curve experiments were performed in the vacuum chamber to observe how altering the environment of a sample affects the friction. These experiments were performed on a sample with 5 micron diameter spheres deposited from aqueous solution. No motion was observed in the optical region during these decoupling curve runs. Friction laws (n) for these experiments were determined using methods outlined in chapters 3 and 5 of this thesis. All of the experiments resided in the strong coupling regime of the Dybwad model which allowed for calculation of slip times. These slip time values were computed relative to the inertial loading point (largest (magnitude) shift in frequency from resonance) as shown in figure 6.17. The runs performed in air and vacuum show similar decoupling curve trends as well as friction laws. The vacuum experiment resulted in a slightly more viscous like friction law (less decoupling) which suggested that the average particle adhesion increased as a result of introducing vacuum. The dry nitrogen environment showed transition if frictional behavior from a “slightly more viscous” than “Coulomb like” friction law to a slipping mechanism that was inversely proportional to the cube of velocity. This type of friction law ($F \propto v^{-n}$) was observed in the decoupling curve experiments performed on 15 micron spheres (figures 16.14ab). The implication from this result is that the removal excess water layers on the surface can cause 5 micron spheres that strongly bonded to the surface and behave like ordinary physisorbed systems into a slipping mechanism similar to what was observed for the larger 15 micron particles.

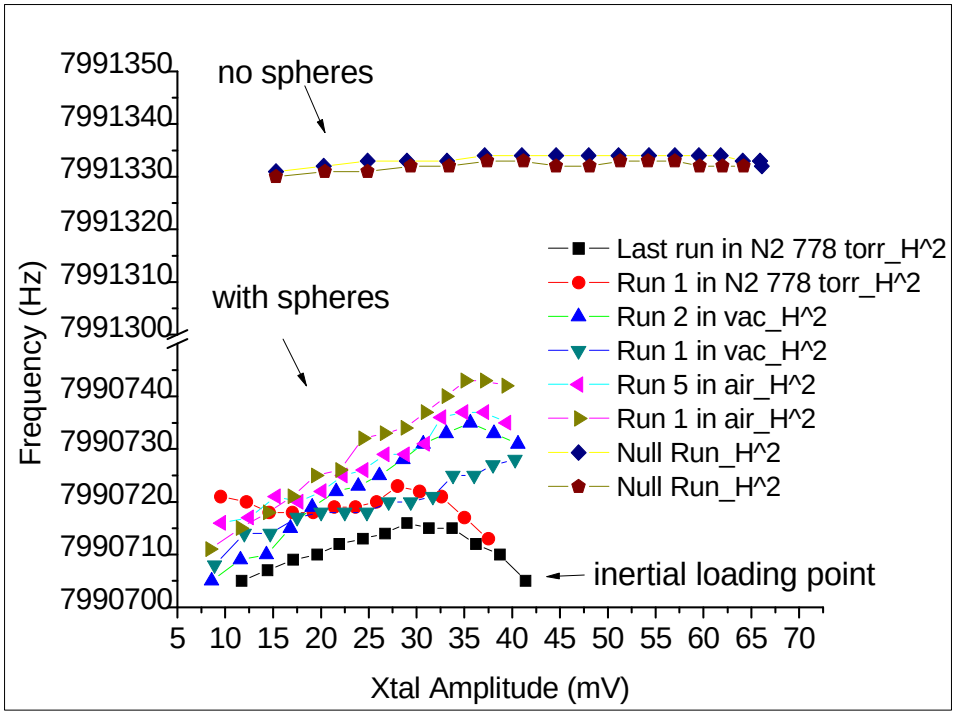

Figure 6.17 - Decoupling curves (forward runs only) for the same sample studied in the varied environments of air, vacuum (1E-3 torr), and dry nitrogen (N2). The H^2 denotes that the mounting orientation is horizontal or parallel with the surface (normal to gravity).

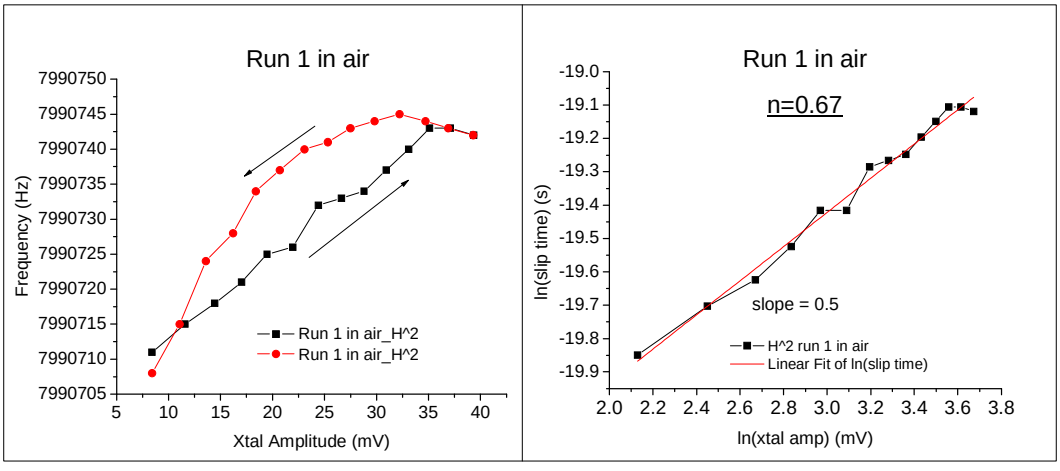

Figure 6.18 -First decoupling curve run in air (approximately 35% r.h.) is shown in (a). The friction analysis of the forward sweep in the decoupling curve is shown in (b).

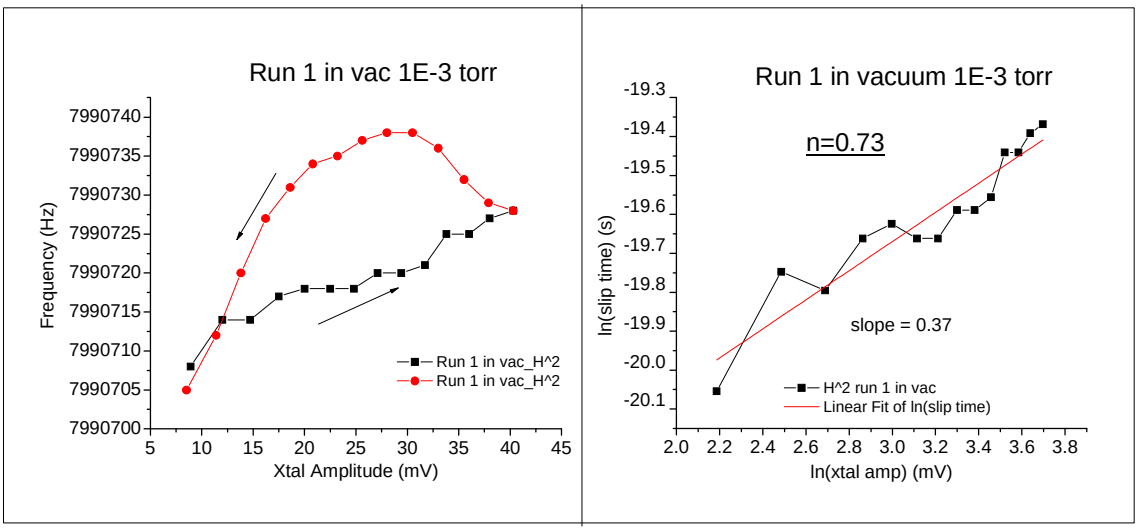

Figure 6.19 - First decoupling curve run in 1E-3 torr vacuum environment is shown in (a). The friction analysis of the forward sweep in the decoupling curve is shown in (b).

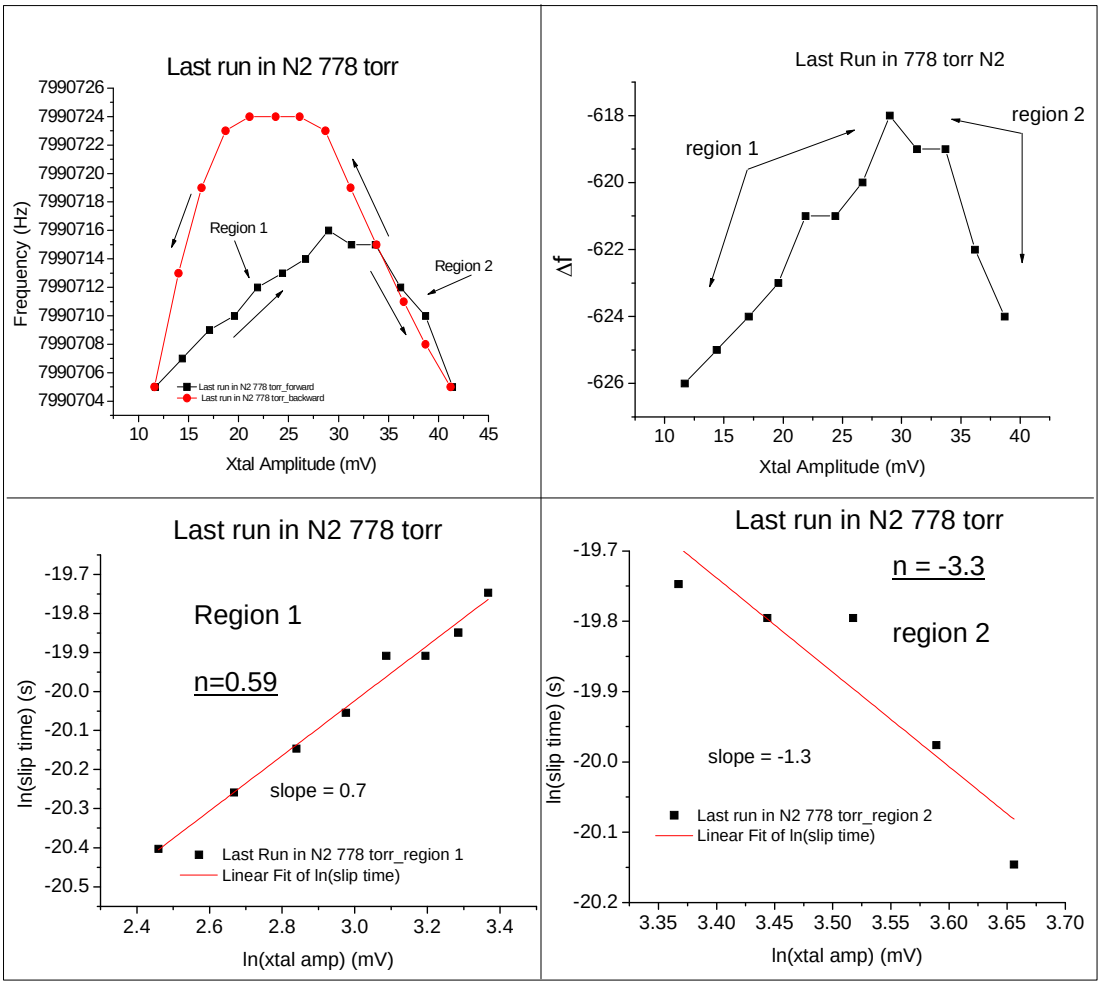

Figure 6.20 - Last decoupling curve run in 778 torr dry nitrogen environment is shown in (a). The frequency shift from resonance of the forward decoupling curve run is shown in (b). Friction analysis of the forward sweep in the decoupling curve is shown in (c) and (d).

6.6 PARTICLE MOTION

When studying the dynamics and motion of the microspheres on the QCM electrode it was not uncommon for us to generate sphere motion by rapidly varying our power supply to create a jerk response in the crystal that would aid in removing the stronger bonds. When this was not sufficient in generating motion we moved to a stronger power source and in

doing so observed some very interesting behavior. The microspheres on the surface of a QCM experience an extreme shear force resulting from the high frequency oscillation of the QCM that governs there observed surface dynamics. The rapidly changing direction of this force causes particles to "ratchet" along the surface of the electrode. A maximum value for the distance a microsphere (we report here results for the 5 micron diameter spheres) travels for the duration the peak force acts on the sphere can be approximated provided a few assumptions. The first assumption is that kinematic equations apply for the non inertial reference frame of an oscillating QCM. If we solve the problem for the time $(1/2f_0)$ at which the peak force acts on the microsphere we find that this force acts in one direction making it a reasonable approximation to assume the acceleration is constant thus allowing the use of kinematic equations. The next assumption is that the microsphere is stationary which is artificial since the microsphere before detachment is initially moving at a velocity equal to the velocity of the QCM however, the direction in which that vector is pointing is not so obvious due to a lack of knowledge regarding the bond rupture mechanism. As a result we assume set the initial velocity to zero to provide an "order of magnitude" approximation of sliding distance. In the absence of friction the one dimensional sliding distance becomes $\frac{A\pi^2}{2}$ were A is the oscillation amplitude of the QCM. An oscillation amplitude A=21nm (which was easily achieved by our strong power source) would result in a sliding distance of 0.1 microns. The shortest time span we could observe with our dvd recorder was 0.01s. The measurement of 0.1 microns was for the duration of half an oscillation period, in the unlikely case that in 0.01s or 80,000 periods this force only induced

motion in one direction during the observation time a sphere would travel approximately 640 m or 0.4 miles. We stated previously that particles tightly bound to the surface via capillary interaction are more likely to undergo a coulomb type friction mechanism during bond rupture. Inserting this resistive term into our distance approximation we obtain

$$d_{sliding} = \frac{n_{odd}^2}{2}\left[\pi^2 A - \frac{\mu_k F_{adh}}{4 m_s f_0^2}\right]. \qquad (6.10)$$

where n_{odd} is the total number of odd cycles (periods), A is the amplitude of oscillation, μ_k is the coefficient of kinetic friction, F_{adh} is the force of adhesion (capillary or Van der Waals), $m_s = 7 \times 10^{-14} kg$ is the mass of the loading (5 micron diameter) particle, and f_0 is the resonant frequency (8 MHz) of QCM.

Plugging in typical values $\mu_k = 0.5$ and $F_{adh} = F_{cap} = 2\mu N$ results in a decrease of approximately 55 nm per half cycle which would result in a sliding distance over a period 0.01s to now be 228 m or 0.1 miles which is an appreciable decrease in motion. This example is of course highly unrealistic since the particle has an "equal" probability to be translated in either direction along the surface. When analyzing the dynamics this competing aspect is immediately obvious especially when drive levels are high and motion is substantial. In the Vittorias[8] experiment they observed 3 main modes scenarios of particle dynamics from analyzing deformation patterns. They found that it is not uncommon for microspheres to remain at one location for a large number of periods before sliding. The authors observed shear deformation patterns which indicates the spheres were sliding however, this does not rule out the possibility of rolling. One particularly interesting observation was particles leaving the surface in via hopping from place to place. We hooked

the sample shown in figure 6.5 up to our strong power source to stimulate particle motion on this wet surface. We observed many interesting dynamics including the hopping described earlier. Particles generally moved in along the direction of oscillation however, if they were confined in cracks or defects on the surface the followed the path of the defect or pinning site until the oscillation was sufficient to eject it from its potential barrier. This may aid in achieving controlled or at the very least enhancing microparticle manipulation and control via intentional defect regions for "guiding" microparticles. We also observed what appeared to be motion influenced by charge interactions between microparticles. These cases involved microspheres in sync with out actually touching its neighbor. Since our surface was wet we observed many interesting dynamics influenced by the water on the surface. For aggregated microsphere islands whose contacts were completely immersed we observed in real time the water ejecting from the many contacts within the island.

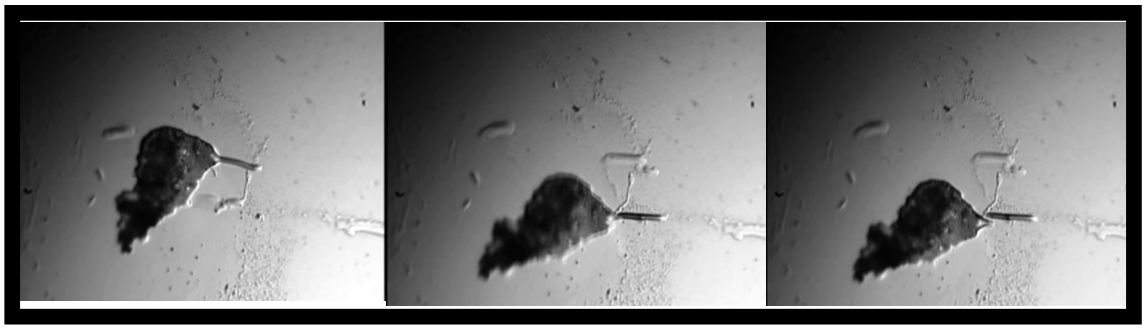

Figure 6.21 - Dynamics of a partially immersed cluster of aggregated spheres during rapidly varying the drive voltage of our strong power source. We observed that the shear stresses were sufficient enough to squeeze water from confined regions within the cluster.

In this study we have demonstrated methods for interpreting average particle behavior on during QCM experiments mainly through realizing the possibility of wet decoupling. We have shown overwhelming evidence that the effects of water during QCM experiments can not be ignored and in many cases govern the dynamics as a whole on the surface. The affects of dissipation (bandwidth shift) were not reported on in this study however, it is important to realize that water will have a huge affect on the dissipation data especially under a wet decoupling mechanism. We introduced a new method for decreasing the presence of water during QCM experiments and provided sufficient evidence that upon landing the overall system force of adhesion is greatly reduced and reflected in both the decoupling and delta frequency plots. Particle transfer experiments have the potential for many fundamental applications of better understanding the friction mechanism at microscale. It is possible with a customized chamber one could measure the friction force directly after a transfer experiment by orienting the chamber vertically (figure 6.16) in a controlled manner recording the dynamics and rotation angle during the experiment. In this study we have

found that the analysis of decoupling curves can be quite complex due to the inconsistent bond strength of the spheres on the surface and the multiple paths spheres can take once in motion. Due to the nature of the deposition and the sub-monolayer surface configuration hysteresis and non uniformity can somewhat be expected in these decoupling curves. The notion of micro particle sorting as suggested by the observed particle motion is not a straight forward task especially in humid/wet environments. However, it may be easier to achieve such control and sorting in a dry environment such as particles on the surface after a transfer experiment. Future work must be done to see if movement can be better controlled and understood.

Acknowledgments:

The authors would like to acknowledge Edward Stevens for his help in constructing images.

6.7 REFERENCES

1. Hirst, E. R.; Yuan, Y. J.; Xu, W. L.; Bronlund, J. E., Bond-rupture immunosensors--A review. *Biosensors and Bioelectronics* 2008, *23* (12), 1759-1768.

2. Rivet, C.; Lee, H.; Hirsch, A.; Hamilton, S.; Lu, H., Microfluidics for medical diagnostics and biosensors. *Chemical Engineering Science* 2011, *66* (7), 1490-1507.

3. Dybwad, G. L., A sensitive new method for the determination of adhesive bonding between a particle and a substrate. *Journal of Applied Physics* 1985, *58* (7), 2789-2789.

4. Flanigan, C. M.; Desai, M.; Shull, K. R., Contact Mechanics Studies with the Quartz Crystal Microbalance. *Langmuir* 2000, *16* (25), 9825-9829.

5. D'Amour, J. N.; Stålgren, J. J. R.; Kanazawa, K. K.; Frank, C. W.; Rodahl, M.; Johannsmann, D., Capillary Aging of the Contacts between Glass Spheres and a Quartz Resonator Surface. *Physical Review Letters* 2006, *96* (5), 058301-058301.

6. Ellis, J. S.; Thompson, M., Acoustic physics of surface-attached biochemical species. *HFSP Journal* 2008, *2* (4), 171-177.

7. Dultsev, F. N.; Ostanin, V. P.; Klenerman, D., "Hearing" Bond Breakage. Measurement of Bond Rupture Forces Using a Quartz Crystal Microbalance. *Langmuir* 2000, *16* (11), 5036-5040.

8. Vittorias, E.; Kappl, M.; Butt, H.-J.; Johannsmann, D., Studying mechanical microcontacts of fine particles with the quartz crystal microbalance. *Powder Technology* 2010, *203* (3), 489-502.

9. Seah, P. J. C. a. M. P., The quartz crystal microbalance; radial/polar dependence of mass sensitivity both on and off the electrodes. *Measurement Science and Technology* 1990, *1* (7), 544-555.

10. Sauerbrey, G., Verwendung von Schwingquarzen zur Wägung dünner Schichten und zur Mikrowägung. *Zeitschrift für Physik* 1959, *155* (2), 206-222.

11. Johannsmann, D., Viscoelastic, mechanical, and dielectric measurements on complex samples with the quartz crystal microbalance. *Physical Chemistry Chemical Physics* 2008, *10* (31), 4516-4516.

12. (a) Dultsev, F. N.; Speight, R. E.; Fiorini, M. T.; Blackburn, J. M.; Abell, C.; Ostanin, V. P.; Klenerman, D., Direct and Quantitative Detection of Bacteriophage by "Hearing" Surface Detachment Using a Quartz Crystal Microbalance. *Analytical Chemistry* 2001, *73*

(16), 3935-3939; (b) Cooper, M. A., Biosensing using rupture event scanning (REVS) . *Measurement Science and Technology* 2003, *14* (11), 1888-1893.

13. Derjaguin, B., Untersuchungen über die Reibung und Adhäsion, IV - Theorie des Anhaftens kleiner Teilchen. *Kolloid-Zeitschrift* 1934, *69* (2), 155-164.

14. Israelachvili, J., *Intermolecular and Surface Forces*. Elsevier: (1985-2004); Vol. 2.

15. Mate, C. M., *Tribology on the small scale a bottom up approach to friction,lubrication, and wear*. Oxford University Press: New York, 2008; Vol. 1, p 333.

16. Deresiewicz, R. D. M. a. H., Elastic spheres in contact under varying oblique forces. *Journal of Applied Mechanics* 1953, *20*, 327-344.

17. Peachey, J.; Van Alsten, J.; Granick, S., Design of an apparatus to measure the shear response of ultrathin liquid films. *Review of Scientific Instruments* 1991, *62* (2), 463-463.

CHAPTER 7 – STUDIES OF DYNAMICS OF MICROSPHERES IN VARIED FRICTION REGIMES

7.1 WATER DECOUPLING EXPERIMENT IN AIR

In the sections that follow below unless otherwise stated I deposited 15 micron polystyrene sphere from aqueous solution onto the electrode of a QCM in ordinary (30% - 40% rh) lab air. With this in mind a baseline experiment was performed to show the effect a dried water layer has on the surface of our experimental QCM. This baseline was important in determining the true "null" frequency behavior of our sample. When analyzing the frictional behavior of the microspheres deposited on the surface it was extremely important to have the proper mass loading frequency value so that slip time (frictional) measurements would be as accurate as possible. The water droplet was deposited in the same manner as microspheres. It was drawn from a glass pipette and blown with helium flow to remove bulk water layers, the sample was then left out to air dry overnight before experiments were performed. The results of this experiment are displayed below in figure 7.1. The dried water layer is in the strong coupling regime of the Dybwad model[1] (negative shift from resonance) which means the particles are strongly coupled to the surface and the Sauerbrey equation[2] can be used to approximate the mass of the film which is approximately 70 ng. Friction laws "n" and slip times were calculated using methods outlined in chapters 3, 5, and 6 of this thesis. As shown in figure 7.1 (b) the frictional behavior throughout a forward sweep of a decoupling curve is not always uniform and thus the plots are split into regions in order to obtain a more detailed

description of the actual physical response of the system. The results (7.1 (c) and 7.1 (d)) show that a dried water layer decouples with a Coulomb like friction law and behaves like typical[3] (see chapter 5) physisorbed particles. The slip times for this experiment ranged between 1.5-12.6 ns. In later experiments the range of crystal (xtal) amplitude values swept during forward decoupling curve runs exceeds the maximum value of 67 mV achieved in this water null run. In these cases the analysis is completed by finding the equation of the line associated with the decoupling curve and extending this line out to the needed xtal amplitude values. This estimation is supported by the results reported in chapter 5 that show (physisorbed particle) decoupling continues at a constant rate once the previous maximum amplitude is exceeded.

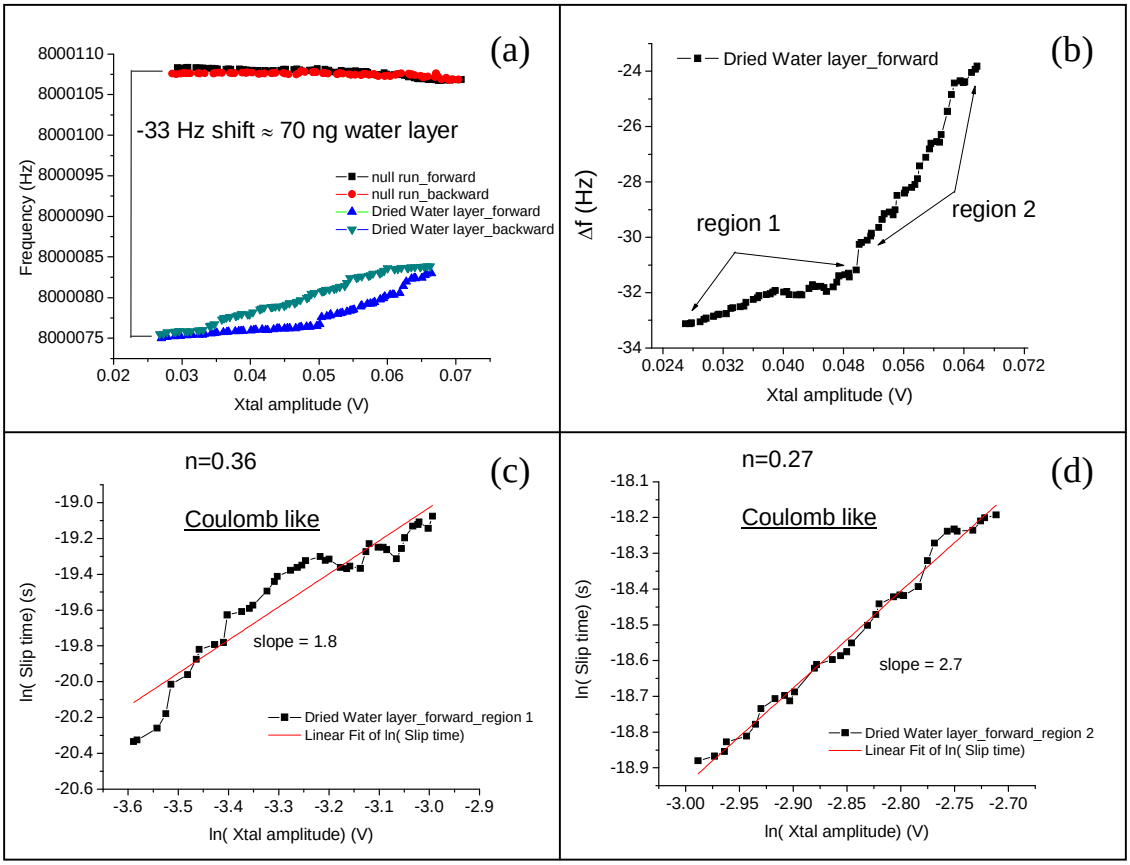

Figure 7.1 - Results of water decoupling experiment in air.

7.2 EXPERIMENT IN AIR OF 15 MICRON SPHERES DEPOSITED FROM AQUEOUS SOLUTION IN HORIZONTAL ORIENTATION

In the following experiment shown in figures 7.2-7.8 15 micron diameter polystyrene microspheres were deposited from aqueous solution (in the same manner as the water droplet experiment) on the same QCM that was used to perform the water decoupling experiment. Three decoupling curve runs were performed on this sample and the detailed analysis of the frictional behavior is outlined in the sections that follow.

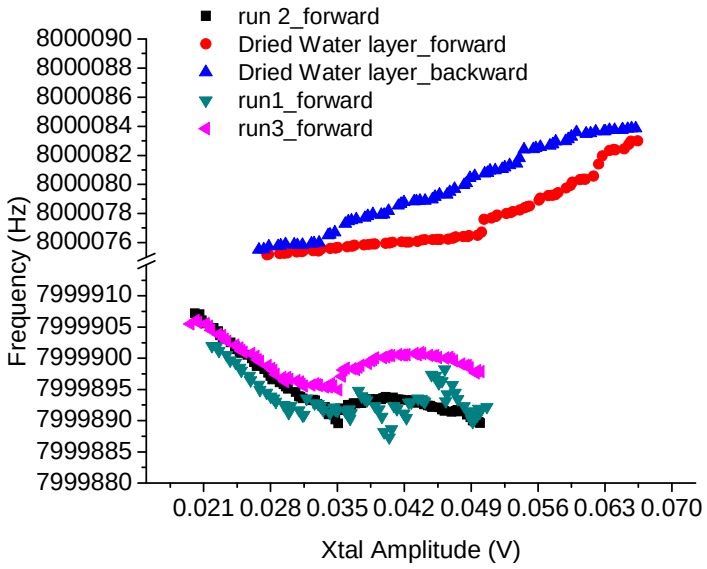

Figure 7.2 - A plot of the water decoupling curve experiment with the forward decoupling curve runs of the three experiments performed after microspheres were deposited.

From figure 7.2 above shows that the microspheres were initially in the strong coupling regime of the Dybwad model. Microspheres with this size (15 microns) have been observed[4] to fall near the intermediate regime (between strong and weak coupling) of the Dybwad model. This suggest that if sufficient changes are made in the average coupling strength of the particles the system could move to the weak coupling regime. In section 7.3 we present data that shows this is indeed the case. The trend in the decoupling curves above suggest that the friction mechanism these particles undergo is different then that of physisorbed particles.

7.2.1 RUN 1 FRICTION ANALYSIS

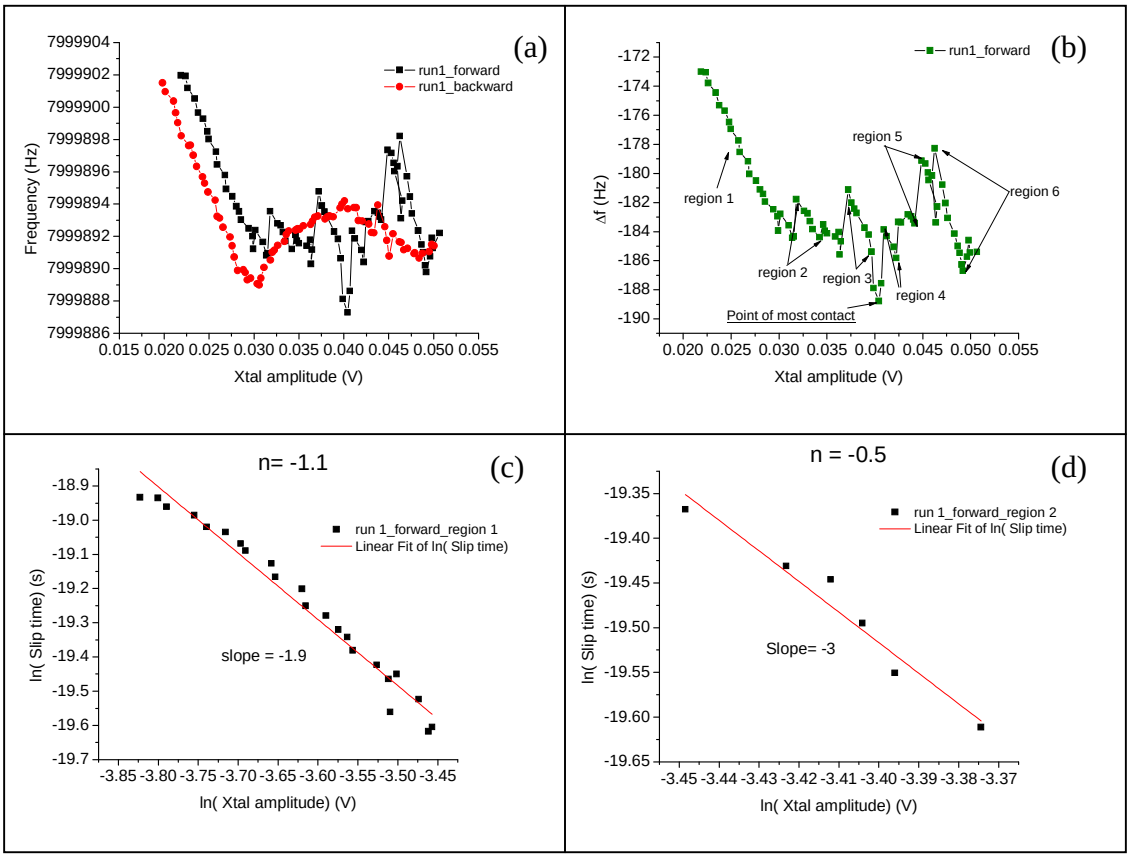

Figure 7.3 - Friction analysis of the first decoupling curve run

The decoupling curve shown in figure 7.3 a shows an initial decrease in frequency with several jagged “stick-slip” like events that follow. This type of downward trend (also shown in 7.3b) suggest a “Mindlin like” slipping mechanism according to previous studies[4] however, after analyzing the regions outlined in 7.3b we observed slipping mechanism that is different then what is expected of Mindlin like slipping (n>1). As previously discussed in chapters 3,5, and 6 the slip time of sliding particles is a function of the mass or “inertial” frequency shift. For small physisorbed particles such as films this value is the shift in

frequency from resonance observed when the sample is initially oscillated as shown in section 7.1 for the water decoupling experiment. Performing a decoupling curve on these type of particles only increases (lowers the mass via "decoupling") the frequency from the initial mass loading shift this however is not the case for the trend shown in figure 7.3a-b. From chapter 3 of this thesis I discussed how the shift in frequency from mass loading is directly proportional to the contact area of the loaded particles and the QCM. The observed trend suggest that the mass/contact area of surface particles increases as the velocity of the substrate is increased (xtal amplitude). The data above implies that the slipping mechanism involved in this experiment is one in which the average contact area of the particles increases with increased shearing. This type of behavior has been observed before[5] for 3mm copper spheres under tangential loading against a sapphire flat. The authors observed a growth in the contacting junction (contact area increase) between sphere and flat as the tangential force increased. In figure 7.3b the area labeled "point of most contact" (-188.7 Hz) is the value used for the mass loading frequency in the slip time calculations which ranged from 1.3-6 ns. For all sloped regions (1-4, and 6) shown in figures 7.3c-d and 7.4abd the friction law or slipping mechanism observed for the particles was inversely related to velocity ($n<1$). In region 5 the analyzed portion was a transition region or "stick" region between 2 sloped or slipping regions. This transition region exhibited a Coulomb like (n close to zero with very little velocity dependence) friction mechanism. No particle motion was observed in the optical region during these experiments (runs 1-3).

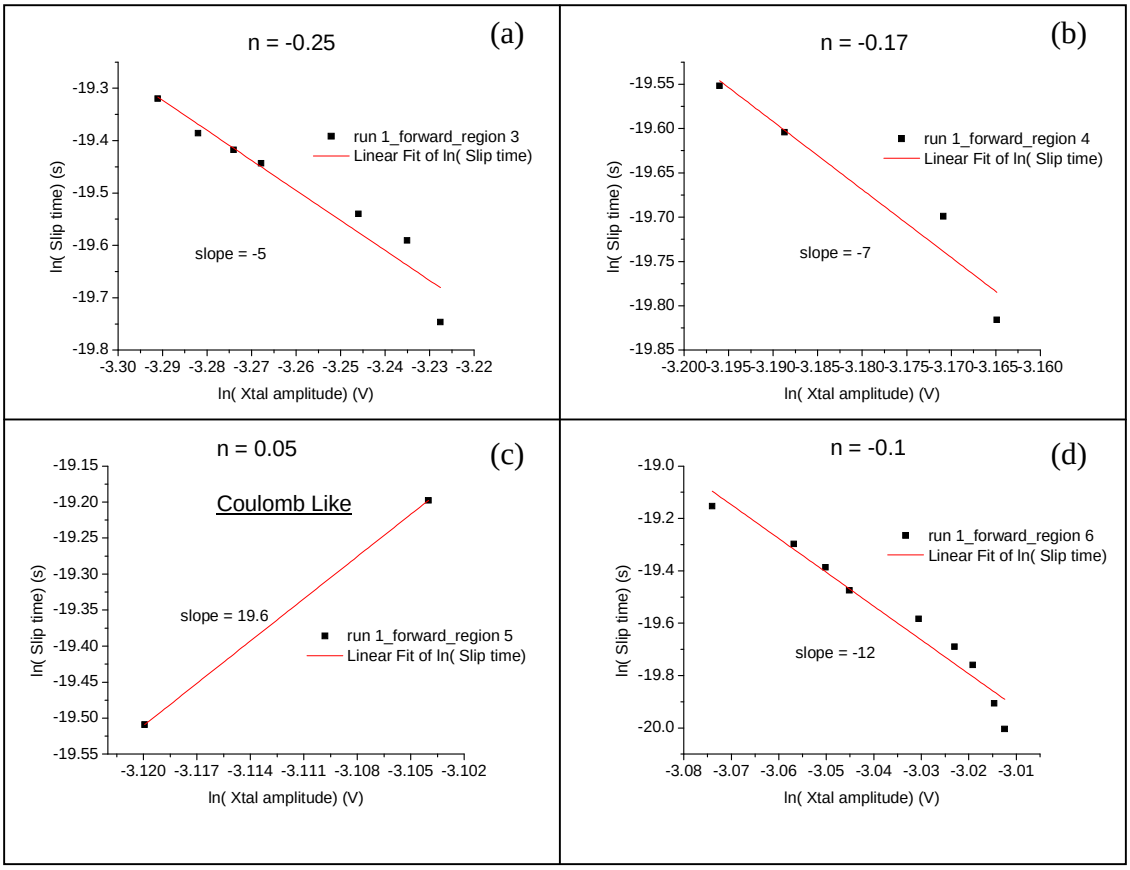

Figure 7.4 -Ccontinued friction analysis of run 1

7.2.2 RUN 2 FRICTION ANALYSIS

The decoupling curve shown in figure 7.4a is “smoother” than what was shown in run 1 and displays less frequent slipping (sloped) regions than what was observed for the initial run. This may indicate that as successive decoupling curve experiments are performed less particles are mobile on the surface as a result of migration to pinning sites from the initial run. The overall trend of the decoupling curve is however quite similar to what was observed for the initial run. As indicated by figures 7.5 and 7.6 when slipping (downward slopping regions) the force law that the particles follow is inversely proportional to velocity whereas,

the transition regions (jumps in the graph) are a mixture of viscous and Coulomb like friction laws.

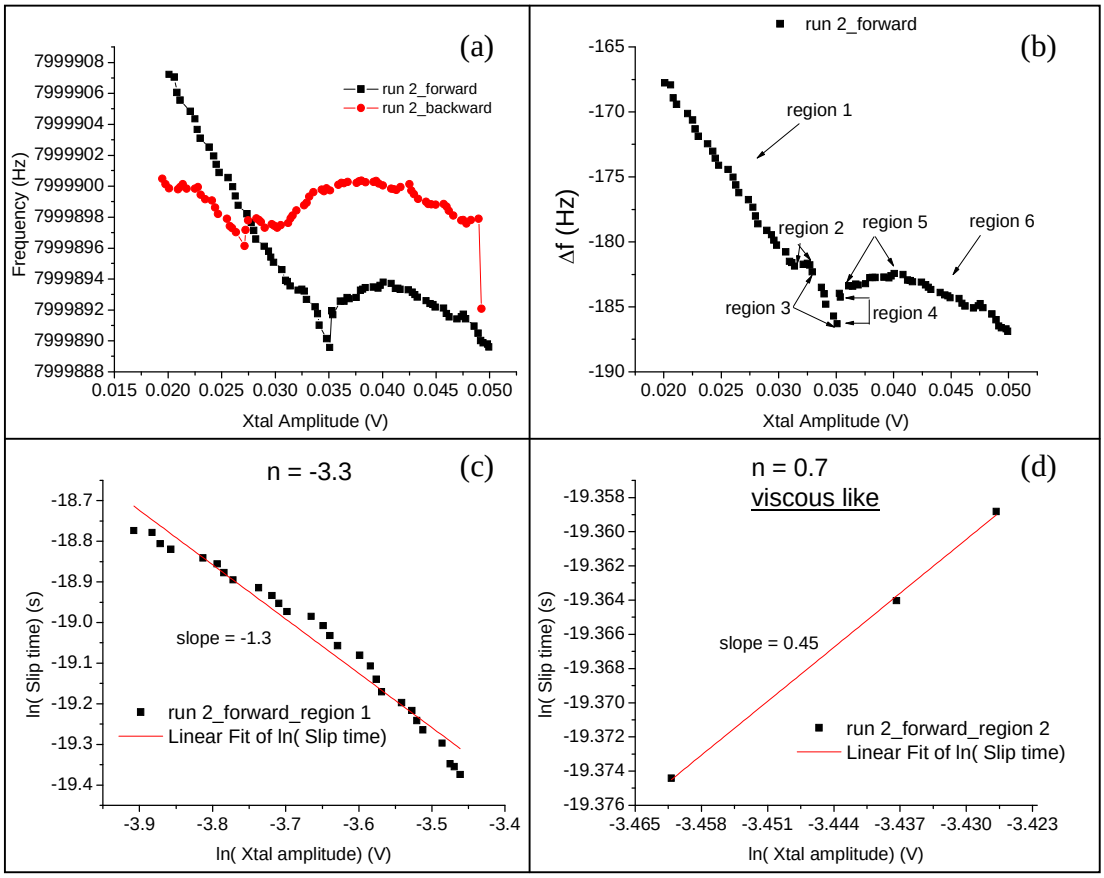

Figure 7.5 - Friction analysis of Run 2 decoupling curve

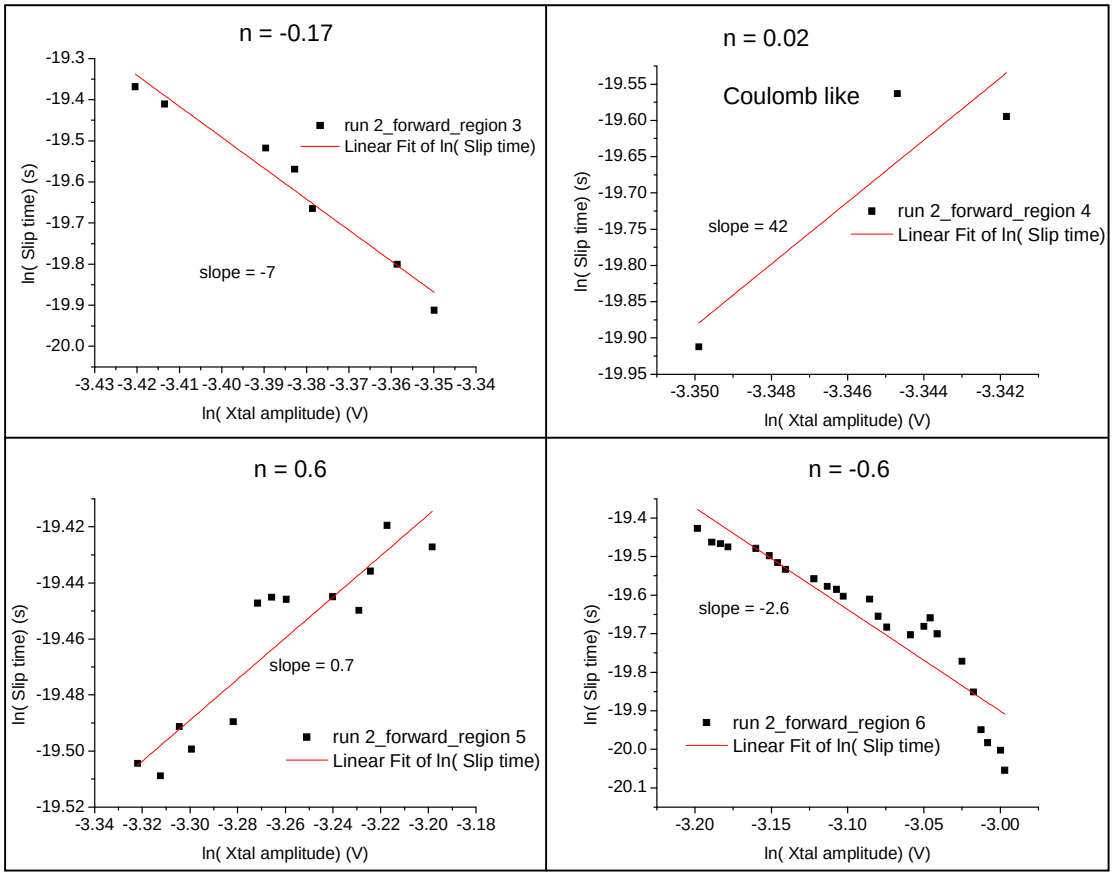

Figure 7.6 - Continued friction analysis of Run 2

7.2.3 RUN 3 FRICTION ANALYSIS

The analysis performed in figures 7.7 and 7.8 show that the friction law has completely changed from what was observed in the two previous runs. It is reasonable to assume from this observation that the majority of the particles on the surface have moved to pinning sites and when pinned the friction law changes from one that is inversely proportional to velocity to one that is observed for granular particles a “Mindlin” like partial slip.

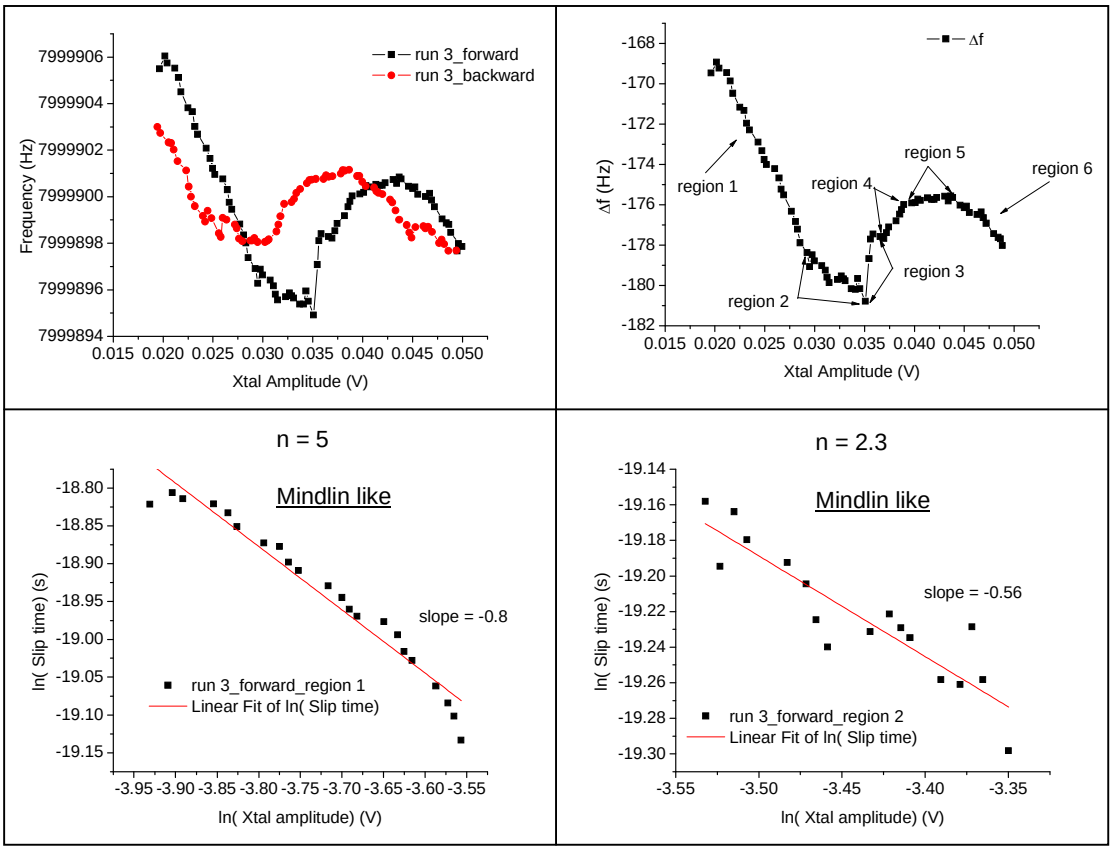

Figure 7.7 -Friction analysis of Run 3

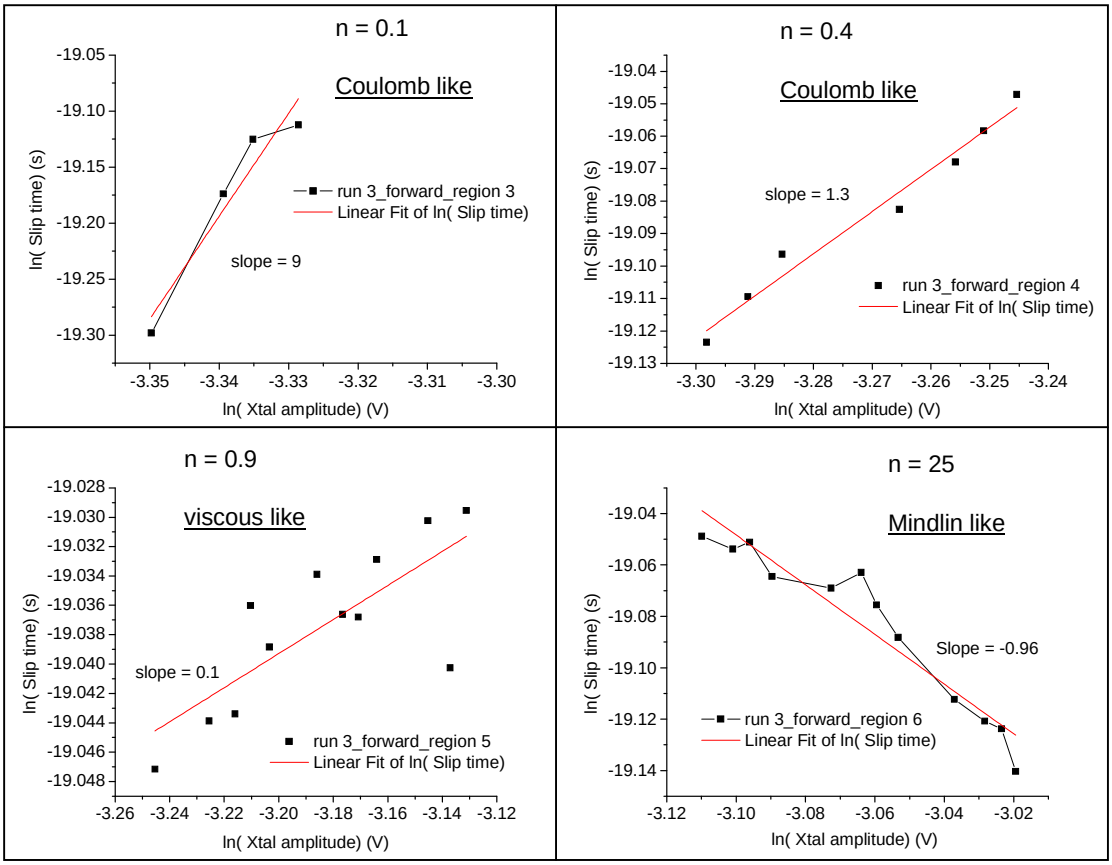

Figure 7.8 - Continued friction analysis of Run 3

7.3 EXPERIMENT IN AIR OF 15 MICRON SPHERES DEPOSITED FROM AQUEOUS SOLUTION IN HORIZONTAL ORIENTATION AFTER INTENTIONALLY DISRUPTING SURFACE BY INDUCING PARTICLE MOTION.

No motion was observed for the decoupling curves studied in section 7.2. In order to generate motion on the surface the sample was connected to a separate oscillator circuit that was tuned to output a larger voltage. When doing so significant motion was observed with

fraction of spheres leaving the surface. Once the motion generation experiment was complete the sample was connected back on the original electronics to perform additional decoupling curves. The aim was to observe the effect shaking and depinning of the particles would have on the decoupling curves. We found that system as indicated by figures 7.9 and 7.10 moved into the weak coupling regime of the Dybwad model. This was an interesting find but, not a complete surprise since particles of this size (15 microns) have been observed in the literature[4] to fall in to the intermediate coupling regime of the Dybwad model. Detailed friction analysis was not performed for this experiment since our method requires that the particles are in the strong coupling regime of the Dybwad model as discussed in chapter 3 of this thesis.

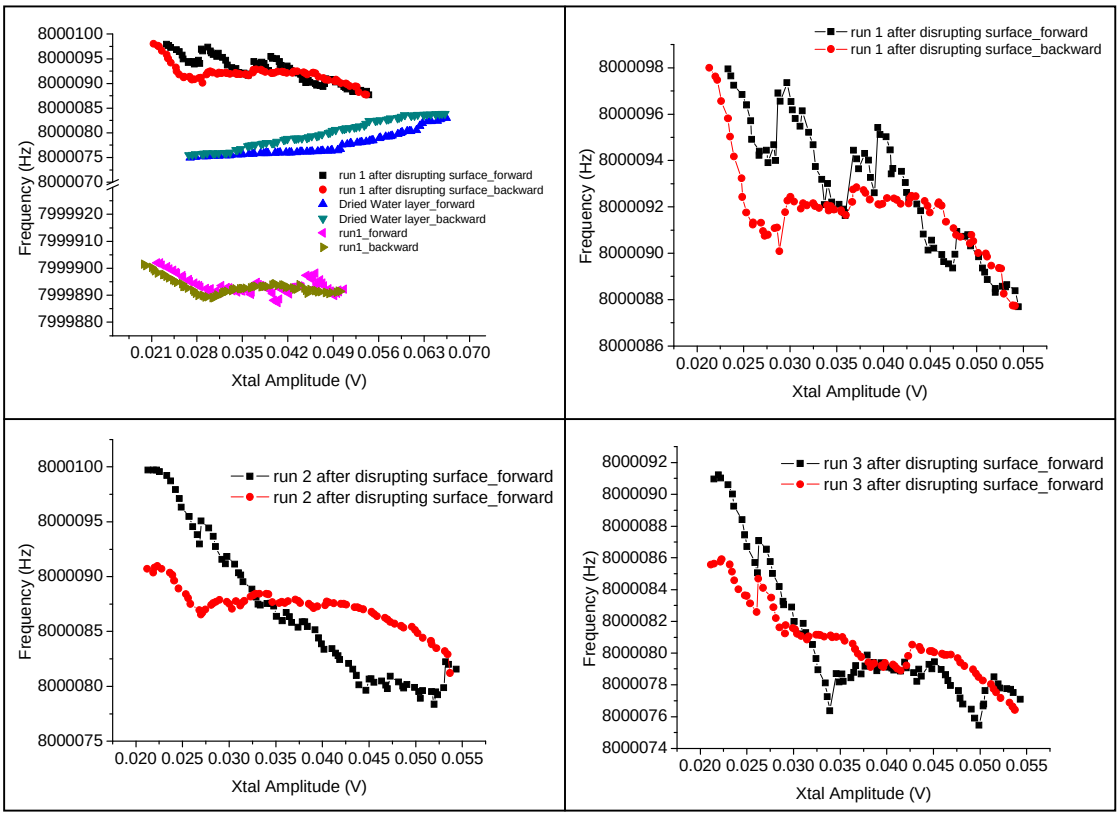

Figure 7.9 - Decoupling curves after motion generation

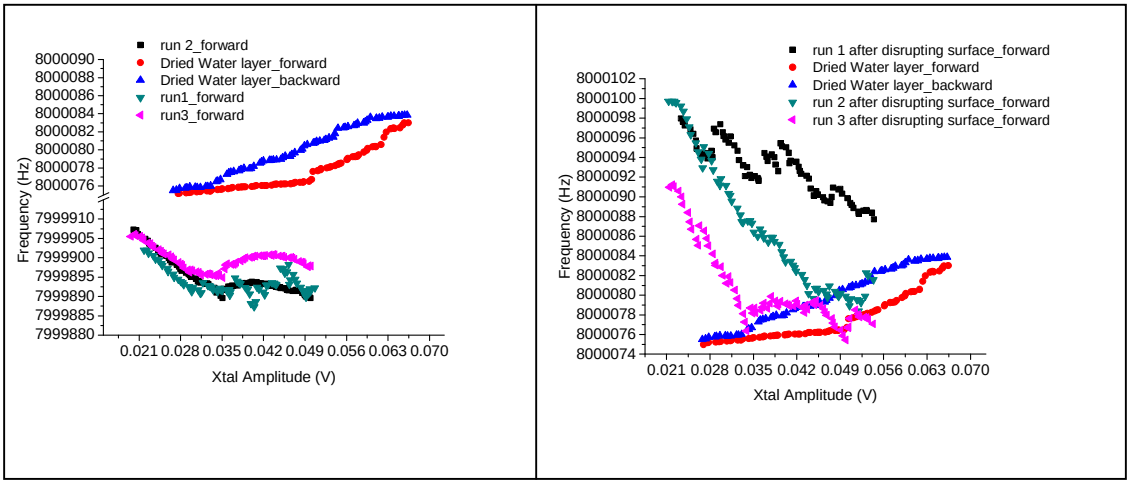

Figure 7.10 - Decoupling curves before (a) and after (b) motion generation plotted with the water decoupling experiment.

7.4 EXPERIMENT IN AIR OF 15 MICRON SPHERES DEPOSITED FROM AQUEOUS SOLUTION IN VERTICAL ORIENTATION AFTER INTENTIONALLY DISRUPTING SURFACE BY INDUCING PARTICLE MOTION.

After performing a the third decoupling curve run in the experiment shown in figure 7.9 the sample was rotated into the vertical orientation (parallel with gravity) with oscillation direction perpendicular with gravity (VH orientation). When performing the first decoupling curve an immediate change in the surface behavior was observed as suggested by the direction of the decoupling curve. The transition for horizontal orientation to the vertical orientation moved the particles further into the weak regime as indicated by the rise in frequency from the horizontal runs studied in figure 7.9 to the vertical runs shown in figure 7.11. This observation provides strong evidence that the acceleration of gravity has an observable affect on the decoupling behavior of microparticles (15 micron in this case) during QCM experiments. After the initial varied behavior in the decoupling curve observed in run 1 the decoupling trend returned to what was observed in the previous experiment performed in the horizontal orientation.

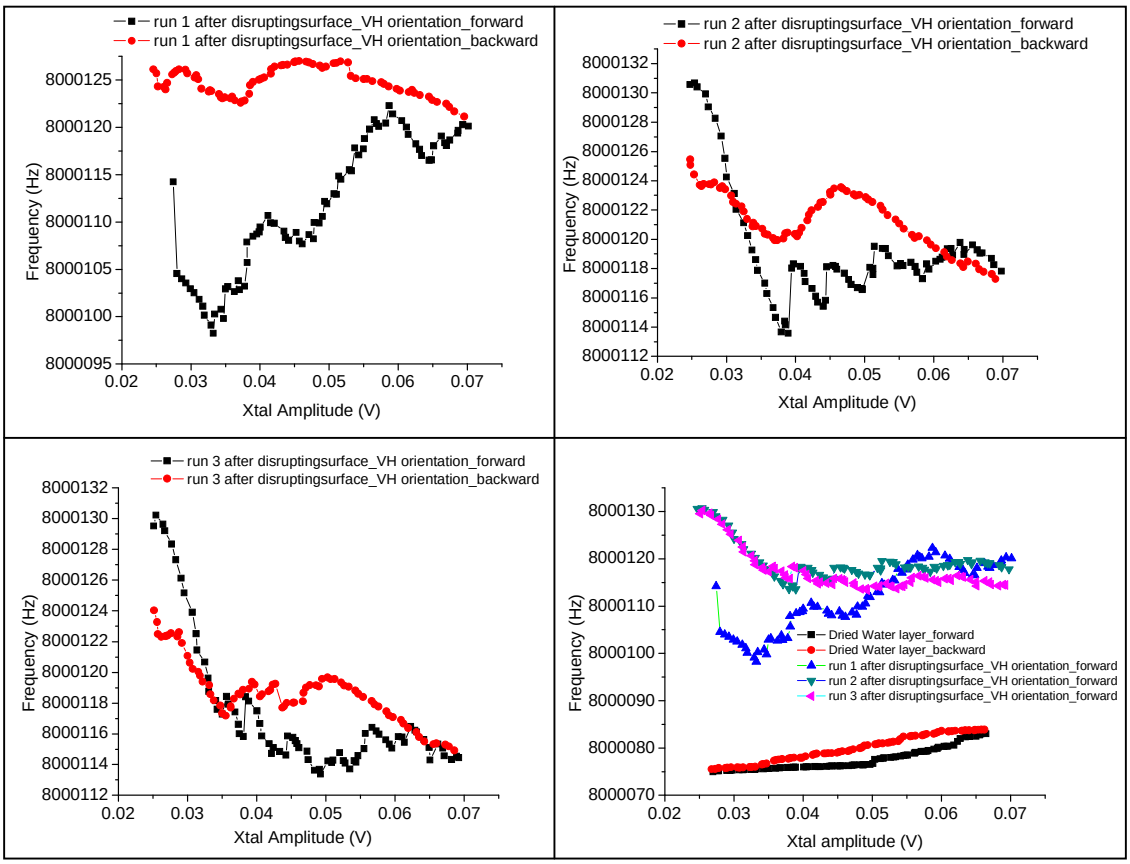

Figure 7.11 - Decoupling curves after placing sample into vertical orientation

7.4.1 EXPERIMENT IN AIR OF 15 MICRON SPHERES DEPOSITED FROM AQUEOUS SOLUTION IN VERTICAL ORIENTATION AFTER INTENTIONALLY DISRUPTING SURFACE A SECOND TIME

After running three decoupling curves in the vertical (vh) orientation the sample was once again connected to the stronger output electronics to generate motion and disrupt the surface. Substantial particle motion accompanied by some particle loss was observed in the optical region during these motion generation runs. After the motion generation runs were finished the surface was scanned and I observed not all of the particles were removed from the surface. The sample was then connected to the original electronics and decoupling curve

runs were performed as usual. As indicated by figure 12 the particles moved back to the strong coupling regime where they originally resided. Detailed friction analysis was performed on these particles and reported on for each run in figures 7.13-7.15. The frictional behavior of the particles was similar to what was observed in section 7.2 with the main exception being the slip time vales for these experiments were approximately an order of magnitude larger than what was calculated for the initial runs in 7.2.

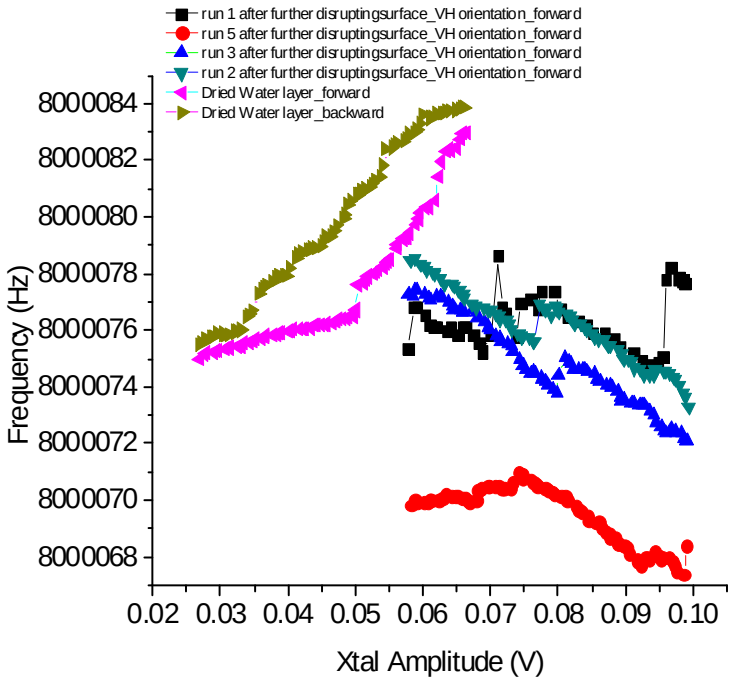

Figure 7.12 - Decoupling curves after disrupting surface in the vertical orientation plotted with the water decoupling experiment.

7.4.2 FRICTION ANALYSIS OF RUN 1

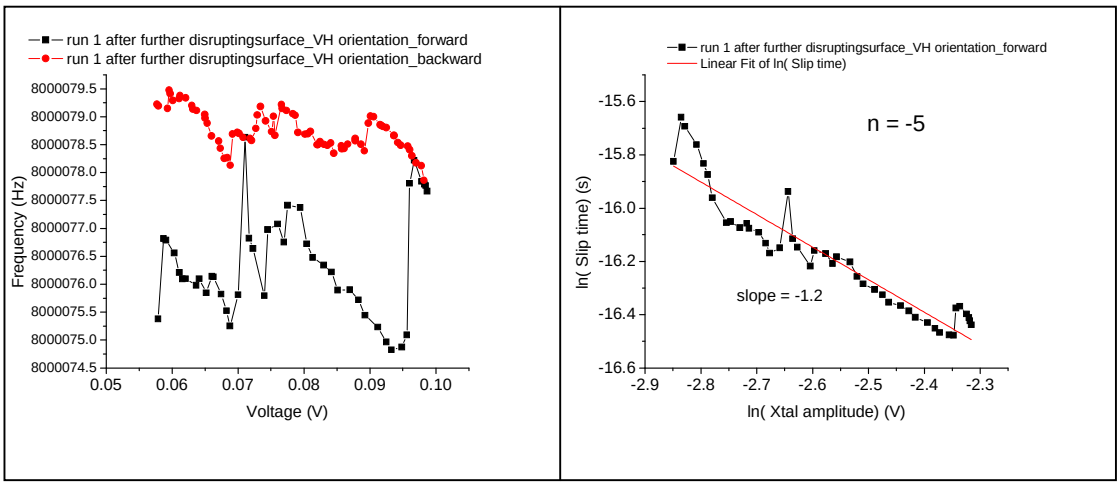

Figure 7.13 - Friction analysis of first decoupling curve run after disrupting surface in the vertical orientation.

7.4.3 FRICTION ANALYSIS OF RUN 2

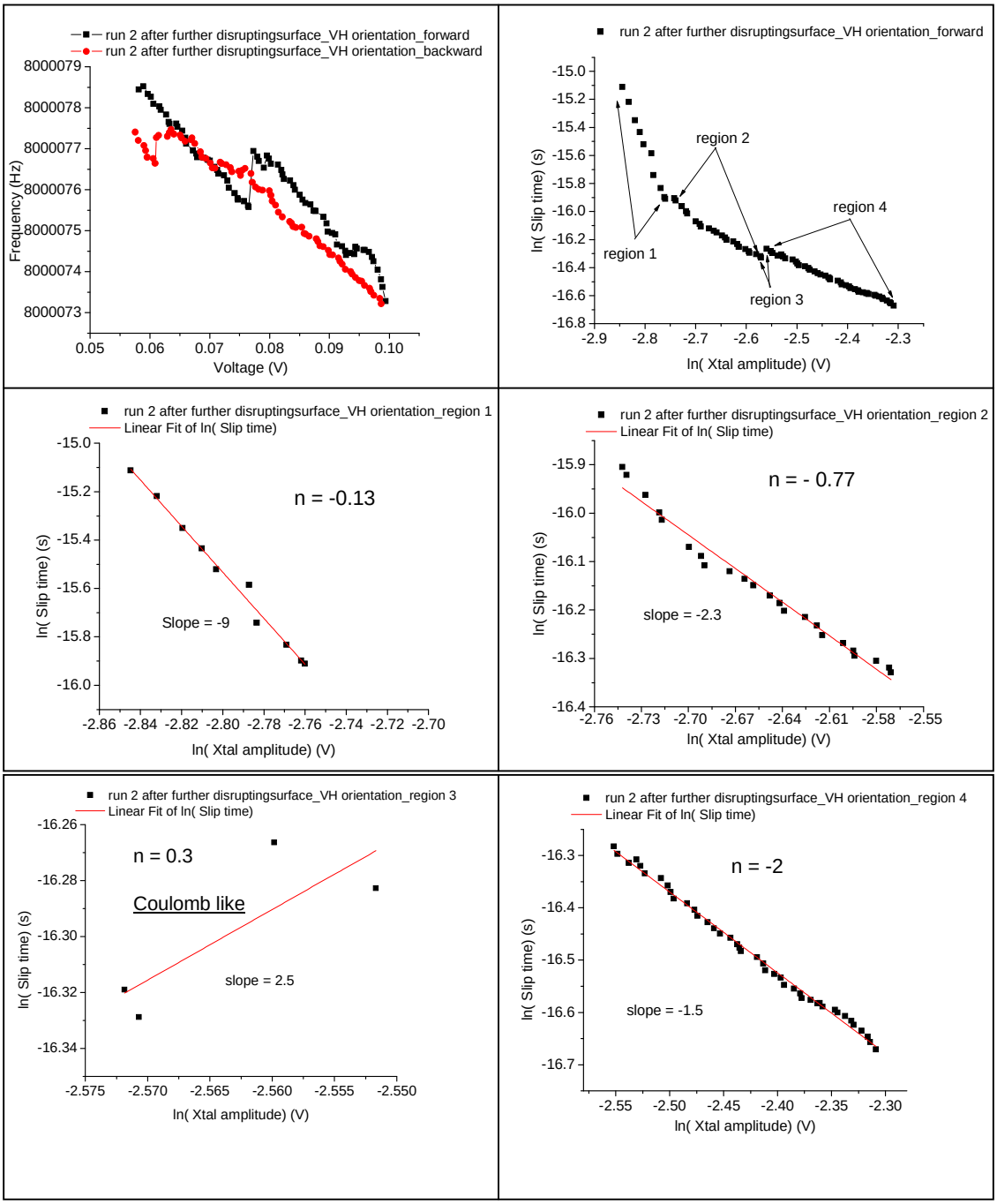

Figure 7.14 - Friction analysis of second decoupling curve run after disrupting surface in the vertical orientation

7.4.4 FRICTION ANALYSIS OF RUN 3

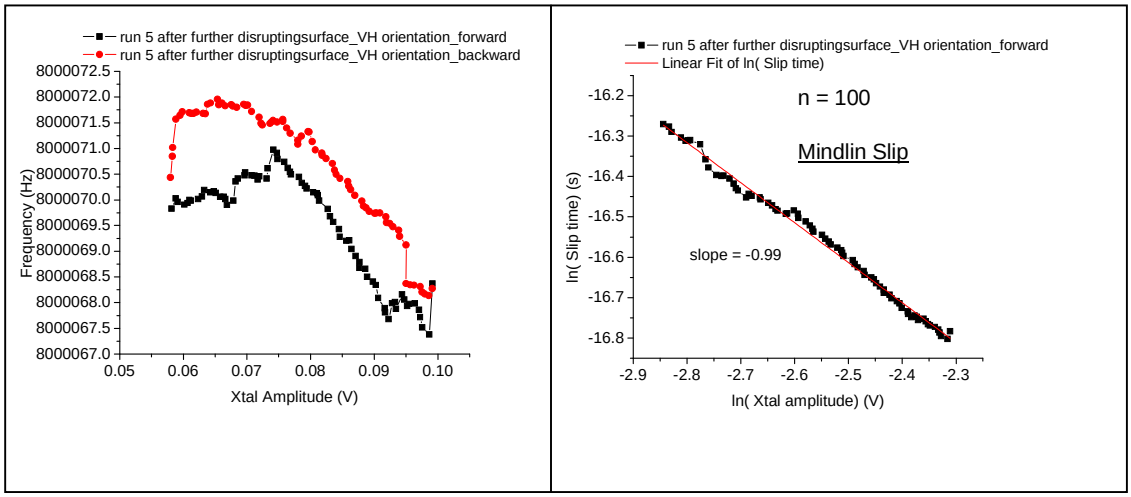

Figure 7.15 - Friction analysis of fifth decoupling curve run after disrupting surface in the vertical orientation

7.5 VARIATION IN MICROPARTICLE COUPLING AS A FUNCTION OF TIME

From the previous sections above I have shown several examples of how the friction associated with 15 micron polystyrene spheres varies with substrate velocity (xtal amplitude). In the sections that follow data is reported on for microspheres at “constant” (velocity is not truly constant since the direction is changing with each oscillation of the QCM) substrate velocity (xtal amplitude). The data from sections 7.5.1 and 7.5.2 show the behavior of the microspheres in different environments and deposited it different ways. The experiment shown in 7.5.1 was deposited in the usual way from aqueous solution however, the experiment shown in figure 7.5.2 was deposited via transfer experiment as described in detail in chapters 2 and 6. In both experiments slow changes in coupling (frequency) were

observed for both experiments. The frequency of occurrence for these varying coupling events where similar for both experiments (30-40 minutes) but the main difference was the shape of these events. The sample deposited from aqueous solution (wet deposition) in figure 7.16 displayed jagged stick-slip like events similar to what was observed during the decoupling curve runs in the earlier sections. The dry deposition sample figure 7.17 displays a smooth roughly sinusoidal response with a frequency of about 30 minutes. Figure 7.18 shows the first decoupling curve run after several frequency response curves were performed. This decoupling curve run demonstrated of a single sphere supports the statement that particles of this size are in the intermediate coupling regime. The details concerning these observed slow coupling changes is currently not well understood. It was suggested in a previous study[4] that QCMs may not be the best devices for generating Mindlin microslip processes. If the observed behavior coupling behavior is Mindlin in nature it is indeed possible that the observed long periods in coupling changes is a reflection of the QCM measurement device coupled with friction at the sphere flat contact region. During decoupling curve runs the surface particles are experiencing additional forces from the varying oscillation amplitude of the QCM which would aid in initiating the “micro-slip” mechanism. According to our previous decoupling curve experiments (sections 7.2-7.4) the observed slipping mechanism or force law for these fixed crystal amplitude experiments is more than likely a force law that is inversely proportional to velocity.

7.5.1 15 MICRON SPHERES DEPOSITED FROM AQUEOUS SOLUTION IN AIR

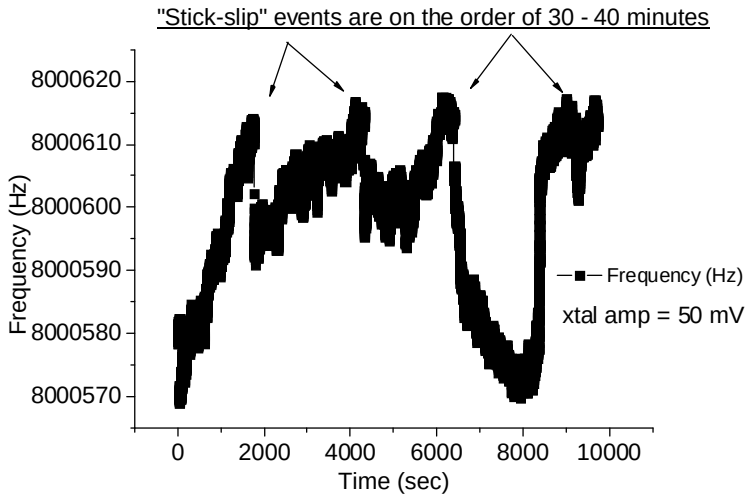

Figure 7.16 - Frequency response over time of a different sample of 15 micron spheres deposited from aqueous solution.

7.5.2 SINGLE 15 MICRON SPHERE CAUGHT DURING TRANSFER EXPERIMENT IN 7E-2 TORR VACUUM ENVIRONMENT IN HORIZONTAL ORIENTATION

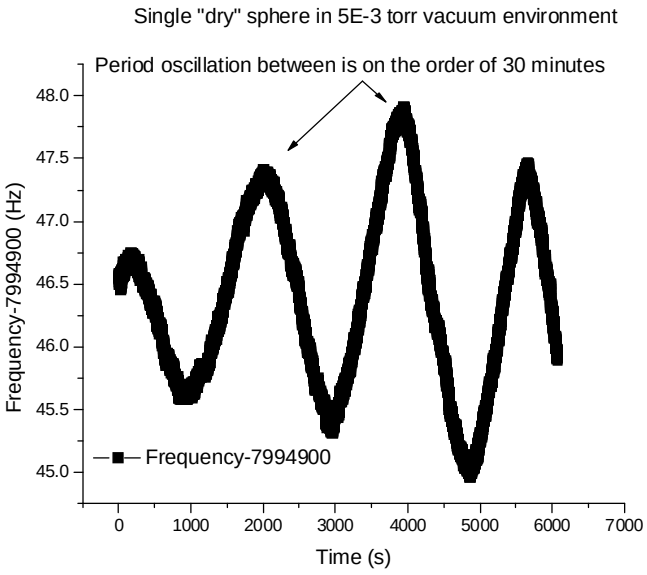

Figure 7.17 - Frequency response over time of a single15 micron sphere deposited in vacuum environment.

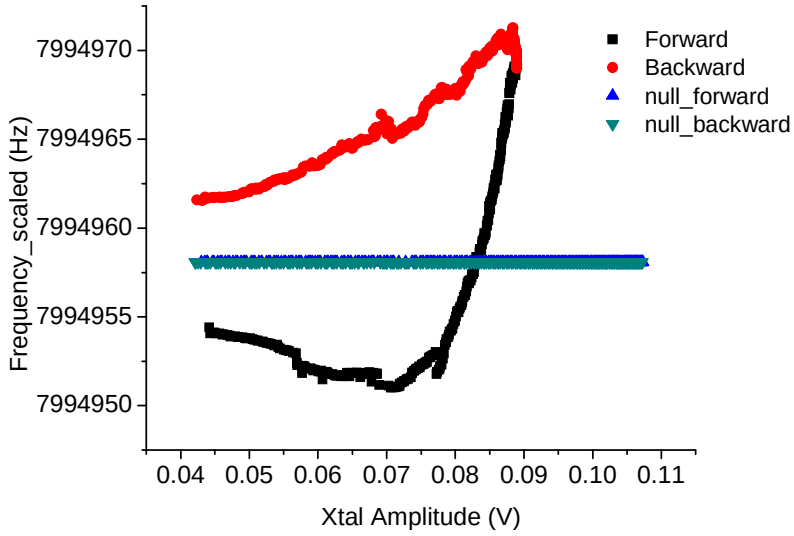

Figure 7.18 - First decoupling curve run of single sphere

7.6 REFERENCES

1. Dybwad, G. L., A sensitive new method for the determination of adhesive bonding between a particle and a substrate. *Journal of Applied Physics* **1985,** *58* (7), 2789-2789.

2. Sauerbrey, G., Verwendung von Schwingquarzen zur Wägung dünner Schichten und zur Mikrowägung. *Zeitschrift für Physik* **1959,** *155* (2), 206-222.

3. Krim, J.; Watts, E. T.; Digel, J., Slippage of simple liquid films adsorbed on silver and gold substrates. *Journal of Vacuum Science & Technology A: Vacuum, Surfaces, and Films* **1990,** *8* (4), 3417-3420.

4. Vittorias, E.; Kappl, M.; Butt, H.-J.; Johannsmann, D., Studying mechanical microcontacts of fine particles with the quartz crystal microbalance. *Powder Technology* **2010,** *203* (3), 489-502.

5. Etsion, I., Revisiting the Cattaneo--Mindlin Concept of Interfacial Slip in Tangentially Loaded Compliant Bodies. *Journal of Tribology* **2010,** *132* (2), 020801-9.

CHAPTER 8: CONCLUSIONS AND FUTURE WORK

8.1 CONCLUSIONS

In this study, methods for interpreting average particle behavior during QCM experiments have been discussed. We have shown overwhelming evidence that the effects of water during QCM experiments can not be ignored and in many cases govern the dynamics as a whole on the surface. The affects of dissipation (bandwidth shift) were not reported on in this study however, it is important to realize that water will have a huge affect on the dissipation data especially under a wet decoupling mechanism where large amounts of water are present. In this study we have found that the analysis of decoupling curves can be quite complex due to the inconsistent bond strength of the spheres on the surface and the multiple paths spheres can take once in motion. Due to the nature of the deposition and the sub-monolayer surface configuration hysteresis and non uniformity can somewhat be expected in these decoupling curves.

8.2 SUGGESTED FUTURE WORK

A new method was introduced in this thesis for decreasing the presence of water during QCM experiments and provided sufficient evidence that upon landing the overall system force of adhesion was greatly reduced and the behavior was reflected in both the decoupling and delta frequency plots. In the future these experiments should include dissipation measurements to further support arguments involving the friction mechanism at the contact. Particle transfer experiments have the potential for many fundamental

applications of better understanding the friction mechanism at the microscale. It is possible with a customized chamber similar to the one I use in this thesis that one could measure the friction force directly after a transfer experiment. This could be accomplished by catching a sphere on the target QCM which would be oriented horizontally. Using a camera mounted directly on the chamber to illuminate the target, one could in principle very carefully rotate the vacuum chamber (monitoring the angle) and estimate a static coefficient of friction (assuming pure roll without slip) by angle at which the particle begins to rotate during the experiment. It is possible that the transfer experiment could be performed multiple times with in a properly constructed chamber to achieve even drier contacts where surface dynamics could be probed in a more controlled environment. The notion of micro particle sorting as suggested by the observed particle motion is not a straight forward task especially in humid/wet environments. However, it may be easier to achieve such control and sorting in a dry environment such as particles on the surface after a transfer experiment. Future work must be done to see if movement can be better controlled and understood.